

NATIONAL LIBRARY
OTTAWA



BIBLIOTHÈQUE NATIONALE
OTTAWA

6245

NAME OF AUTHOR..... L. A. Vienneau.....

TITLE OF THESIS..... INTERNAL FRICTION IN COLD-WORKED

.....NICKEL.....

UNIVERSITY..OF ALBRTA., EDMONTON.....

DEGREE FOR WHICH THESIS WAS PRESENTED. Ph.D.....

YEAR THIS DEGREE GRANTED..... 1970.....

Permission is hereby granted to THE NATIONAL LIBRARY
OF CANADA to microfilm this thesis and to lend or sell copies
of the film.

The author reserves other publication rights, and
neither the thesis nor extensive extracts from it may be
printed or otherwise reproduced without the author's
written permission.

(Signed)..... *L. A. Vienneau*.....

PERMANENT ADDRESS:

Laboratory of Atomic and Solid State
..... Physics

Clark Hall.....

Cornell University.....

DATED... May 19..... 1970

Ithaca, 14850 New York

THE UNIVERSITY OF ALBERTA

INTERNAL FRICTION IN COLD-WORKED NICKEL

BY

© LEONARD ARTHUR VIENNEAU

A THESIS

SUBMITTED TO THE FACULTY OF GRADUATE STUDIES IN
PARTIAL FULFILMENT OF THE REQUIREMENTS FOR THE
DEGREE OF DOCTOR OF PHILOSOPHY

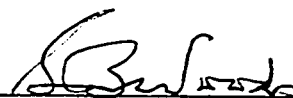
DEPARTMENT OF PHYSICS

EDMONTON, ALBERTA

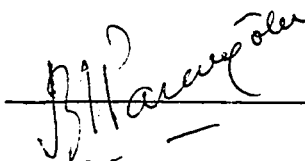
SPRING, 1970

UNIVERSITY OF ALBERTA
FACULTY OF GRADUATE STUDIES

The undersigned certify that they have read,
and recommend to the Faculty of Graduate Studies for
acceptance, a thesis entitled "INTERNAL FRICTION IN
COLD-WORKED NICKEL", submitted by Leonard Arthur Vienneau
in partial fulfilment of the requirements for the degree
of Doctor of Philosophy.



Supervisor



External Examiner

Date 2 January 1970

ABSTRACT

The problem of internal friction in cold-worked metals has interested researchers since the original work of Bordoni (1949). The mechanical relaxation effect known as the Bordoni peak, consisting of a large maximum in the temperature dependence of the internal friction, has been of prime interest. As early as 1957, the dislocation kink theory of Seeger et al was able to account for the primary features of the peak, particularly the activation energy. This theory and the several versions of it have not however been able to explain the spectrum of the Bordoni relaxation.

The work presented here is an experimental study of internal friction in cold-worked nickel. A comparison of the Bordoni peak in nickel with that of copper has indicated that the modifications of the Seeger et al theory given by Paré (1961) and Hobart (1969) cannot account for the spectrum of the Bordoni peak. We have found that the Bordoni peak in nickel is accompanied by a subsidiary peak similar to the Niblett-Wilks peak in copper. We present measurements of the subsidiary peak in copper and nickel which lend support to the Thompson and Holmes (1959) proposal that several discreet relaxations are present in the vicinity of the Bordoni peak.

The theoretical considerations by Seeger and Schiller (1962) on the effects of kink-kink interactions are also discussed.

A third relaxation peak which occurs in cold-worked nickel was also studied. It is shown that this effect arises from the interaction of dislocations with hydrogen impurities and can be identified with the hydrogen cold-work peak in iron (Gibala, 1967) and tantalum (Mazzolai and Nuovo, 1969). This is contrary to the Sommer and Beshers (1966) proposal that this third peak can be identified with the Bordoni relaxation. Our measurements on tantalum have revealed a previously unreported relaxation peak which is introduced by cold work. Possible explanations for this peak are discussed.

We have found that under certain conditions, the internal friction of cold-worked nickel exhibits a "plateau" region near liquid helium temperatures. This effect is compared with similar results that have been reported for iron by Bruner (1960) and Vienneau (1968). The measurements are discussed in terms of magnetic relaxation, that is, stress induced motion of magnetic domain walls in the presence of dislocations.

FOR.

Dianne, Tony, Todd and Natasha

TABLE OF CONTENTS

<u>Chapter</u>		<u>Page</u>
I.	INTRODUCTION	1
II.	THEORY OF ACOUSTIC RELAXATION	6
	A. General theory	6
	B. Thermally activated relaxation	9
	C. Relaxation processes with a spectrum of relaxation times	10
	D. Experimental considerations	18
III.	EXPERIMENTAL TECHNIQUE	20
	A. The cryostat	20
	B. The excitation and detection of vibrations	21
	C. Measurements of internal friction	26
	D. Temperature measurement	28
IV.	EXPERIMENTAL RESULTS	31
	A. Nickel	32
	i) The P_1 relaxation peak	34
	ii) The subsidiary peak P_2	47
	iii) The P_3 relaxation peak	53
	iv) Cold working and magnetic damping	58
	B. Copper	64
	i) The Bordoni peak	67
	ii) The Niblett-Wilks peak	69
	C. Tantalum	76
	D. Iron	86

V.	DISCUSSION	101
	A. The relaxation peaks	101
	i) The Bordoni peak	101
	ii) The δ -peak in tantalum and niobium	127
	iii) The hydrogen cold-work peaks	132
	B. Magnetic damping effects	146
VI	CONCLUSIONS	153
	BIBLIOGRAPHY	157

LIST OF TABLES

<u>Number</u>		<u>Page</u>
I.	Experimental results for the P_1 (Bordoni) peak in nickel	39
II.	Experimental results for the P_2 (Niblett-Wilks) peak in nickel	51
III.	Comparison of σ_P^0/μ for various metals	130
IV.	Summary of the energies related to the hydrogen cold-work peak	140

LIST OF FIGURES

<u>Figure</u>		<u>Page</u>
2.1	The variation of the real and imaginary compliances with $\omega\tau$.	8
2.2	The function $f_2(x,\beta)$ for several values of the parameter β .	14

2.3	The dependence of $f_2(0,\beta)$, the maximum value of $f_2(x,\beta)$ on the width of the distribution	15
3.1	Schematic of the cryostat set up to measure damping of flexural normal modes in disk shaped samples.	22
3.2	Schematic of cryostat set up for the study of internal friction in normal modes of bar-shaped samples.	23
3.3	Block diagram of excitation and detection system	25
3.4	(a) Typical resonance curve for normal mode of a sample	27
	(b) Typical recording of the decay of free vibrations in a sample	27
4.1	The effect of various amounts of cold work on the internal friction in nickel	33
4.2	Temperature dependence of Q^{-1} at three frequencies in a nickel sample deformed 12%.	36
4.3	Temperature dependence of the resonant frequency f_0 for three normal modes studied in figure 4.2	37
4.4	Activation energy plot for the P_1 peak in nickel	40
4.5	The dependence of Q^{-1}/Q_m^{-1} on x for the P_1 peak in nickel	42
4.6	The variation of β vs T^{-1} determined from the shape of the P_1 peak in nickel deformed 12%	45

4.7	Comparison of β versus T^{-1} for the P_1 peak after various treatments of a nickel sample	48
4.8	The P_2 peak in nickel deformed 12%	50
4.9	Activation energy plot for the P_2 peak in nickel	52
4.10	The effect of hydrogen charging on the Q^{-1} versus T curve in cold worked nickel	55
4.11	The effect of increasing cold-work on the P_3 peak in nickel	56
4.12	The effect of magnetic saturation on Q^{-1} at low temperatures in lightly cold-worked nickel	60
4.13	Temperature dependence of Q^{-1} in a nickel sample used by Schiller (1955)	62
4.14	Magnetic field dependence of Q^{-1} and the resonant frequency f_0 of the Schiller sample at 4.2°K	63
4.15	Temperature dependence of Q^{-1} for two modes of a copper sample deformed 25%	68
4.16	Temperature dependence of β for the Bordoni peak in copper	70
4.17	The Niblett-Wilks peak separated from the total Q^{-1} curves in figure 4.15	72
4.18	The Niblett-Wilks peak for a copper sample deformed 10%	73
4.19	The effect of various amounts of cold working on the Bordoni peak in copper	75
4.20	The temperature dependence of Q^{-1} in annealed tantalum	78

4.21	The effect of cold work on Q^{-1} versus temperature in tantalum	79
4.22	Q^{-1} versus temperature in cold worked tantalum at two frequencies	81
4.23	Resonant frequency as a function of temperature for two modes in figure 4.22	82
4.24	Activation energy plot for the δ -peak in tantalum	83
4.25	Dependence of Q^{-1} on temperature in iron at four frequencies	87
4.26	The frequency dependence of the anomalous internal friction in iron	89
4.27	The internal friction in iron after various annealing treatments	90
4.28	Magnetic field dependence of Q^{-1} for the extensional modes of a bar shaped iron sample	92
4.29	The magnetic field dependence of Q^{-1} for the torsional modes of a bar shaped sample	94
4.30	Normalized frequency dependence of Q^{-1} in iron at low temperatures	95
4.31	Temperature dependence of the normalizing frequency ω_0	97
4.32	Q^{-1} versus ω/ρ for various annealing treatments in iron	99
4.33	The temperature dependence of Q^{-1} after irradiation	100
5.1	The elastic energy of a dislocation in a periodic lattice	108

CHAPTER 1

INTRODUCTION

The fact that solids, and in particular metals, do not behave in a perfectly elastic manner is a well known phenomenon. A consequence of this deviation from ideal behavior is that sound waves and mechanical vibrations cannot progress in a solid with undiminished intensity. This phenomenon, variously referred to by terms such as acoustic damping or internal friction, has been the subject of many investigations for over a century. The most important results in the early literature have been reviewed by Zener (1948).

The earliest theoretical consideration of significance dealing with internal friction considered the solid to contain one or more ordering processes through which the stress of a sound wave could relax. Zener (1948) has presented a phenomenological theory of stress relaxation. This theory introduces first order terms in the stress and strain rate into the normal (Hooke's law) elastic stress-strain relationship. As a consequence subsequent experimental investigations have generally been attempted to delineate the ordering or relaxation processes that cause internal friction.

Of the many internal friction sources that have been studied, most attention has been focussed on extended faults in metals, primarily dislocations. Read (1941) was the first to suggest that part of the internal friction in metals is caused by the stress-induced motion of dis-

locations. The interest in dislocation motion is primarily due to the role these faults play in the plastic flow of solids under large stresses (see for instance, Cottrell, 1953). It is reasonable to expect that an understanding of the motion of dislocations under the small stresses present in a sound wave would lead to a better understanding of their motion under larger stresses. This knowledge would of course be of fundamental importance to the theory of the strength of materials.

The experimental investigations of internal friction have uncovered a large number of effects which can be attributed to dislocation motion (see for example, Mason, 1966 a). From the varied nature of these effects, it has become increasingly clear that dislocations can undergo a variety of different modes of motion and that simple models such as that of the Granato-Lücke (1956) theory cannot account for all of these. These difficulties occasioned the introduction of the kink concept into the theory of internal friction (Seeger, 1956). This concept has given the best overall picture of dislocation internal friction (Seeger and Schiller, 1966 and Alefeld, 1967).

One of the prominent features of dislocation internal friction is the Bordoni relaxation effect (Bordoni, 1954). This relaxation arises from a type of dislocation motion which is thermally activated. Although there have been many theoretical models proposed for the interpretation

of the Bordoni effect (Niblett, 1966) the most widely accepted theory is that of Seeger et al (1957). This proposal attributes the Bordoni effect to stress relaxation caused by the generation of double kinks in dislocations. The Bordoni effect exhibits itself as a peak in the internal friction versus temperature curve and the major problem with the Seeger et al model is its failure to explain the large width of this peak. Attempts to modify the theory of this effect have been reported by Paré (1961) and more recently by Hobart (1969). The Seeger theory demonstrates that the generation of double kinks is a thermally activated process and a calculation is given for the activation energy involved. Paré introduced the concept of internal stresses into the theory and from this postulated that double kink generation involves a continuous spectrum of activation energies. He also showed that the shape of the Bordoni peak in copper is consistent with such a spectrum. Paré's proposal however could not account completely for the width of the peak. Hobart pointed out that the activation energy spectrum could be affected by dislocation splitting and by taking this into consideration he was able to account for the width of the Bordoni peak.

From an experimental point of view, the situation is more complicated. The review by Niblett (1966) shows that there is no agreement in the literature on whether or not the width of the Bordoni peak can be attributed to a

spectrum of activation energies, since from the shape of the peak alone the spectrum cannot be determined uniquely (Bordoni, 1961). A second, less important, problem with the Seeger model is its failure to explain relaxation peaks, similar to the Bordoni peak, that have been observed in cold worked b.c.c. metals (Chambers, 1966).

The present study consisted of measurements of the internal friction in cold worked nickel an f.c.c. metal. The peaks that were observed were compared with those in copper and tantalum. This procedure provided new information on the Bordoni peak and the peaks in b.c.c. metals. Evidence will be presented to show that both types of peaks occur in nickel. The peak identified with the b.c.c. type relaxation in this work was first observed by Sommer and Beshers (1966) and interpreted by these authors as the Bordoni peak. The evidence to be presented here will show that this peak is hydrogen cold work peak. The b.c.c. relaxation peaks are now known to be of this type (Mazzolai and Nuovo, 1969). This study has also shown that tantalum, a b.c.c. metals, exhibits a previously unreported peak at temperatures lower than that of the hydrogen cold work peak. The peak observed in nickel at a lower temperature than the cold work peak (Berry, 1962) is shown to be accompanied by a smaller subsidiary peak on its low temperature side. The double peak is compared with the Bordoni peak which has a similar subsidiary peak and the

result favors a discreet spectrum as first proposed by Thompson and Holmes (1959). This is discussed in terms of the Paré-Hobart proposal.

Another type of ordering process which is known to occur in ferromagnetic metals such as nickel is that associated with the induced motion of magnetic domain walls (Bozorth, 1951). The internal friction in cold worked nickel was found to exhibit an anomalous effect at low temperatures similar to the "plateau region" in iron, first observed by Heller (1959) and associated with magnetic internal friction. The author wrote an M.Sc. thesis in 1968 on the 'Anelasticity of Iron at Low Temperatures' which consisted primarily of an investigation of the plateau region. These results along with more recent measurements will be compared with the anomaly in nickel.

CHAPTER 2

THEORY OF ACOUSTIC RELAXATION

A. General theory of acoustic relaxation

Only a brief review of simple relaxation theory will be given here since it has been covered in detail in a previous thesis (Vienneau, 1968). This treatment follows the work of Zener (1948) for relaxation in a "standard linear solid" using a single relaxation time.

In a standard linear solid the stress-strain relation is assumed to contain first-order terms in the stress and strain rates. It is usually written (for one dimension) in the form:

$$J_R \sigma + \tau_\sigma J_u \dot{\sigma} = \varepsilon + \tau_\sigma \dot{\varepsilon} \quad , \quad (2.1)$$

where σ is the stress component, ε is the strain component, J_u and J_R are the unrelaxed and relaxed compliances respectively, and τ_σ is the relaxation time at constant stress. The difference between the relaxed and unrelaxed compliances is defined as the relaxation of the compliance, δJ , that is:

$$\delta J = J_R - J_u \quad . \quad (2.2)$$

In the case of acoustic relaxation we are interested in the dynamic response of the solid described by equation (2.1). Given an oscillating stress:

$$\sigma = \sigma_0 e^{i\omega t} \quad , \quad (2.3)$$

where σ_0 is the stress amplitude and ω is the circular frequency, it is seen from equation (2.1) that the strain

is given by:

$$\varepsilon = J^*(\omega) \sigma . \quad (2.4)$$

The complex compliance $J^*(\omega)$ is usually written:

$$J^*(\omega) = J_1(\omega) - i J_2(\omega) \quad (2.5)$$

where:

$$J_1(\omega) - J_u = \frac{\delta J}{1 + \omega^2 \tau^2} \quad (2.6)$$

and,

$$J_2(\omega) = \delta J \frac{\omega \tau}{1 + \omega^2 \tau^2} . \quad (2.7)$$

The variations of J_1 and J_2 with $\omega \tau$ are illustrated in figure 2.1.

The complex compliance indicates that the strain lags behind the stress by a phase angle ϕ given by:

$$\tan \phi = J_2/J_1 . \quad (2.8)$$

The quantity $\tan \phi$, called the internal friction is usually expressed in the form:

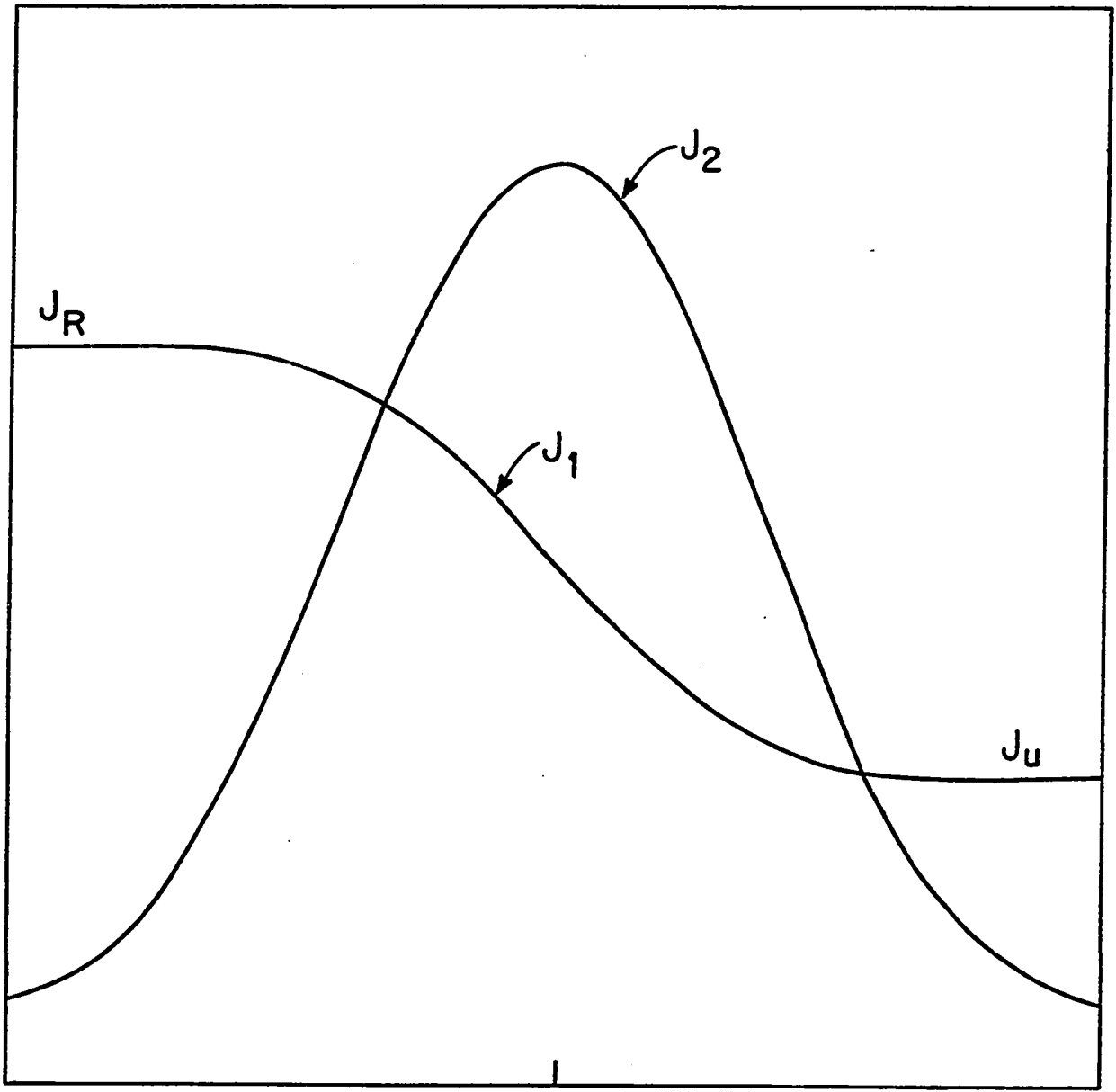
$$\tan \phi = \frac{\Delta}{(1+\Delta)^{1/2}} \frac{\omega \tau}{1 + \omega^2 \tau^2} , \quad (2.9)$$

where Δ , called the relaxation strength, is given by:

$$\Delta = J/J_u . \quad (2.10)$$

FIGURE 2.1

THE VARIATION OF REAL AND IMAGINARY COMPLIANCES
WITH $\omega\tau$, SHOWING THE RELAXING EFFECTS AT $\omega\tau = 1$.



$\text{Log } \omega \bar{\tau}$

The internal friction, $\tan \phi$, given by equation (2.9) has a maximum at $\omega\tau = 1$, given by:

$$(\tan \phi)_m = \frac{1}{2} \frac{\Delta}{(1+\Delta)^{1/2}} . \quad (2.11)$$

It is easily shown that the phase angle ϕ is related to the power P dissipated by the oscillating strain and that this relation is given by (Zener, 1948):

$$\tan \phi = \frac{P}{\omega E} , \quad (2.12)$$

where E is the total elastic energy of the oscillating strain. It is seen from this expression that $\tan \phi$ is a measure of the damping of the strain wave, i.e., sound wave.

B. Thermally activated relaxation

In the last section, the relaxation time was treated as a parameter. However τ may often be expressed as a function of one or more variables. For example, in a thermally activated relaxation process the relaxation time obeys an Arrhenius rate equation (Zener, 1948) and is given by:

$$\ln \tau = \ln \tau_0 + \frac{W}{kT} . \quad (2.13)$$

The quantity τ_0 is called the limiting relaxation time, W is the activation energy for the process, k is Boltzmann's constant and T is the absolute temperature.

The peak in the $\tan \phi$ vs $\ln \omega \tau$ curve may be experimentally observed in two ways. One may either vary the frequency ω or the relaxation time τ (via the temperature). The latter method is often the more convenient since the relaxation time may vary through several orders of magnitude for a relatively small variation in temperature. The maximum internal friction will of course occur when $\omega \tau = 1$. If we combine this condition with equation (2.13), we find that:

$$\ln \omega = \ln \tau_0^{-1} - W/kT_m, \quad (2.14)$$

where T_m is the temperature at which maximum damping occurs. This dependence of T_m on the frequency of vibration ω enables one to determine W and τ_0 experimentally. A plot of $\ln \omega$ versus T_m^{-1} will have its slope equal to W/k and its intercept equal to $\ln \tau_0^{-1}$.

C. Relaxation processes with a spectrum of relaxation times

Many relaxation processes which might be expected to obey equation (2.9) exhibit a peak which is much wider than the theoretical prediction. This is interpreted as the result of a spectrum of relaxation times being associated with the processes rather than a single relaxation time as implied by equation (2.9) (Zener, 1948). The observed acoustic relaxation is thus the average of many individual

processes whose relaxation times are distributed about a most probable value τ_m .

In the analytical treatment of this behavior one uses a normalized distribution function $\psi(\ln \tau)$. The individual processes, characterized by $\ln \tau$ and falling in the range $d(\ln \tau)$, are assumed to contribute to the relaxation of the compliance an amount dJ given by (Staverman and Schwarzl, 1956):

$$dJ = \delta I \psi(\ln \tau) d(\ln \tau) \quad . \quad (2.15)$$

Thus equations (2.6) and (2.7) may be rewritten as:

$$d [J_1(\omega) - J_u] = \frac{dJ}{1 + \omega^2 \tau^2} \quad , \quad (2.16)$$

and,

$$d [J_2(\omega)] = dJ \frac{\omega \tau}{1 + \omega^2 \tau^2} \quad . \quad (2.17)$$

These equations may be integrated using equation (2.15) to obtain:

$$J_1(\omega) = J_u + \delta J \int_{-\infty}^{+\infty} \frac{\psi(\ln \tau)}{1 + \omega^2 \tau^2} d(\ln \tau) \quad , \quad (2.18)$$

and,

$$J_2(\omega) = \delta J \int_{-\infty}^{+\infty} \frac{\omega \tau}{1 + \omega^2 \tau^2} \psi(\ln \tau) d(\ln \tau) \quad . \quad (2.19)$$

Equations (2.18) and (2.19) reduce to (2.6) and (2.7) if $\psi(\ln \tau)$ is taken to be a Dirac delta function.

The treatment of the integrals in the above equations depends, of course, on the form of $\psi(\ln \tau)$. It has been found however that the shapes of $J_1(\omega)$ and $J_2(\omega)$ functions is not very sensitive to the form of the distribution function (Berry and Nowick, 1961 a). The width of the distribution function is the primary parameter effecting J_1 and J_2 . It is thus possible to assume a particular form for $\psi(\ln \tau)$ without greatly affecting the generality of the treatment. The following section is based on the work of Berry and Nowick (1961 a and b) in which the Gaussian distribution is used to study equations (2.18) and (2.19).

We now introduce the variable z given by:

$$z = \ln \tau / \tau_m \quad (2.20)$$

and then the Gaussian distribution function is given by:

$$\psi(z) = \frac{1}{\beta\sqrt{\pi}} \exp(-z^2/\beta^2). \quad (2.21)$$

The parameter β is the half width of $\psi(z)$ at e^{-1} of its maximum value. Using the variable,

$$x = \ln \omega \tau_m \quad , \quad (2.22)$$

and substituting (2.21) into (2.18) and (2.19) we obtain:

$$\frac{J_1(x) - J_u}{\delta J} = \frac{1}{\sqrt{\pi}} \int_{-\infty}^{+\infty} e^{-u^2} \frac{du}{1+\exp[2(x+\beta u)]} \equiv f_1(x, \beta) \quad , \quad (2.23)$$

and

$$\frac{J_2(x)}{\delta J} = \frac{1}{\sqrt{2\pi}} \int_{-\infty}^{+\infty} \exp(-u^2) \operatorname{sech}(x+\beta u) du \equiv f_2(x, \beta). \quad (2.24)$$

Since the integrals involved cannot be evaluated in terms of tabulated functions, numerical calculations are required using β as a parameter. For $\beta=0$, the Gaussian distribution function becomes the Dirac δ -function and, as mentioned earlier, this corresponds to the case of a single relaxation time.

The numerical calculations of the function $f_2(x, \beta)$ in equation (2.24) were carried out by Berry and Nowick (1961 a). The result of these calculations is illustrated in figure 2.2 by a normalized plot of f_2 versus x for various values of β . It is noted that f_2 has a maximum value at $x=0$ given by:

$$f_2(x, \beta) \Big|_m = f_2(0, \beta) ; \delta\tau_m = 1 . \quad (2.25)$$

The quantity $f_2(0, \beta)$ is illustrated in figure 2.3 as a function of β . It should also be noted that the width of the peak in $f_2(x, \beta)$ increases with β and it is easily shown that the asymptotic form of f_2 for large β is given by (Berry and Nowick 1961):

$$f_2(x, \beta) = \frac{\sqrt{\pi}}{2\beta} \exp(x^2/\beta^2) . \quad (2.26)$$

An examination of the function $f_1(x, \beta)$ indicates two things of importance. This function is an antisymmetric function in x whose value at $x=0$ is $\frac{1}{2}$ irrespective of the value of β . The slope $2f_1(x, \beta) / \partial x \Big|_{x=0}$ however decreases at

FIGURE 2.2

THE FUNCTION $f_2(x, \beta)$ FOR SEVERAL VALUES OF THE
PARAMETER β . (AFTER BERRY AND NOWICK, 1961)

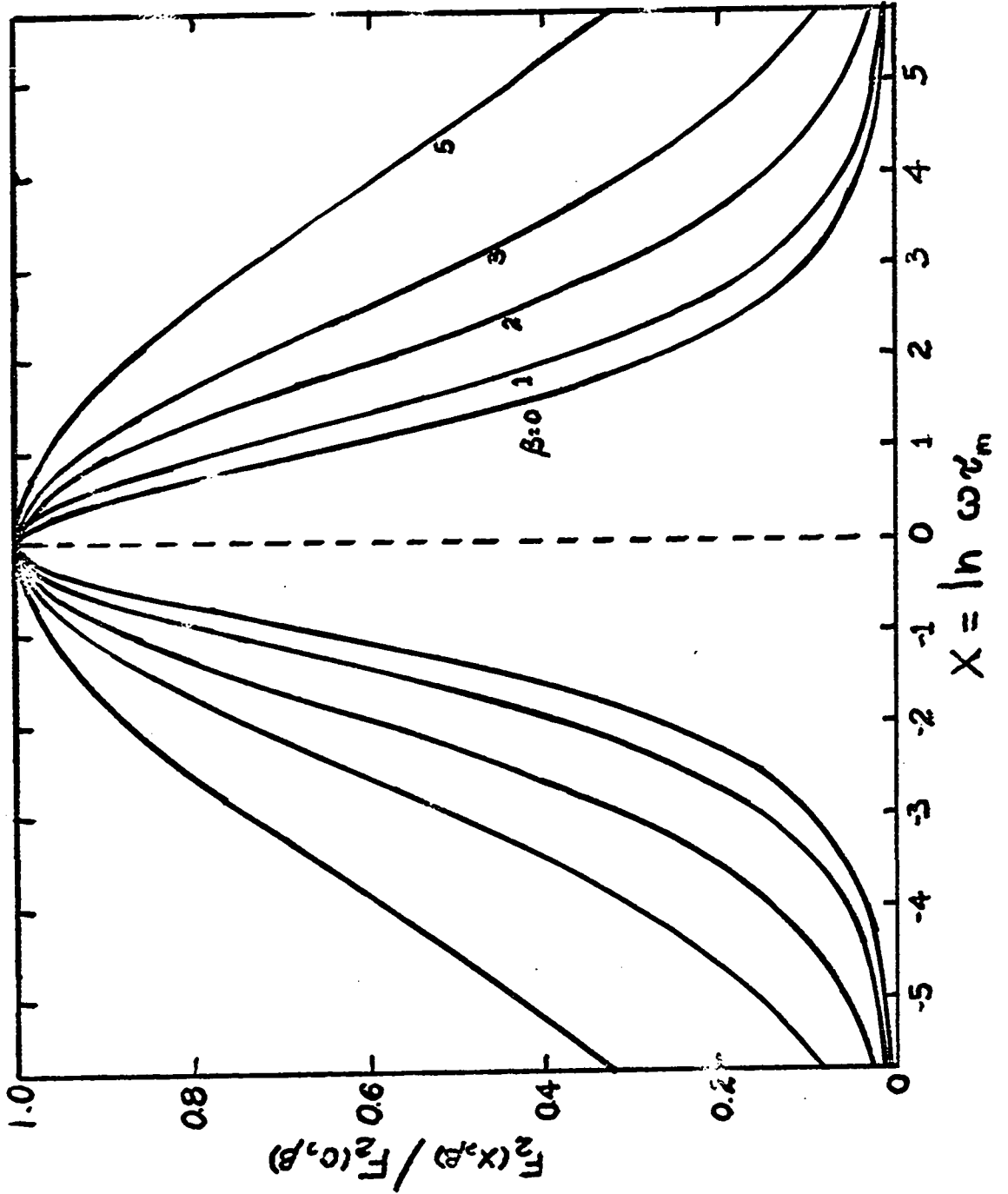
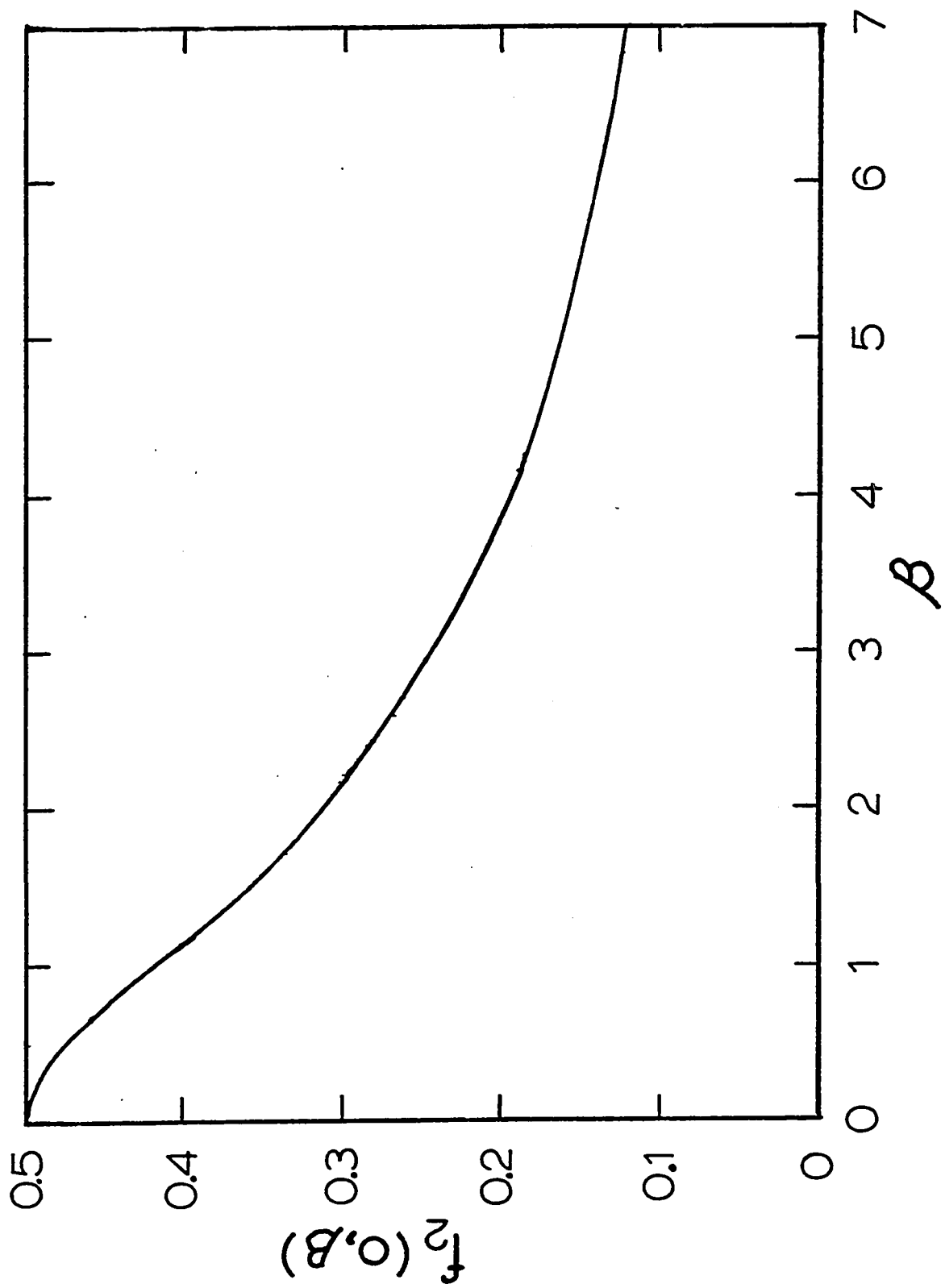


FIGURE 2.3

THE DEPENDENCE OF $f_2(0, \beta)$, THE MAXIMUM VALUE OF
 $f_2(x, \beta)$, ON THE WIDTH OF THE DISTRIBUTION



β is increased. Numerical calculations of $f_1(x, \beta)$ have been tabulated by Yager (1936) in his treatment of dielectric relaxation.

We must now consider the possibility of a temperature-dependent distribution parameter β . The discussion has up to now been concerned with a distribution in the quantity $\ln \tau$. In the case of a thermally-activated relaxation process, $\ln \tau$ was found to be dependent on temperature; according to equation (2.13),

$$\ln \tau = \ln \tau_0 + \frac{W}{kT} \quad (2.13)$$

It is clear from this equation that a distribution in $\ln \tau$ is due either to the existence of a distribution in $\ln \tau_0$ or in the activation energy W , or in both. It will now be shown that it is possible to differentiate between a spectrum in $\ln \tau_0$ and one in W by the resulting form of the spectrum in $\ln \tau$.

In general terms it is known that the variance of a linear function of several random variables x_i is given by:

$$\text{Var} \left[\sum_{i=1}^n a_i x_i \right] = \sum_{i=1}^n \sum_{j=1}^n a_i a_j \text{Cov}[x_i, x_j] \quad (2.27)$$

where a_i are constants and $\text{Cov}[x_i, x_j]$ is the covariance of the pair of random variables x_i and x_j (see for example, Jenkins and Watts, 1968). It is also known that if x_i has a Gaussian distribution, the linear function on the left

hand side of equation (2.7) will also have a Gaussian distribution. The above relation was applied to equation (2.13) by MacDonald and Barlow (1961) with the assumption that $\ln \tau_0$ and W are random variables with Gaussian distributions of width β_0 and β_W respectively. They also assumed that these two distributions were independent of one another. This leads to a Gaussian distribution in $\ln \tau$ with its width β given by:

$$\beta = \left[\beta_0^2 + \left(\frac{\beta_W}{kT} \right)^2 \right]^{1/2} . \quad (2.28)$$

We note that unless β_W vanishes (distribution in $\ln \tau_0$ only), β is a function of temperature. If β_0 vanishes, we see that β is given by

$$\beta = \frac{\beta_W}{kT} . \quad (2.29)$$

We thus see that an activation energy spectrum is distinguished from a limiting relaxation time spectrum in that it causes a temperature dependent spectrum in $\ln \tau$. Berry and Nowick have shown that if β_W and β_0 are not independent of one another then the resulting spectrum in $\ln \tau$ can be approximated by a Gaussian distribution whose width is:

$$\beta = \beta_0 + \frac{\beta_W}{kT} . \quad (2.30)$$

This equation would apply when W and τ_0 are mutually dependent on a parameter with a distribution of values.

The above results provide a method of determining the source of a spectrum in $\ln \tau$ for a thermally-activated relaxation process. The problem is now one of determining β versus T and comparing with equations (2.28) to (2.30).

D. Experimental considerations

The theory presented above gives a description of the dynamic response functions f_1 and f_2 and assumes that these are measured quantities. In practice however these functions cannot be measured directly and it is necessary to consider the method of arriving at them from the experimentally determined quantities. Internal friction experiments normally yield the quantity $\tan \phi$ and the magnitude of the elastic compliance $J = (J_1^2 + J_2^2)^{1/2}$. From equation (2.8) we see that:

$$J_2 = J_1 \tan \phi. \quad (2.31)$$

Combining this result with equation (2.24), we get:

$$f_2(x, \beta) = \frac{J_1}{\delta J} \tan \phi. \quad (2.31)$$

In the case of thermally-activated relaxation processes, we have seen that it is advantageous to increase $\tan \phi$ as a function of temperature at a constant frequency. Using equations (2.13) and (2.22) we see that the variable x , in this case, is given by:

$$x = \ln \omega \tau_m = \frac{W_m}{k} [T^{-1} - T_m^{-1}] , \quad (2.32)$$

where W_m is the most probable activation energy. Thus, if J_1 and δJ are known, the function $f_2(x, \beta)$ can be calculated. This calculation can be simplified by assuming that $\delta J \ll J_1$ (usual case) and that both δJ and β are independent of temperature. Under these assumptions equation (2.31) becomes

$$\frac{f_2(x, \beta)}{f_2(0, \beta)} = \frac{\tan \phi}{\tan \phi \Big|_{T_m}} \quad (2.33)$$

The last two equations can now be used to put the experimental data in the form used in figure 2.2 and a comparison can be made to arrive at a value of β for the relaxation peak in question. If β is dependent on temperature, equation (2.33) must be corrected slightly to take into account the resulting temperature dependence of $f_2(0, \beta)$. This correction is small in most cases (Berry and Nowick, 1961).

CHAPTER 3

EXPERIMENTAL TECHNIQUE

The details of the experimental technique, for the most part were described in an earlier thesis (Vienneau, 1968). The internal friction was measured by a resonance technique with a system capable of frequencies ranging from 4 kHz to 300 kHz. The temperature of the sample could be varied from room temperature to liquid helium temperatures. It was also possible to measure the internal friction as a function of magnetic field from zero to 1 kOe.

A. The Cryostat

The cryostat used in making the measurements was very similar in design to that described by Bordoni et al (1959). Since its original description (Vienneau, 1968) this cryostat has been modified to allow the measurement of internal friction for several different types of vibrations. The flexural vibrations in thin disk-shaped samples could be investigated by the mounting technique illustrated schematically in figure 3.1. The sample was supported by resting it on three pins which made contact with it on a nodal circle of the normal flexural mode to be used in the measurement. Shallow holes were drilled into the sample at the points of contact for stability. This type of mount contributes very little to the damping of vibration in the sample.

The torsional and extensional vibrations of bar-shaped sample were studied using the mounting technique illustrated in figure 3.2. This mount also involved the

supporting of the sample by 3 pins which made contact with it at nodal points. The mounting pins in this case are lightly spring loaded and the sample is suspended from the nodes.

B. The excitation and detection of vibrations

The so-called electrostatic driving technique was used to excite normal modes of vibration in the sample. This involved the placing of an electrode near the surface of the sample at an antinodal point (see E in figure 3.1 and E¹ in figure 3.2). An oscillating voltage (25-150 volts) was then applied to the electrode with the sample being held at ground potential through one of the mounting pins. By considering the electrode-sample system as a parallel plate capacitor, Nuovo (1961) demonstrated that the applied voltage V produces a force on the sample which is proportional to V^2 and has a frequency that is twice that of V . If appropriate frequency is chosen, the driving voltage will produce a resonance by causing the sample to vibrate in its normal mode.

The surface of the samples was made parallel to that of the electrodes by the adjusting screws illustrated in the diagrams. The distance between the sample and the electrode was adjustable from the exterior of the cryostat via a control rod which also served as an electrical connection to the electrode. The electrode to sample distance was

FIGURE 3.1

SCHEMATIC OF CRYOSTAT SET UP TO MEASURE DAMPING
OF FLEXURAL NORMAL MODES IN DISK SHAPED SAMPLES

E - Electrode
S - Sample
1,2,3 - Sample mounting pins
1,2 - thermocouple pins
3 - ground pin
A,B,C - Three point adjustment for
electrode-sample parallelism

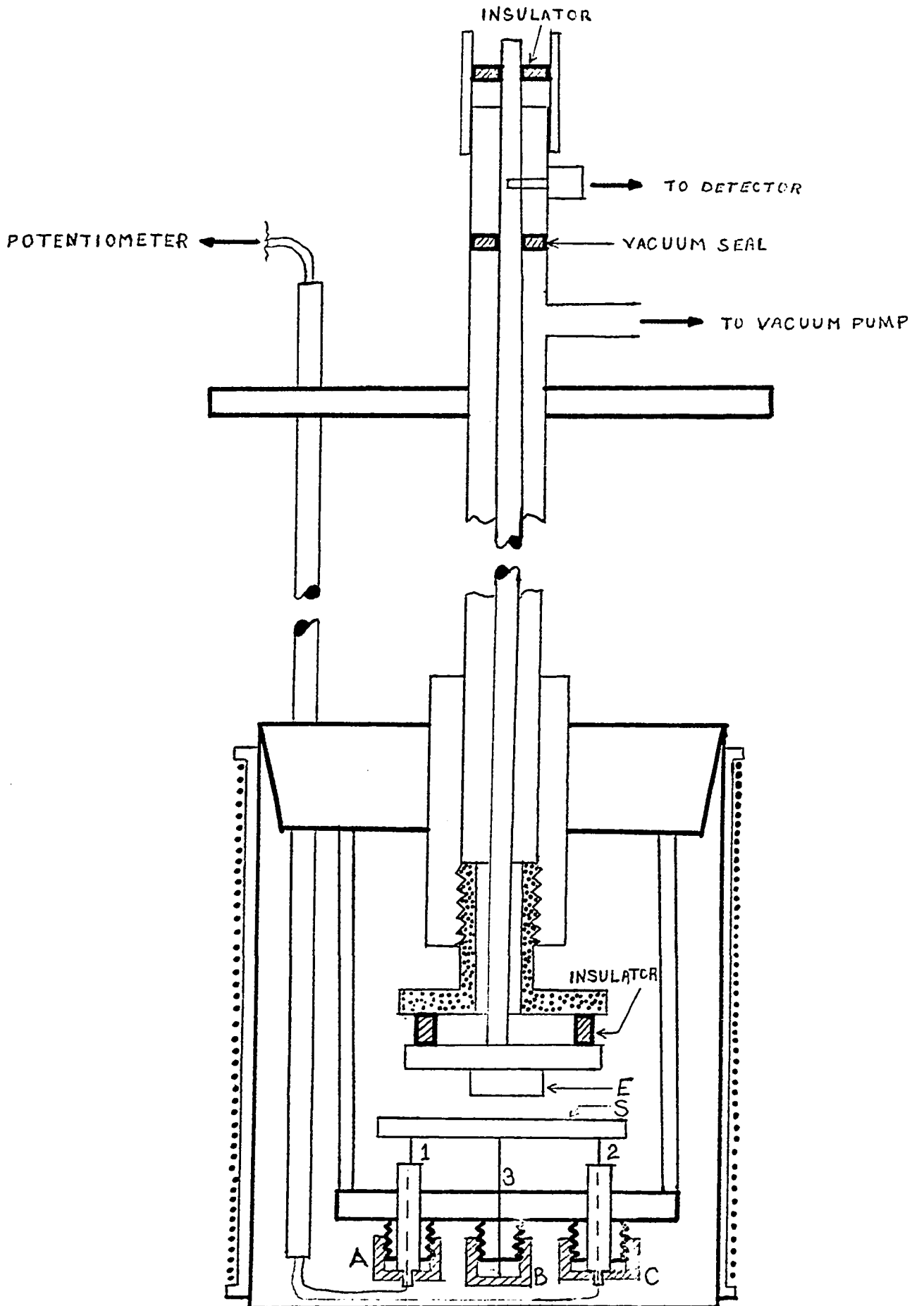
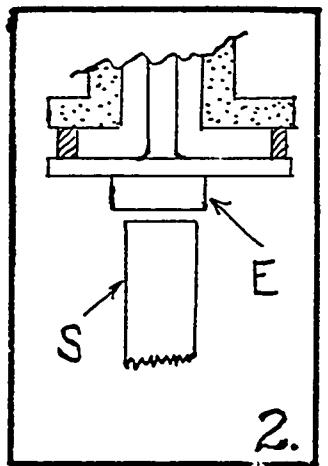
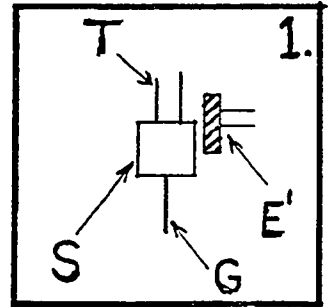
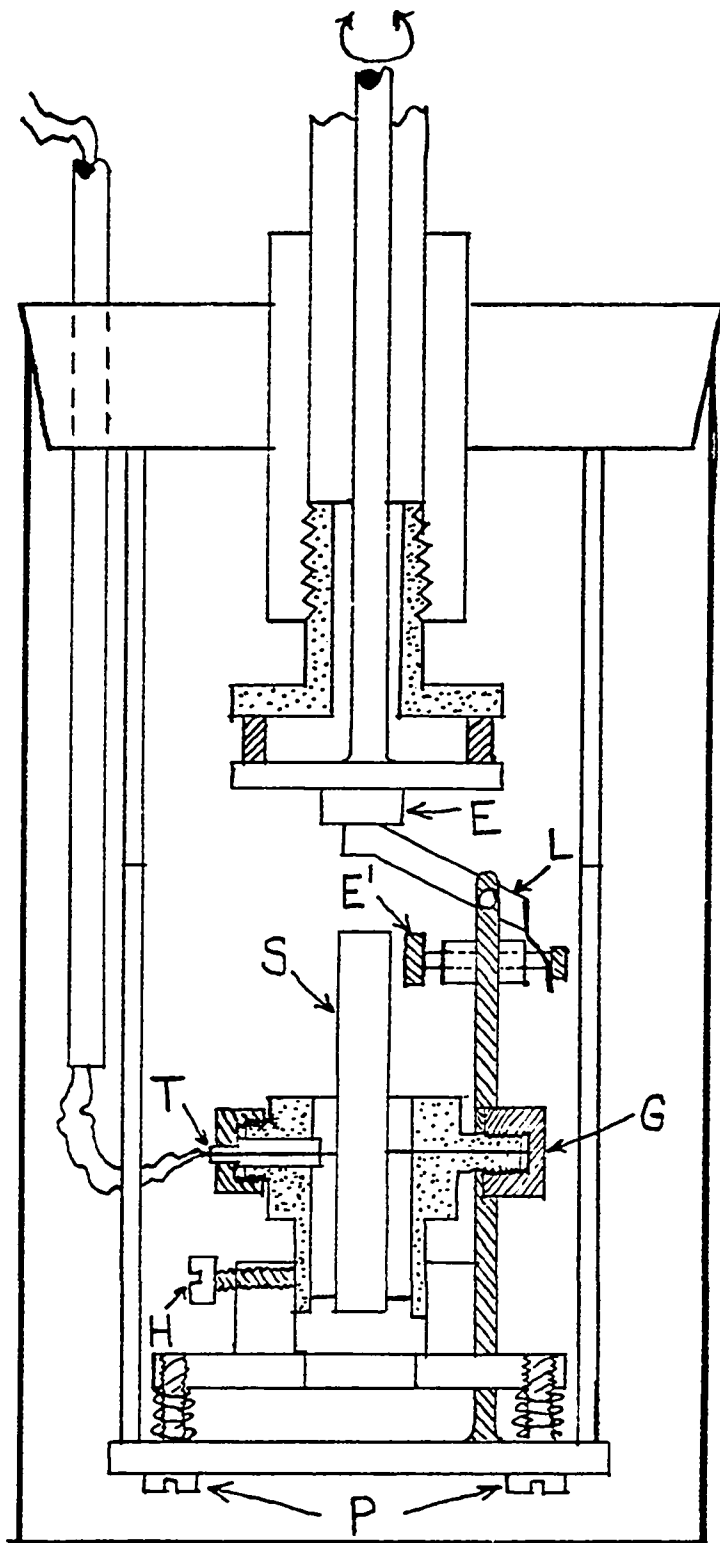


FIGURE 3.2

SCHEMATIC OF CRYOSTAT SET UP FOR THE STUDY OF
INTERNAL FRICTION IN NORMAL MODES OF BAR-SHAPED
SAMPLES

- E - Electrode
S - Sample
P - Three point sample-electrode parallelism adjustment
T - thermocouple pins
G - ground pin
E¹ - auxiliary electrode for torsional modes
L - lever system to transform vertical motion of E
into horizontal motion of E¹
- Inset 1 - Torsional mode arrangement showing relative
position of E¹ and S.
- Inset 2 - Extensional mode arrangement showing relative
position of E and S with E¹ removed.



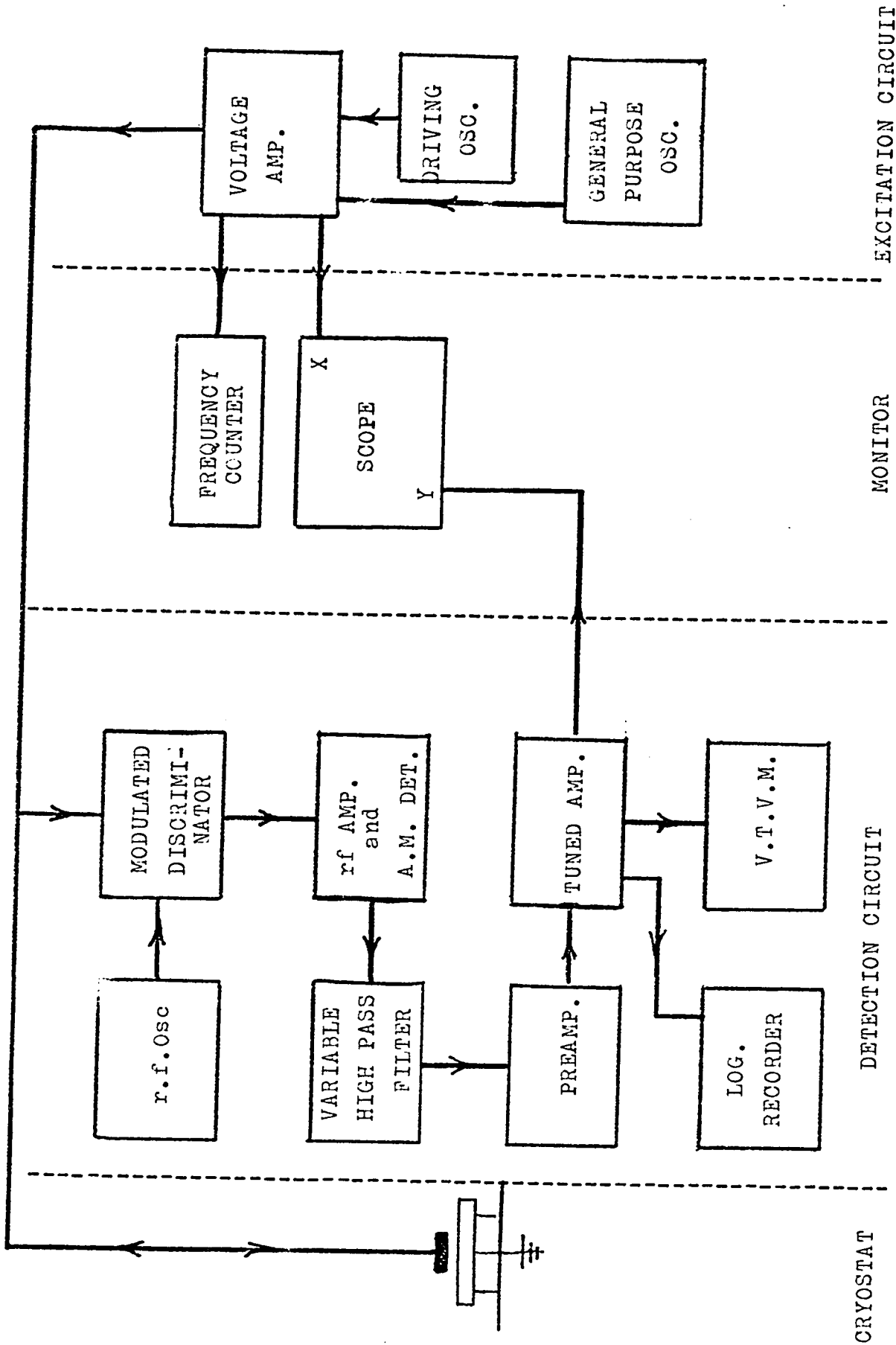
typically 0.1 mm. The position of the electrode with respect to the samples for the three different types of vibration is illustrated in figures 3.1 and 3.2.

As well as its function in the excitation of vibration, the electrode served as the basis of the detection system with the control rod as the common electrical connection for both functions. The block diagram in figure 3.3 illustrates the electronic system and its connection to the electrode. The oscillator-amplifier combination used for the driving voltage had an output capability of 0-250 volts at frequencies ranging from 2 kHz to 300 kHz. The voltage amplifier was similar to that described by Nuovo (1961) and the oscillator was described by Vienneau (1968).

The detection of the vibration produced in the sample was based on the modulated discriminator system, described by Nuovo (1961). This technique detects the change in capacitance of the electrode-sample system caused by the vibration of the sample with respect to the electrode. The output of the modulated discriminator is a signal with an amplitude proportional to that of the vibrations in the sample and a frequency equal to that of the vibrations. After this signal had passed through a filtered amplifier system (Vienneau, 1968), it was fed to a vacuum tube voltmeter and a logarithmic level recorder. The frequency was measured by a preset counter to an accuracy of ± 0.1 Hz.

FIGURE 3.3

BLOCK DIAGRAM OF THE EXCITATION AND
DETECTION SYSTEM



C. Measurement of Internal Friction

It has been mentioned several times that the internal friction was measured using normal modes of vibration in the samples. These normal modes are resonant conditions which are described by a quality factor Q . It is easily shown (Zener, 1948) that Q is related to the internal friction by the equation:

$$Q^{-1} = \tan \phi . \quad (3.1)$$

The value of Q^{-1} can be determined from the width of the resonance peak for the normal mode of interest. A typical peak is illustrated in figure 3.4(a) showing the resonant frequency f_0 and the two frequencies at half-maximum amplitude, f_1 and f_2 . By measuring these three frequencies, the internal friction can be determined from the equation:

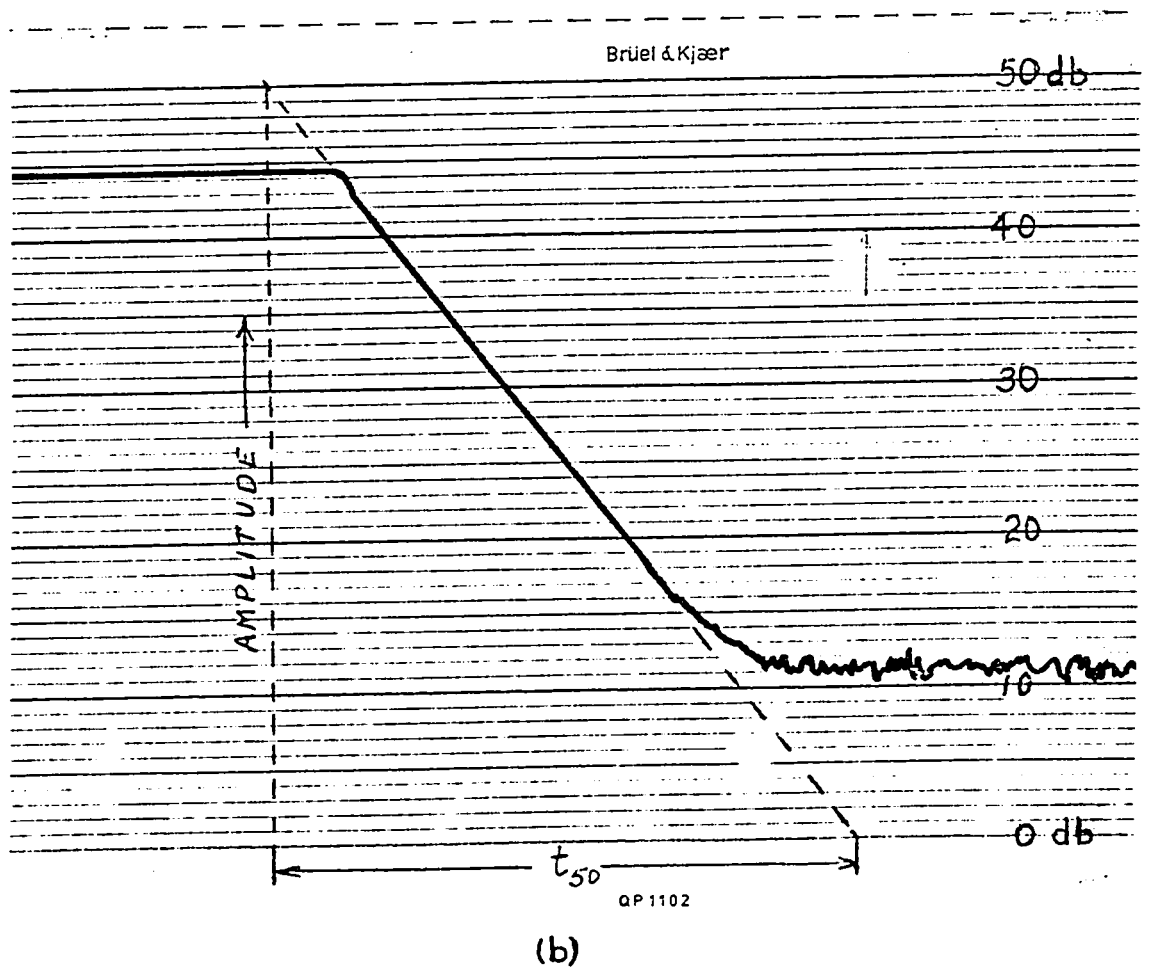
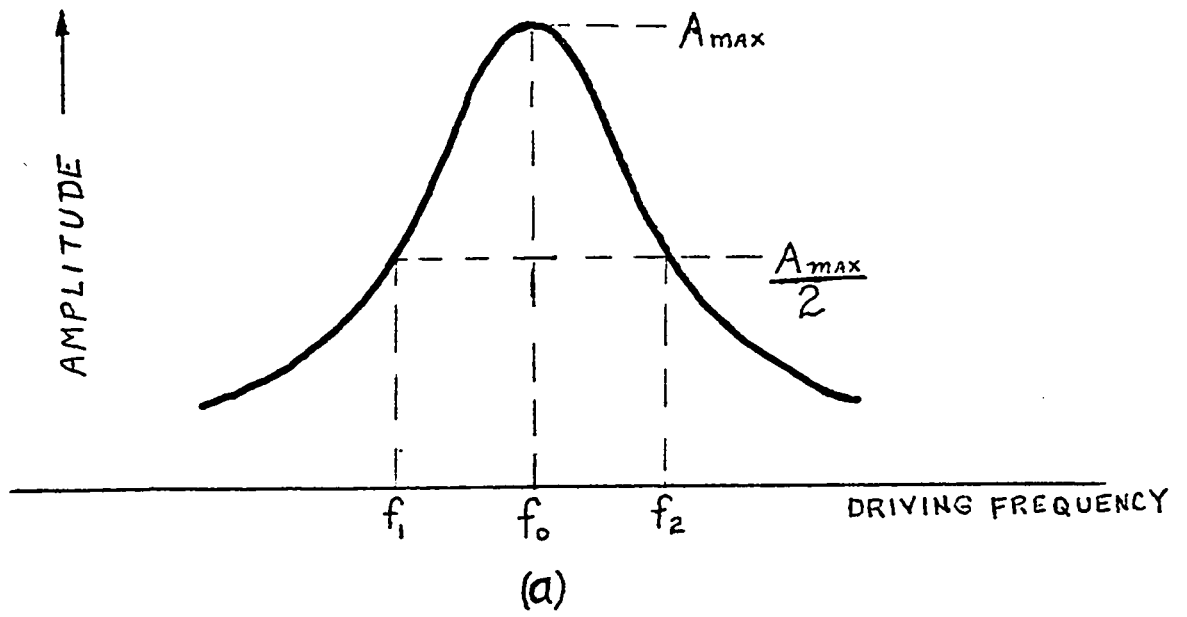
$$Q^{-1} = \frac{f_2 - f_1}{\sqrt{3} f_0} . \quad (3.2)$$

The accuracy of this measurement is determined by the width of the peak and since the uncertainty in f_1 and f_2 is ± 0.1 H_z the peak must be several H_z wide before the measurement of Q^{-1} is satisfactory.

When the resonance peak was too narrow (Q^{-1} small) to be measured accurately in this way, Q^{-1} was determined from the decay rate of the resonant vibrations. This was done by recording the amplitude of vibrations as a function

FIGURE 3.4

- (a) TYPICAL RESONANCE CURVE FOR THE NORMAL MODE OF A SAMPLE SHOWING THE CHARACTERISTIC FREQUENCIES f_0 , f_1 AND f_2 .
- (b) TYPICAL RECORDING OF THE DECAY OF FREE VIBRATION IN A SAMPLE SHOWING THE CHARACTERISTIC TIME t_{50} .



of time on the logarithmic level recorder following cut-off of the driving voltage. The trace of a typical decay is shown in figure 3.4(b). The exponential decay produced a straight line which could be extrapolated to 50 db to arrive at the time t_{50} . After measurement of the resonant frequency, the internal friction was evaluated from:

$$Q^{-1} = \frac{1.833}{f_o \cdot t_{50}} \quad (3.3)$$

The use of equations (3.2) and (3.3) was demonstrated by Nuovo (1961). Satisfactory agreement has been found between the two methods when it was possible to use both at the same time. The error in the measurements of Q^{-1} was one percent or less when the two methods were compared. It should be noted that the 30 db signal to noise ratio indicated by figure 3.4(b) is typical of the conditions encountered during all the measurements to be presented.

D. Temperature measurement

In order to determine the temperature dependence of Q^{-1} it is of course necessary to be able to control and measure the temperature of the sample. The cryostat design allowed the sample temperature to be varied from room temperature to liquid helium temperature. This was effected by slowly cooling the sample chamber over a boiling liquid. Liquid nitrogen was used for cooling from room temperature

to 77°K and liquid helium was used for lower temperatures. The sample was brought into thermal contact with the chamber by helium exchange gas and the temperature was held constant during the measurements by evacuating the sample chamber. The sample mounting technique described provided very effective thermal isolation. The temperature drift during the course of a measurement was 0.1°K or less. In order to avoid errors in Q^{-1} due to this small drift, the resonance peak was scanned in both directions to measure f_0 , f_1 and f_2 . By averaging the resulting Q^{-1} the effect of the temperature dependence of the above frequencies was minimized.

The temperature of the sample was measured by a thermocouple incorporated in the mounting pins. Two of these pins were in the form of 0.3 mm diameter wires, insulated from ground. One wire was constant^w alloy and the other was copper with the sample forming the junction between the two. A reference junction was located in an ice bath outside the cryostat and the emf was determined by standard potentiometric means. The calibration of this thermometer was based on the work of Powell et al (1961) and was described by Vienneau (1968). The estimated error in the temperature determination was $\pm 0.2^\circ\text{K}$ from room temperature to 20°K. The error increased considerably at lower temperatures. When an accurate measurement was

required below 20°K , a germanium resistance thermometer was mounted near the surface of the sample. Temperature measurements could then be made down to 4.2°K with no increase in error.

CHAPTER 4

EXPERIMENTAL RESULTS

The internal friction spectrum of nickel has been the subject of several investigations. The most important of these investigations have dealt with thermally-activated relaxation peaks observed in cold worked specimens or with magnetic damping phenomena. In the former category, work has been done by Berry (1962), Guberman (1963) and by Sommer and Beshers (1966). The earliest work done in the field of magnetic damping in nickel was reviewed by Bozarth (1951). Most of the work of interest that has been done since then has been reviewed by Truell et al (1969). In spite of the large volume of results, there remain many things that are not understood concerning the internal friction of nickel (see for instance Dietz, 1969).

The purpose of this work was to study experimentally several damping phenomena which occur in cold worked nickel and to compare them with the results in other metals. The most important of these were copper, tantalum and iron. This procedure has illustrated many interesting properties of nickel and has also thrown light on damping effects in the other metals mentioned.

The measurements on nickel will be presented first followed by each of the other metals individually. A discussion of the results and a comparison between the different metals will be given in Chapter 5.

A. Nickel

In order to study the effect of cold on the acoustic damping in nickel it was necessary to start with well annealed samples. The material studied was purchased from Johnson Matthey Ltd. (London, England). It was spectrographically standardized, polycrystalline metal the analysis of which showed an impurity content of less than 10 ppm initially; all the samples were annealed at 950°C for 2 hours or more in vacuo. The work of Echigoya and Hayashi (1969) has shown that the treatment would considerably reduce the dislocation density. In this condition, the room temperature internal friction Q^{-1} was very large and its value decreased only slightly at low temperatures. There were variations, from sample to sample, but a representative value of Q^{-1} at room temperature was 5×10^{-2} .

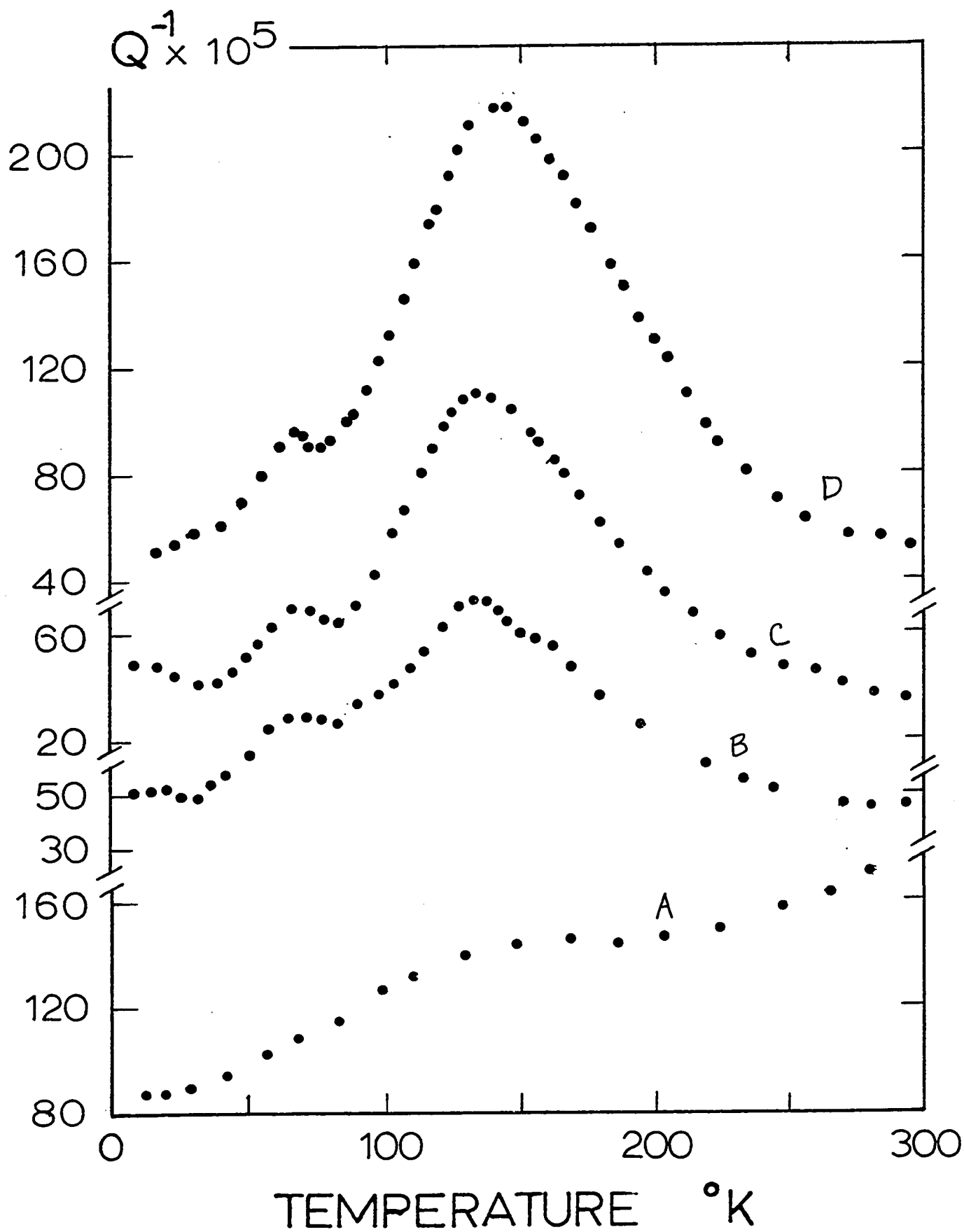
With the initial conditions given above, a disk-shaped sample was cold worked by swaging to various degrees of permanent strain. A summary of these results is presented in figure 4.1 showing the temperature dependence of Q^{-1} after each treatment. The frequency of vibrations, in all cases, was approximately 85 kHz. The percent strain quoted refers to the reduction in the thickness of the sample. The first effect of cold working was to dramatically reduce the large damping observed in the well annealed samples. The amount of cold working is increased, a large peak (to be called P_1) appears in

FIGURE 4.1

THE EFFECT OF VARIOUS AMOUNT OF COLD WORK ON THE INTERNAL FRICTION IN NICKEL. THE VIBRATION FREQUENCY IN ALL CASES WAS APPROXIMATELY 85 kHz .

- A - 1% reduction in thickness
- B - 3%
- C - 5%
- D - 12%

Note: The scale is same for each curve but has been displaced for clarity.



the Q^{-1} curve at about 140°K. This is accompanied by a smaller peak (to be called P_2) in the vicinity of 65°K. A fourth very interesting effect of cold working is the clearly visible increase in Q^{-1} as the temperature is lowered below 50°K for 3% and 5% deformations. This is in contrast to the well-annealed and the slightly cold worked cases where Q^{-1} continuously decreases as the temperature is lowered.

The anomalous rise of Q^{-1} below 50°K and the P_2 peak at 65°K have not been reported in the literature and therefore received detailed study here. The main peak, P_1 , at 140°K, was reported by Berry (1962) and by Sommer and Beshers (1966). These two papers present conflicting interpretations of this peak and the present study was designed to resolve the situation. The latter authors report the presence of another large peak in Q^{-1} curve situated near room temperature. This peak, to be called P_3 , was found to be most prominent for deformations of less than 9%. The results presented here for the pure nickel sample do not show this peak and it was therefore interesting to attempt an explanation of this effect.

i) The P_1 relaxation peak.

The most familiar aspect of the temperature dependence of Q^{-1} , the peak P_1 , will be examined first. This peak is known to be due to a thermally activated relaxation

process (Sommer and Beshers, 1966). This is substantiated by the measurements illustrated in figure 4.2. The three curves represent the dissipation coefficient Q^{-1} for three modes of nickel sample No. 1 after 12% deformation. It is seen that the temperature of maximum damping T_m increases with the frequency of measurement as required by equation (2.14). Thermally-activated relaxation should also cause an inflection in the elastic compliance as seen in figure 2.1. This behavior should be reflected in the temperature dependence of the resonant frequency of each mode (Bordoni, 1960). This inflection point is clearly visible in all three curves given in figure 4.3, although it is partially masked by the normal temperature dependence of the elastic compliance.

It was advisable to make a study of the various parameters of the relaxation since they have not been clearly delineated by past workers. This study included the determination of the activation energy, the limiting relaxation time and an analysis of the spectrum of relaxation times. It is possible to determine the activation energy and the limiting relaxation time from a graph of $k \ln f_m$ versus T_m^{-1} as indicated by equation (2.14). The results obtained in this way must, of course, be interpreted as most probable values in the event the peak is due to a spectrum of relaxation times.

FIGURE 4.2

THE TEMPERATURE DEPENDENCE OF Q^{-1} AT THREE
FREQUENCIES IN A NICKEL SAMPLE DEFORMED 12%

$$f_1 = 22.2 \text{ kHz}$$

$$f_2 = 32.4 \text{ kHz}$$

$$f_3 = 84.9 \text{ kHz}$$

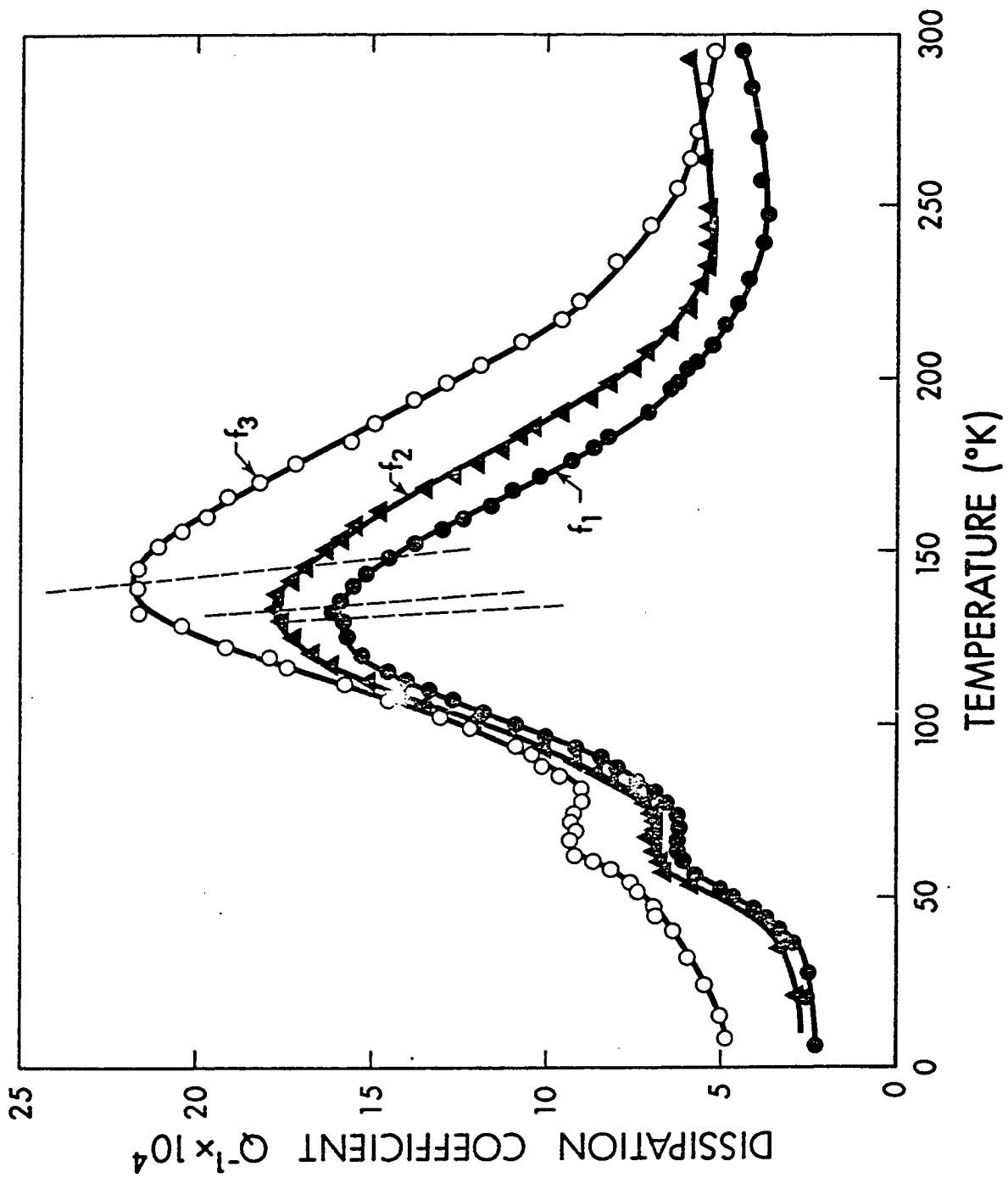
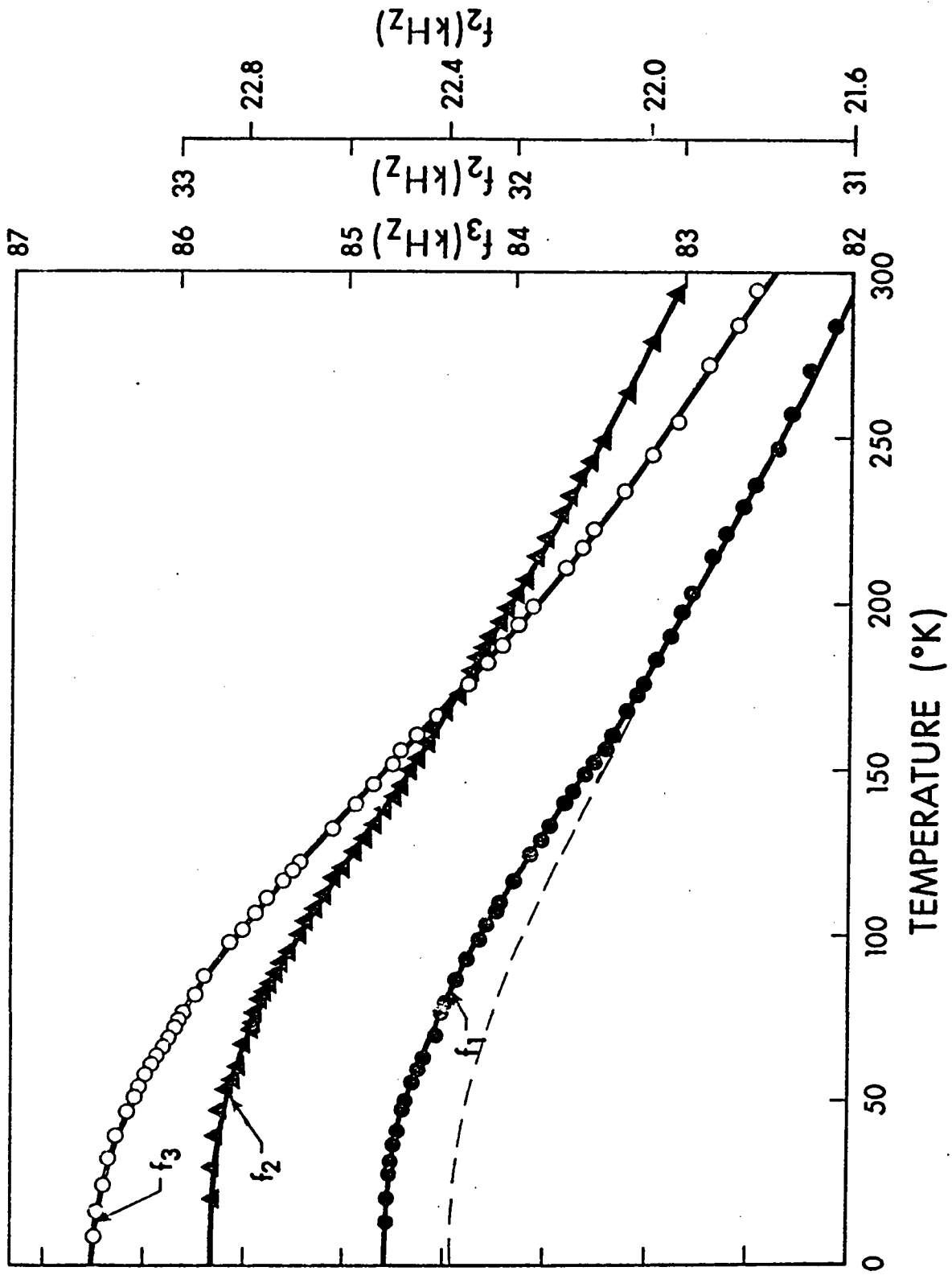


FIGURE 4.3

TEMPERATURE DEPENDENCE OF THE RESONANT FREQUENCY
 f_0 FOR THREE NORMAL MODES STUDIED IN FIGURE 4.2.



The data required to determine the activation energy of the P_1 peak are summarized in table 1. The values given for T_m were determined from the intersection of the axes of the peaks and the experimental curves (Bordoni et al, 1959). These axes are illustrated in figure 4.2 by the dashed lines. The error given is an estimate based on the precision with which the intersection point could be determined and the accuracy of the temperature measurement (given in Chapter 3). Figure 4.4 is a graph of $k \ln f_m$ versus T_m^{-1} and the result is a straight line in agreement with equation (2.14). The activation energy W is equal to the slope of this line and has a value of 0.195 ± 0.02 eV. The error given is determined from the estimated errors in T_m given in table I, and cannot be considered as absolute. The limiting relaxation time τ_0 is found from the intercept and is given by:

$$\ln \tau_0 = -27.6 \quad . \quad (4.1)$$

Since no other determination of W and τ_0 have been reported, a comparison is not possible. The values of T_m reported by Sommer and Beshers, for 30 kHz vibrations, do however fall across the line drawn in figure 4.4.

With the activation energy determined it is now possible to examine the peak for the presence of a spectrum of relaxation times. This is done by assuming the validity

TABLE I
 EXPERIMENTAL RESULTS FOR THE P₁ PEAK

f_m (kHz)	T_m (°K)	Q_m^{-1} [*]
22.2	131±0.4°K	138×10 ⁻⁵
32.4	134±0.4°K	157×10 ⁻⁵
84.9	141.5±0.4°K	186×10 ⁻⁵
119.7	146 ± 1°K	194×10 ⁻⁵

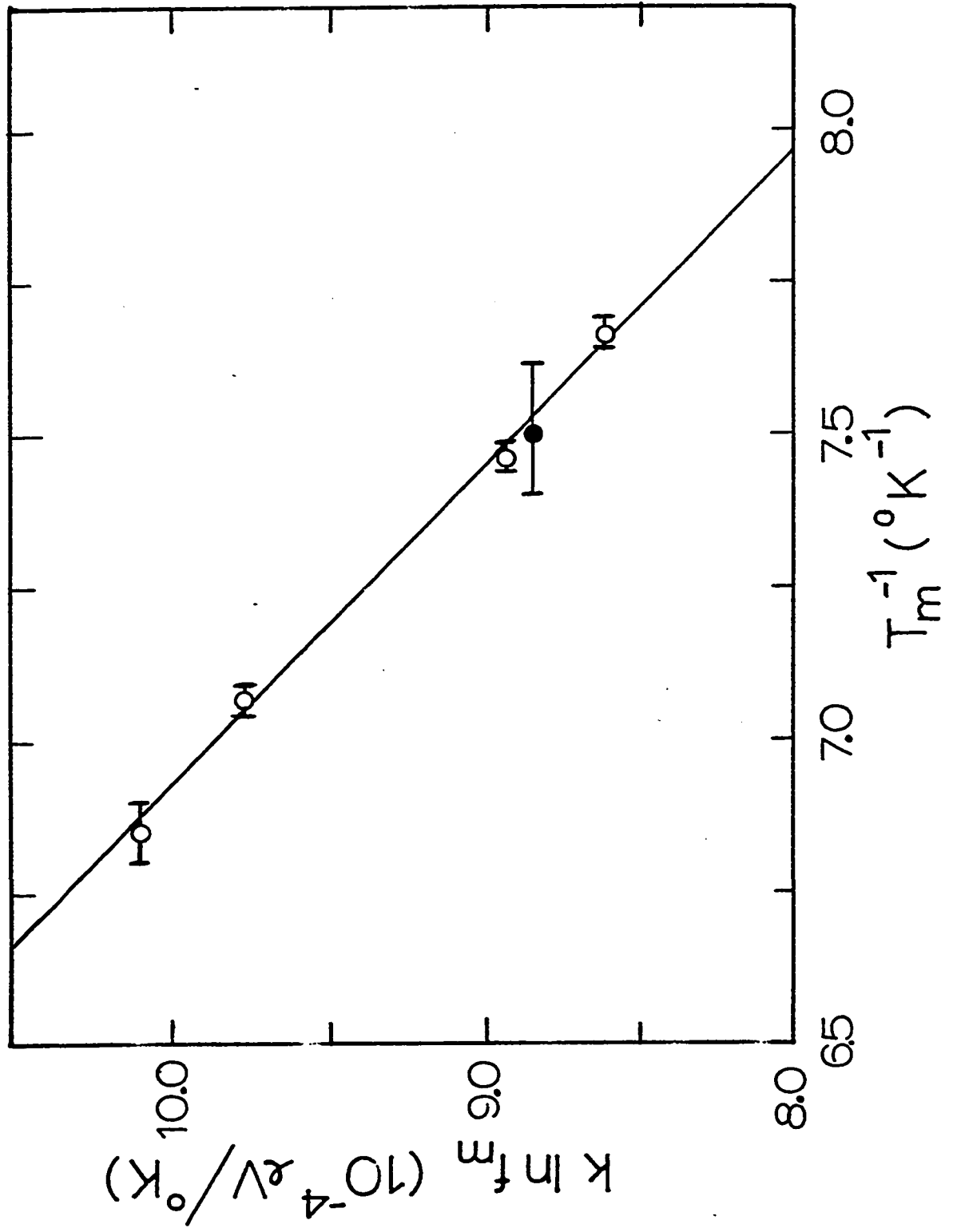
*
 Corrected for background damping.

FIGURE 4.4

ACTIVATION ENERGY PLOT FOR THE P_1 PEAK IN NICKEL

○ - this study

◐ - Sommer and Beshers (1966)

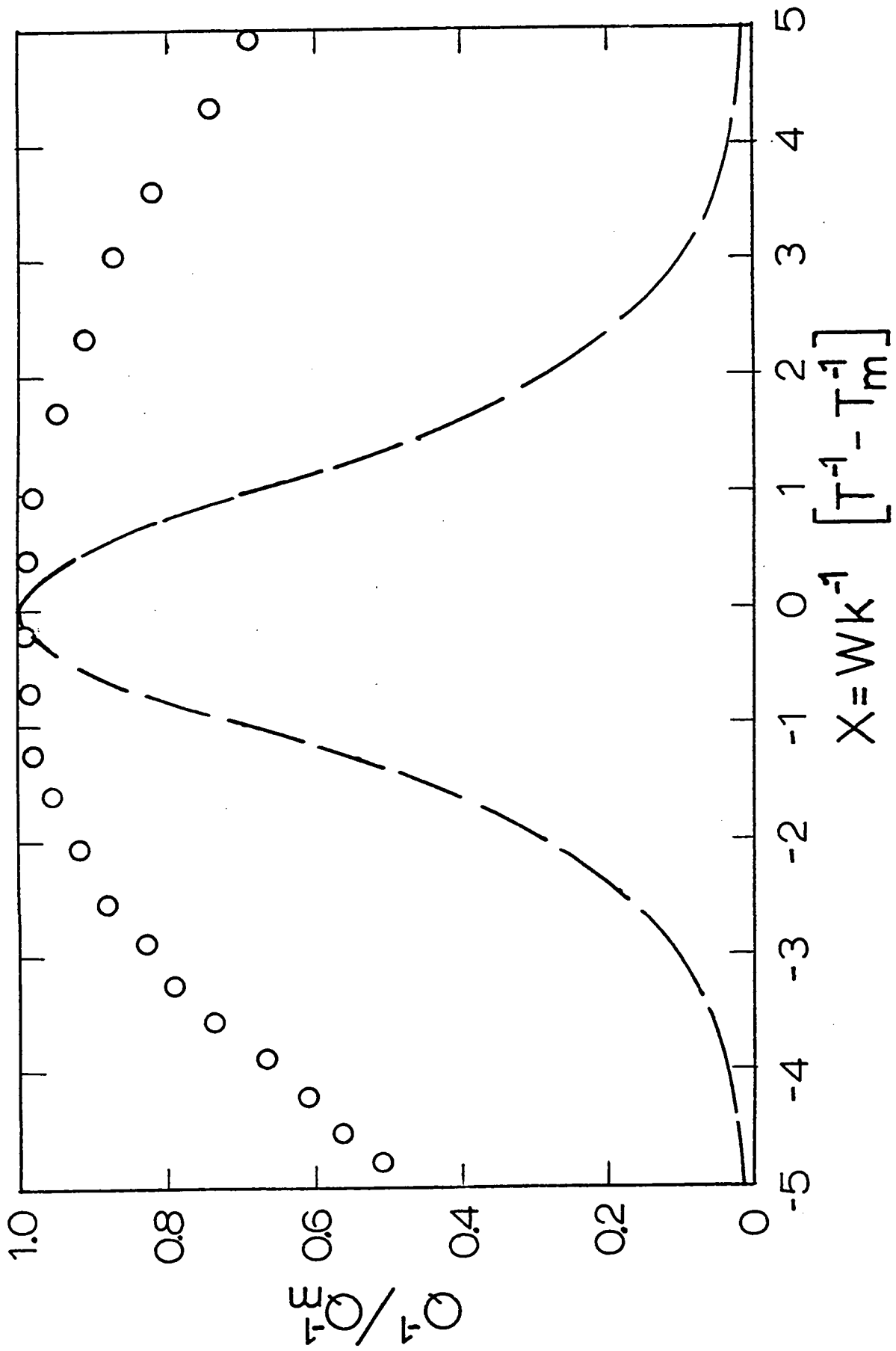


of the assumptions made for equation (2.44) and comparing a graph of Q^{-1}/Q_m^{-1} versus x with the curves in figure 2.2. This comparison is illustrated in figure 4.5 and it is obvious that the experimental curve (circles) is much wider than the prediction for a single relaxation time process. The behavior, as stated in Chapter 2, can be explained by the presence of a spectrum of relaxation times. The normal procedure in this event would be to fit the experimental curve to a curve similar to those in figure 2.2 in order to determine the half width β for the spectrum. This would not be valid in this case because the experimental curve does not have the required symmetry. The function $f_2(x, \beta)$ is an even function of the variable x (equation (2.24)), and therefore should be symmetric about $x=0$. The experimental curve illustrated in figure 4.5 does not have this symmetry. The low temperature side of the peak ($x > 0$) is significantly broader than the high temperature side.

This asymmetry could arise from three different causes. The most obvious consideration would be the subsidiary peak P_2 which might contribute to the damping on the low temperature side. This contribution however should be negligible since P_2 occurs at too low a temperature ($x \approx 17$) to affect the data illustrated in figure 4.4. Another possibility is that the relaxation strength (thus Q_m^{-1}) decreases with increasing temperature. This would render

FIGURE 4.5

THE DEPENDENCE OF Q^{-1}/Q_m^{-1} (CIRCLES) ON X FOR THE P_1 PEAK IN NICKEL COMPARED WITH THE PREDICTION FOR A PROCESS WITH A SINGLE RELAXATION TIME (DASHED LINE)



equation (2.33) invalid; however this possibility is easily discounted by the behavior in figure 4.2 where Q_m^{-1} is shown to increase with temperature. The third possibility lies with the nature of the relaxation time spectrum. If it is assumed that the peak is due to a continuous spectrum then it can be analysed using the treatment given in Chapter 2. In these terms, the asymmetry can be accounted for by a spectrum width β which is an increasing function of T^{-1} . This would be the expected behavior in the case of an activation energy spectrum. The increase in Q_m^{-1} with temperature that is found in figure 4.2, is consistent with such a spectrum. It is known from equation (2.31) that:

$$Q_m^{-1} = \frac{\delta J}{J_1} f_2(0, \beta) \quad ,$$

and since $f_2(0, \beta)$ is a decreasing function of β then Q_m^{-1} must increase with T in the event of an activation energy spectrum. The above discussion leads to the conclusion that each experimental point in figure 4.5 lies on a curve of the type in figure 2.2; however the value of β for each point is different. If it is assumed that the corrections to equation (2.33) arising from the temperature dependence of $f_2(0, \beta)$ are negligible then β may be determined by interpolation of the tabulated values of $f_2(x, \beta)/f_2(0, \beta)$ given by Berry and Nowick (1961). The method can be supplemented by solving equation (2.26) for β when its value is larger

than 7, the maximum value listed in the tables. The results of this analysis for two frequencies are illustrated in figure 4.6 in the form of β versus T^{-1} . It is seen that β increases with T^{-1} along a straight line and that the results appear to be independent of frequency. It should be pointed out that by considering these results as a first order approximation to β vs T^{-1} and applying the corrections required for the resulting temperature dependence of $f_2(0,\beta)$, a repeat of the analysis gave essentially the same straight line. The value of β determined from the width of the peak at the three frequencies is included in the diagram for comparison.

The analysis in figure 4.6 indicates that the shape of the peak is consistent with the temperature-dependent spectrum of equation (2.30). The intercept and the slope of the line yield the half width of the limiting relaxation time and activation energy spectrum respectively. The numerical values are given by:

$$\left. \begin{array}{l} \beta_0 = 1.9 \quad , \\ \text{and} \\ \beta_W = 0.056 \text{ eV.} \quad . \end{array} \right\} \quad (4.2)$$

The deviations from the straight line which occur at $T^{-1} > 10^{-2}$ are due to the presence of the subsidiary peak P_2 and are not considered to be part of the spectrum of P_1 . It is also important to recall that equation (2.30) was derived

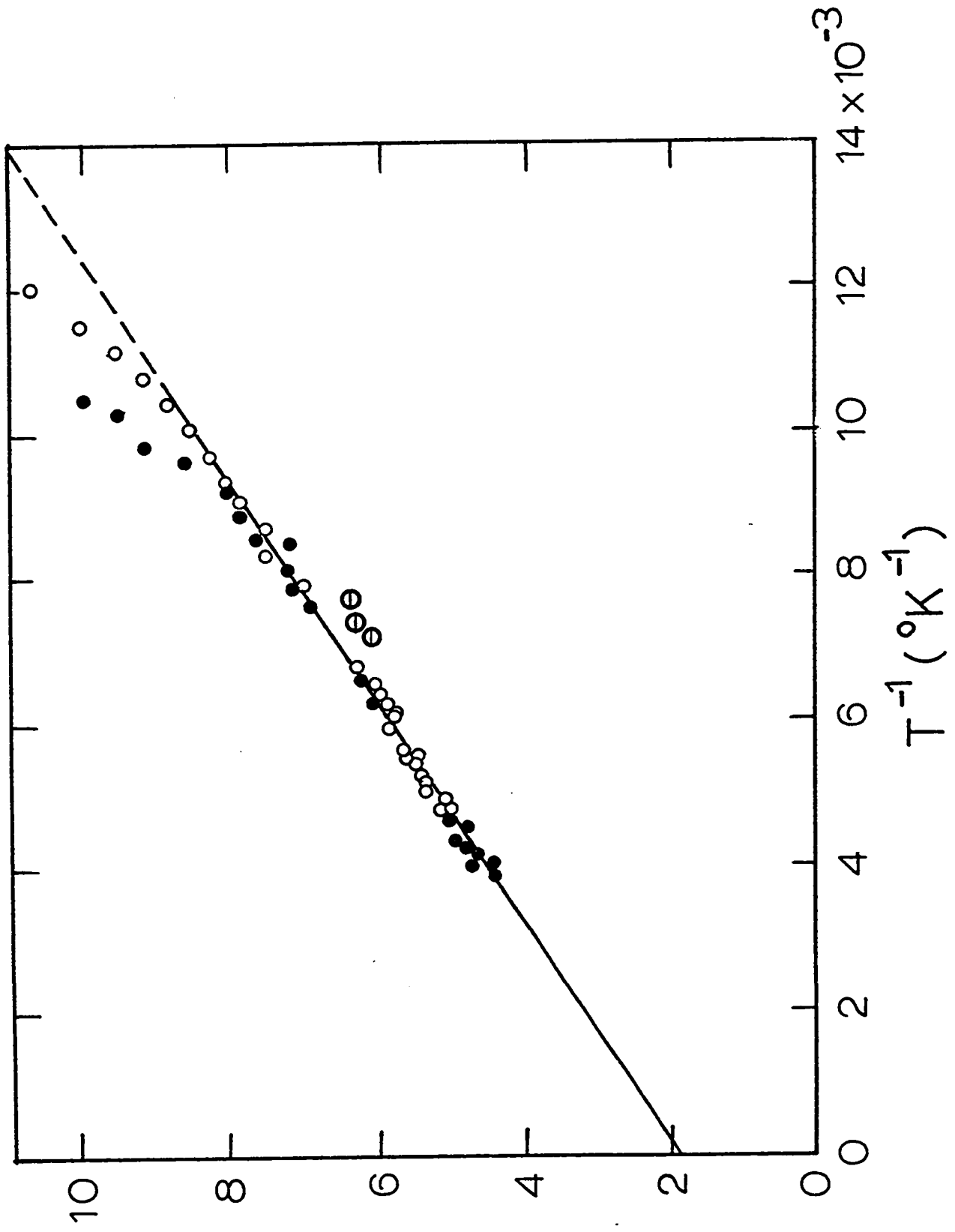
FIGURE 4.6

The variation of β vs T^{-1} determined from the shape of the P_1 peak in nickel deformed 12%.

○ - 32 kHz

● - 85 kHz

The symbols θ represent β determined from the width of the peak at the three frequencies measured.



with the assumption that β_o and β_w were not linearly independent of one another.

The preceding discussion has been based on the measurement of the P_1 peak in a sample deformed 12%. It is of interest to know whether the results are dependent on the amount of cold working or on other parameters such as impurity content. Recalling the measurements illustrated in figure 4.1 it was found that Q_m^{-1} and the peak temperature T_m increased with the amount of cold working. This effect was observed to saturate for the larger deformations. The opposite behavior was observed when the sample was annealed, i.e. Q_m^{-1} and T_m decreased. Due to the limited frequency range it was not possible to determine whether or not the changes in T_m were associated with a change in the limiting relaxation time or in the activation energy. The changes in activation energy, if any, were too small to be detected and therefore shall be neglected in the analysis that follows.

The effects of cold working on the shape of the peak were also studied. For small deformations such as curve A and B in figure 4.1 the peak is not developed enough to perform an analysis similar to that of figure 4.6. The errors in estimating the background would be too large to make the analysis meaningful. The structure observed on the P_1 peak in curve B would also interfere with this

analysis. It is noteworthy that the P_1 peak was found to be poorly formed for several samples which were deformed at approximately 3% as for curve B. This could thus appear to be an important feature of the curve. For larger amounts of cold work, the peak was well defined and smooth.

The analysis of figure 4.6 was repeated on the same sample (12% deformation) after an annealing treatment at 200°C for 10 minutes. This was followed by a further 25% deformation and another analysis of β versus T^{-1} . In figure 4.7, the results are compared with the 12% case represented by the solid line. There appears to be no significant change in the spectrum parameter β , at least for these larger amounts of cold work. The same result was obtained with another sample cold worked to 15% and then electrolytically charged with hydrogen. The effect of dissolved hydrogen was found to be similar to that of annealing the sample, i.e. a lowering of both T_m and Q_m^{-1} .

ii) The subsidiary peak P_2

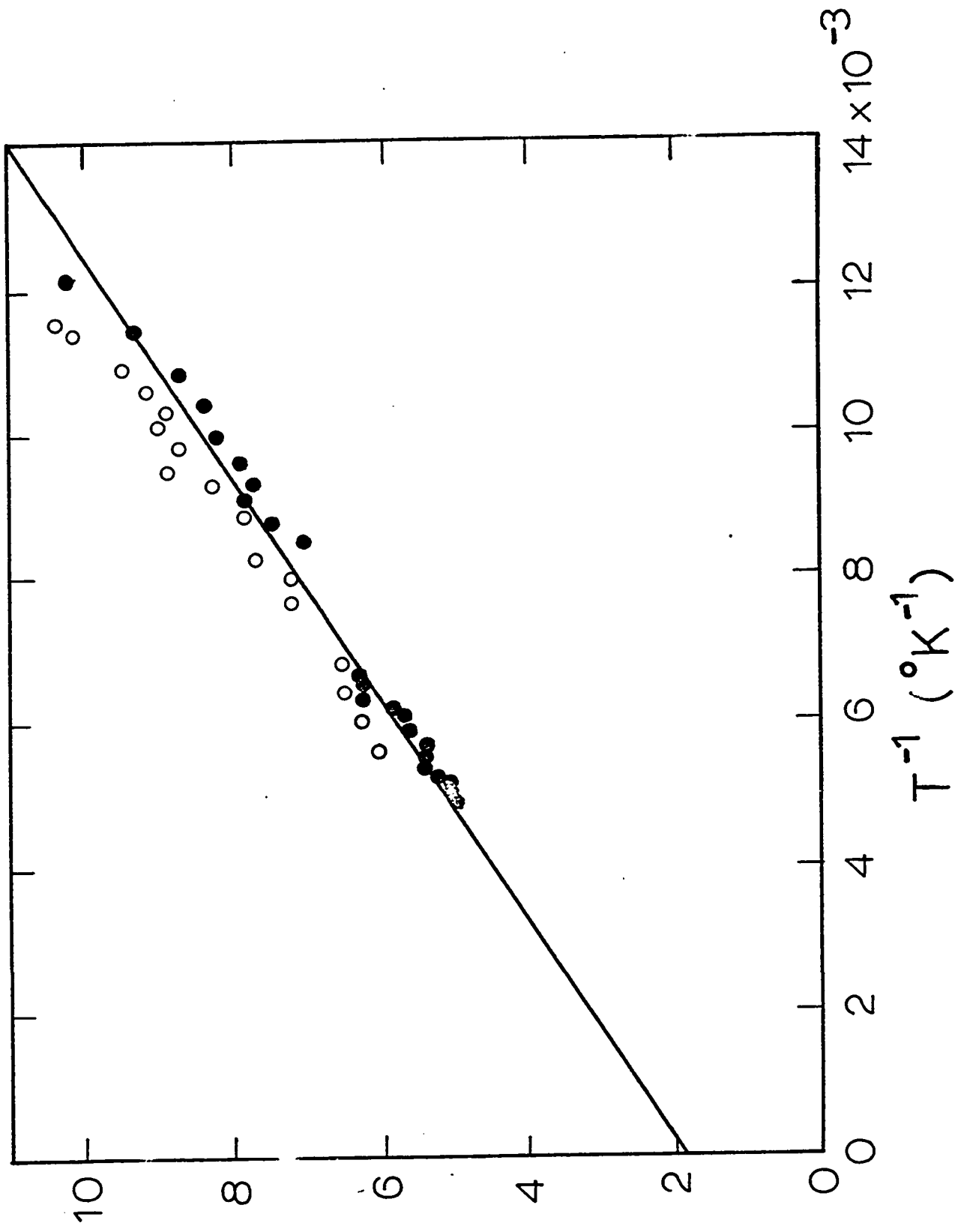
In order to study the damping peak P_2 it is necessary to separate it from the general temperature dependence of Q^{-1} . This is easily done by calculating the contribution to Q^{-1} arising from the main peak P_1 and subtracting it from the total damping. In the temperature range near P_2 , the contribution from P_1 will be given by the asymptotic

FIGURE 4.7

COMPARISON OF β VERSUS T^{-1} FOR THE P_1 PEAK AFTER
 VARIOUS TREATMENTS OF A NICKEL SAMPLE

Symbol	Treatment	* T_m	Q_m^{-1}
—	12% deformation (figure 4.6)	134°K	157×10 ⁻⁵
●	Subsequent anneal at 200°C for 10 minutes	128°K	100×10 ⁻⁵
⊙	Further 25% deformation	137°K	180×10 ⁻⁵

* Values corrected to correspond to a frequency
 of 32 kHz .



form of $f_2(x, \beta)$, that is, equation (2.26). The temperature dependence of β is determined from figure 4.6, by extrapolation of the straight line to low temperatures. The P_1 peak has been subtracted from the three curves in figure 4.2 in this way and the remainder is illustrated in figure 4.8. The result can only be considered as approximate since the relatively small errors in determining the P_1 peak become important when compared to the height of the P_2 peak. It should also be noted that the background damping is of about the same magnitude as the height of the P_2 peak and this contributes considerably to its uncertainty. For these reasons complete analysis, similar to that done for P_1 , cannot be carried out; however it is possible to estimate some of the primary features of the relaxation from the summary in table II.

The frequency dependence of T_m , the temperature of maximum damping, is illustrated in figure 4.9. The slope of the line indicates an activation energy of 0.140 ± 0.035 eV for this relaxation. The intercept is given by $\ln \tau_0 = -25$. It is noteworthy that, although the activation energy of the P_2 peak is smaller than that of P_1 , the limiting relaxation times are approximately the same. The width of the peak indicates that the peak is due to a spectrum of relaxation times. By assuming that the Gaussian distribution can be used to describe this spectrum and then comparing with $\Delta_x(\beta)$ in figure 2.3 it was found

FIGURE 4.8

THE P_2 PEAK IN NICKEL DEFORMED 12%. THE CURVES
CORRESPOND TO THREE FREQUENCIES AS IN FIGURE 4.2.

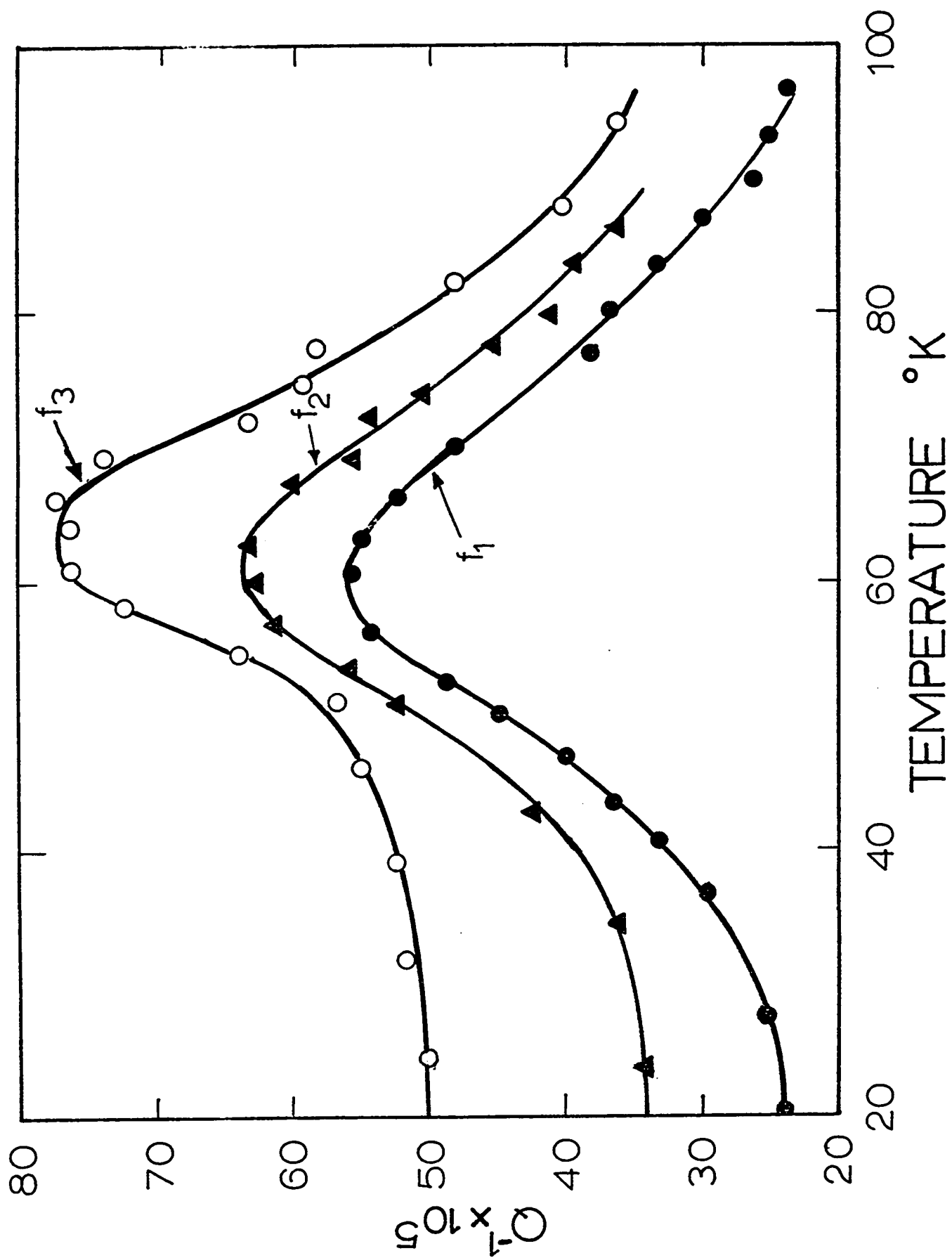


TABLE II
EXPERIMENTAL RESULTS FOR THE P₂ PEAK

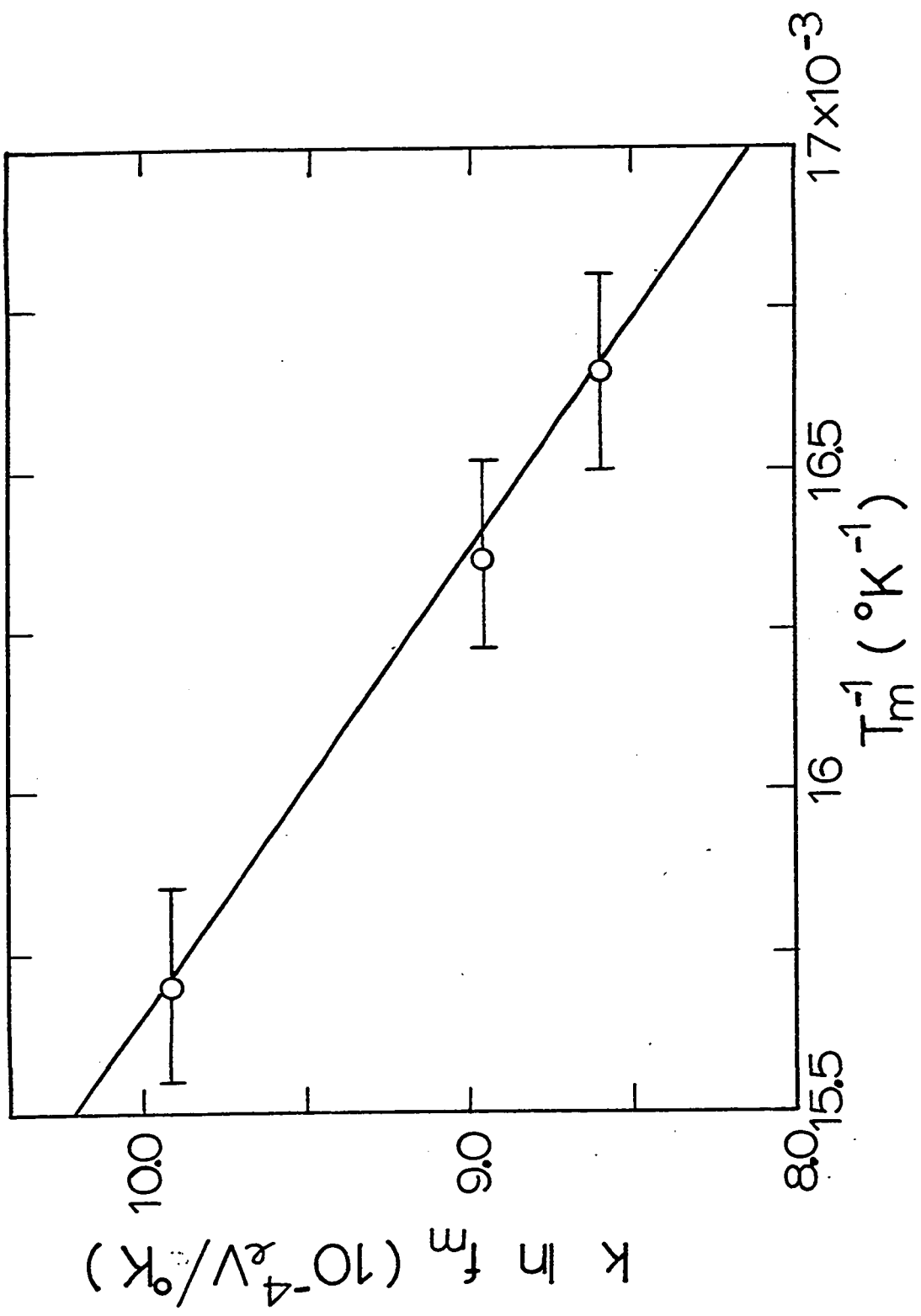
f_m (kHz)	T_m (°K)	Q_m^{-1}
22.3	60.0±0.6	36×10 ⁻⁵
32.7	61.2±0.6	40×10 ⁻⁵
86.0	63.5±0.6	50×10 ⁻⁵

FIGURE 4.9

ACTIVATION ENERGY PLOT FOR THE PEAK IN
NICKEL INDICATING:

$$W = 0.140 \pm 0.035 \text{ eV}$$

$$\ln \tau_0 = -25 \pm 2$$



that β is approximately 7 at temperatures near T_m (60-65°K). The temperature dependence of β , as mentioned earlier, could not be determined. An investigation of the dependence of Q_m^{-1} and T_m on the amount of cold working, annealing treatments and hydrogen charging showed that P_2 is similar to P_1 in these respects.

As mentioned earlier, Berry (1962) identified the P_1 peak with the Bordoni peak in copper but this interpretation has been disputed by Sommer and Beshers (1966) who interpreted a peak (P_3) observed near 250°K (30 kHz) as the Bordoni peak. In view of this, it would be unwise to attempt a comparison between copper and nickel without more information on the P_3 peak.

iii) The P_3 relaxation peak

It has been shown in figure 4.1 that the temperature dependence of Q^{-1} for relatively pure cold worked nickel does not exhibit the P_3 peak reported by Sommer and Beshers (to be noted SB). It was therefore necessary to determine what condition was required in the metal in order to observe it. The samples, on which the SB measurements were made, were reported to contain 5 ppm dissolved hydrogen. This section will present experimental results which indicate that the P_3 peak is not observed in the cold worked state alone but requires the presence of this hydrogen.

The sample used in the study was disk shaped and deformed to 8% reduction in thickness by swaging. An electrolytic charging technique (Haywood, 1969) was then used to introduced H_2 into the metal, using a 0.1N solution of H_2SO_4 as electrolyte. The temperature dependence of Q^{-1} was measured before the charging process and at several stages during the charging. The results are illustrated in figure 4.10. In curve A it is seen that the temperature dependence of Q^{-1} before charging is typical of the behavior shown in figure 4.1. The effects of the first charging are shown by curve B. Both the P_1 and P_2 peaks were considerably reduced, as mentioned earlier. This was accompanied by the appearance of a third peak near $230^\circ K$. In curve C, which was measured after a second charging with H_2 , the P_1 and P_2 relaxations are almost completely quenched, while the new peak has increased to a height comparable with the P_1 peak in the pure material.

This new peak can be identified with the P_3 peak reported by SB, since it occurs within the expected temperature range for the measuring frequency (16 kHz). In order to verify this identification, a study of the effects of various amounts of cold working on H_2 -charged nickel was carried out. The results are summarized in figure 4.11. These results demonstrate that the height of the peak Q_m^{-1} initially increases with the amount of cold working (curves A and B). The P_1 and P_2 relaxation peaks,

FIGURE 4.10

THE EFFECT OF HYDROGEN CHARGING ON THE Q^{-1} VERSUS T
CURVE IN COLD WORKED NICKEL (FREQUENCY 16 kHz).

A - before charging

B - after charging with H₂

C - after further charging

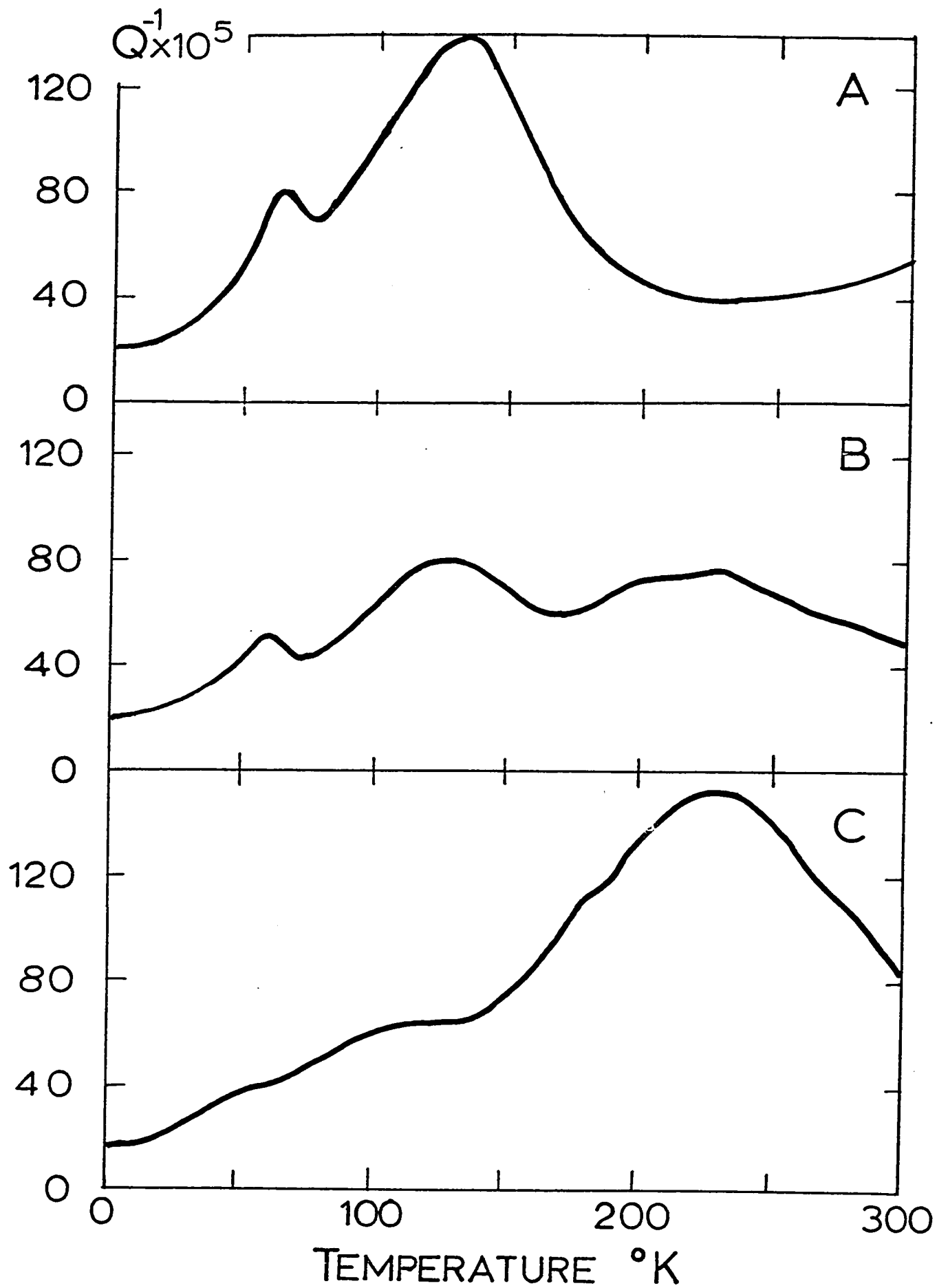


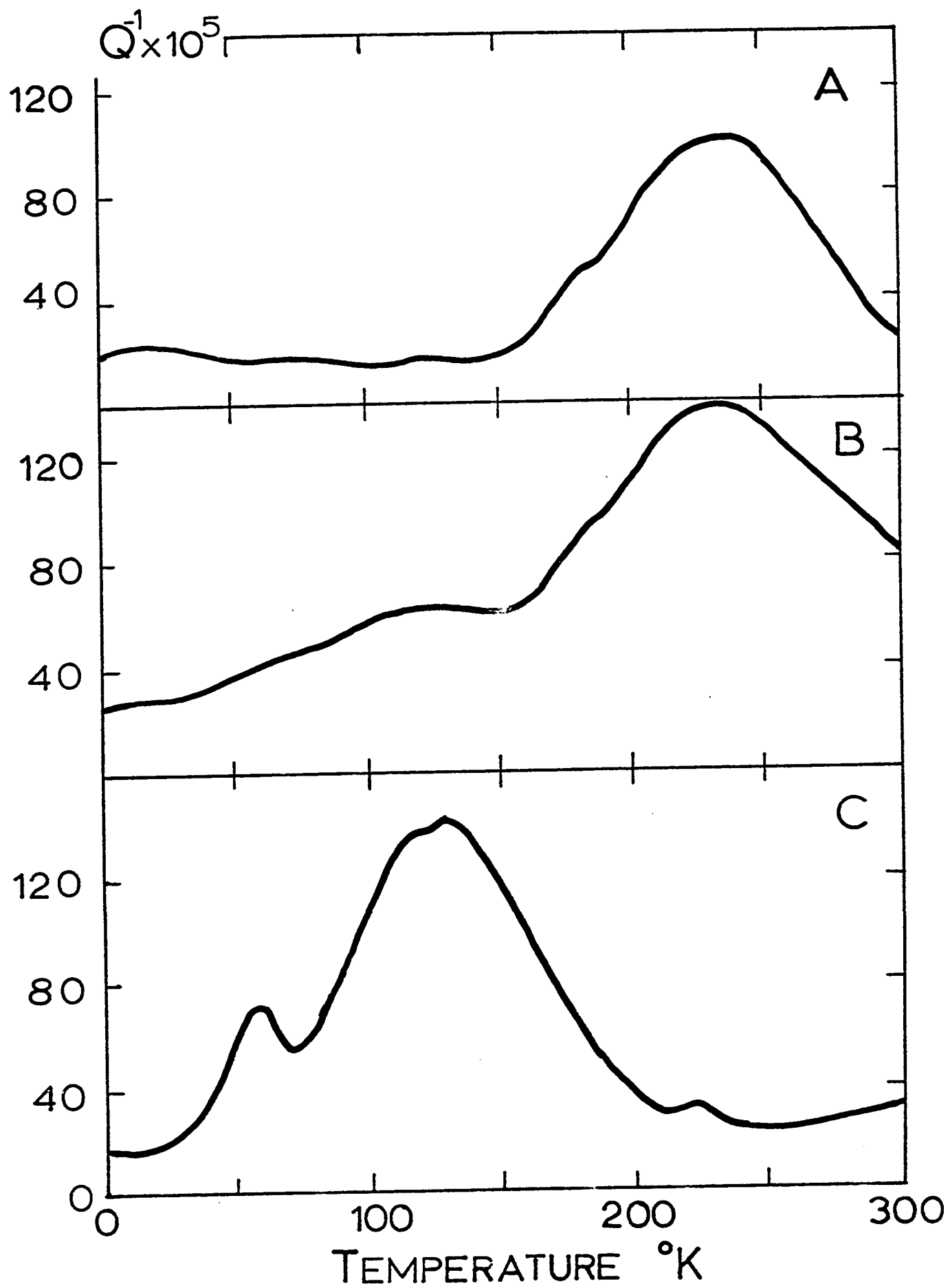
FIGURE 4.11

THE EFFECT OF INCREASING COLD WORK ON THE
 P_3 PEAK IN NICKEL ($f \approx 20 \text{ kHz}$)

A - 2% deformation

B - 7%

C - 15%



under these conditions, are very small compared to the high temperature peak. When the amount of deformation reaches 15% (curve C) it is seen that the value of Q_m^{-1} for the third peak has dropped considerably and the P_1 and P_2 peaks dominate the Q^{-1} versus T curve. These results are in agreement with those reported by SB for the P_3 peak. As shown in figure 4.11, the temperature T_m of the H_2 -induced peak decreases with increasing amount of cold work. This is also in agreement with the SB observations on the P_3 peak. The above points strongly support the identification of the P_3 peak with the hydrogen-induced peak observed here.

An analysis of the P_3 relaxation peak, similar to that carried out for the P_1 peak would not be practical for several reasons. An accurate value of the activation energy could not be obtained although a consolidation of the results from the SB study, the measurement by Berry (1962) and the present work indicate that the activation energy is larger than the P_1 activation energy and of the order of 0.5 eV. No reasonable estimate could be made of the limiting relaxation time.

Due to the uncertainty in the activation energy of P_3 , an analysis of the spectrum of relaxation times is impossible. This difficulty is compounded by the structure in the curve, particularly on the low temperature side of T_m . This structure indicates that the peak

may be formed by two or more overlapping peaks which cannot be taken into account in the analysis. The width of the peak does indicate the presence of a spectrum of relaxation times and the SB results indicate that the width of this spectrum increases markedly with cold working.

It is clear that the P_3 peak in nickel requires both the presence of H_2 and cold working to be observed. This is in marked contrast to both the P_1 peak and the Bordoni peak in copper which are hindered by impurities (Caswell, 1958). The SB identification of the P_3 peak with the Bordoni relaxation mechanism is probably incorrect. The P_3 peak more closely resembles the hydrogen-cold-work peaks observed in tantalum and niobium by Mazzolai and Nuovo (1969). (See Section C of this Chapter.)

iv) Cold working and magnetic damping

The completion of this experimental study on sound absorption in cold worked nickel will consist of a limited discussion of magnetic damping. The large volume of work done on the effect of cold work on magnetic damping, has been reviewed by Brátina (1966). A detailed study of the many phenomena observed would be a very large undertaking; this discussion will therefore be restricted to a single effect observed in nickel during the course of this work which has not been reported in the literature.

It was pointed out for figure 4.1 that in the region of 5% deformation, the temperature dependence of Q^{-1} showed an anomalous rise below 50°K . Although it is not visible in figure 4.1 at 12% deformation, this low temperature damping effect is in fact present. An examination of figure 4.8 shows that the background damping on the low temperature side of the P_2 peak is considerably larger than on the high temperature side. It is also seen that this effect increases with frequency.

In order to determine if this damping effect was caused by the motion of magnetic domain walls in the sample, Q^{-1} was measured with a 1 KOe magnetic field applied along the plane of the disk shaped sample. It is clear that in the magnetically saturated state, this type of damping should not occur because of the absence of domain walls. These measurements are illustrated in figure 4.12 in the form of Q^{-1} vs temperature in the magnetized and unmagnetized states. The difference between these two measurements, which is illustrated by the heavy line, is attributed to magnetic damping. The increase in this damping at low temperatures appears to be present only at intermediate levels of cold work (3% to 12%), that is, it could not be resolved from the Q^{-1} versus T curve of annealed or heavily cold worked samples. This is consistent with the measurements reported by Truell et al (1969) for annealed nickel, in which the magnetic

FIGURE 4.12

THE EFFECT OF MAGNETIC SATURATION ON Q^{-1} AT
LOW TEMPERATURES IN LIGHTLY COLD WORKED NICKEL.

○ — H = 0

● — H = 1 KOe

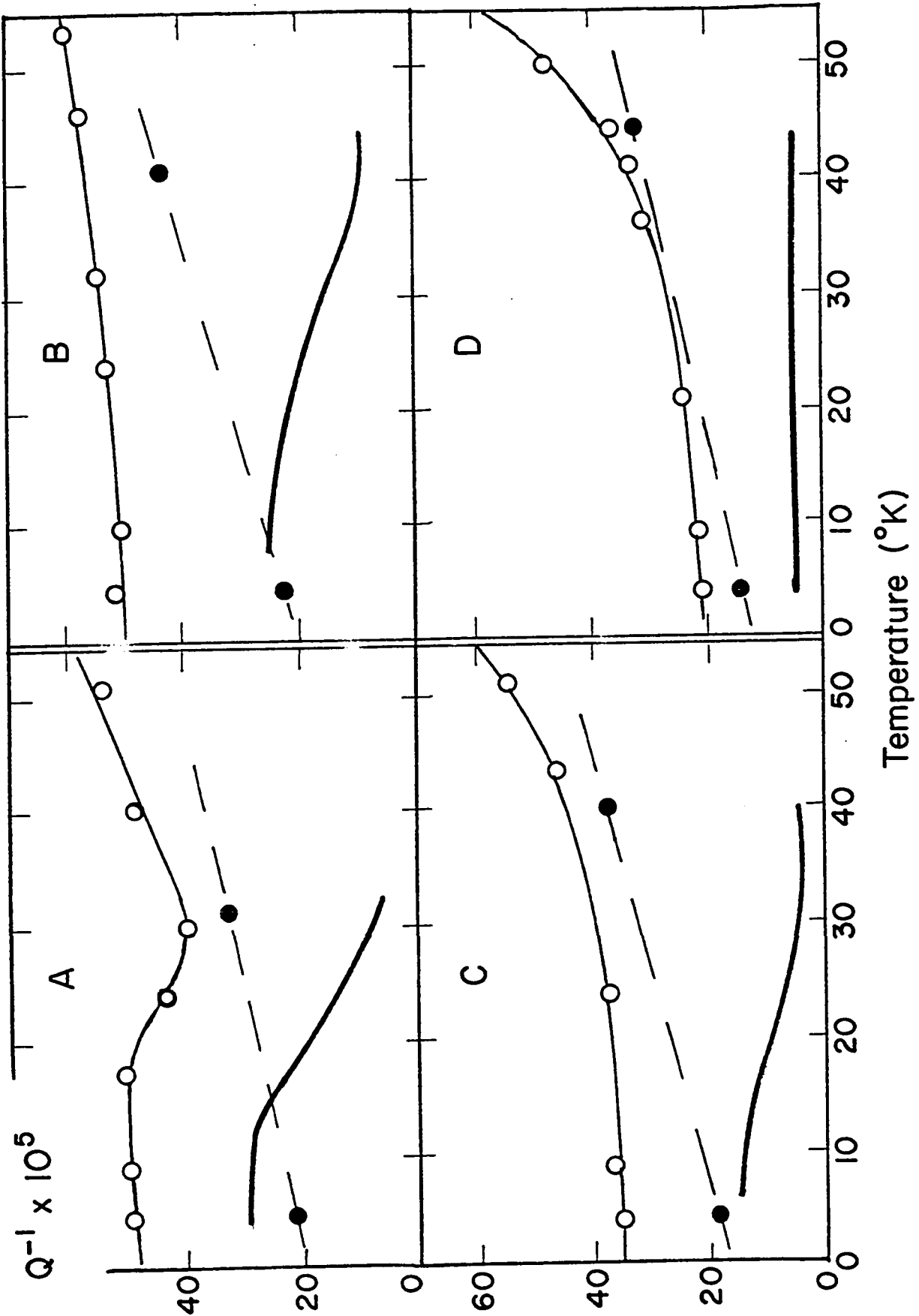
— — difference between two results

A - 5% deformation at 85 kHz

B - 12% deformation at 85 kHz

C - 12% deformation at 34 kHz

D - 12% deformation at 22 kHz



damping was at a minimum and essentially constant below 100°K .

In the course of this work, measurements of Q^{-1} versus temperature were made on a nickel sample obtained from the stock used by Schiller (1955) in his investigation of magnetic damping at room temperature. The results of the measurements on this sample in the "as received" condition are illustrated in figure 4.13. The low temperature magnetic damping was clearly visible in this case because of the absence of the P_1 and P_2 peaks. The mechanical history or the source of the material could not be determined; however an electron microprobe analysis indicated that it contained approximately 0.1% impurity. The sample was probably in a cold worked state since annealing in vacuo brought the Q^{-1} vs T curve into line with the results in the pure annealed samples. It should be noted that these results verify the frequency dependence, inferred from figure 4.12. The magnetic field dependence of Q^{-1} was measured in the Schiller sample at 4.2°K . These results are presented in figure 4.14 and it is seen that the low temperature effect is considerably reduced at fields comparable to the saturation field of nickel. The resonant frequency of the sample is also illustrated showing the effect of the magnetic damping on the elastic compliance.

FIGURE 4.13

TEMPERATURE DEPENDENCE OF Q^{-1} IN A
NICKEL SAMPLE USED BY SCHILLER (1955)

● — 26 kHz
○ — 90 kHz

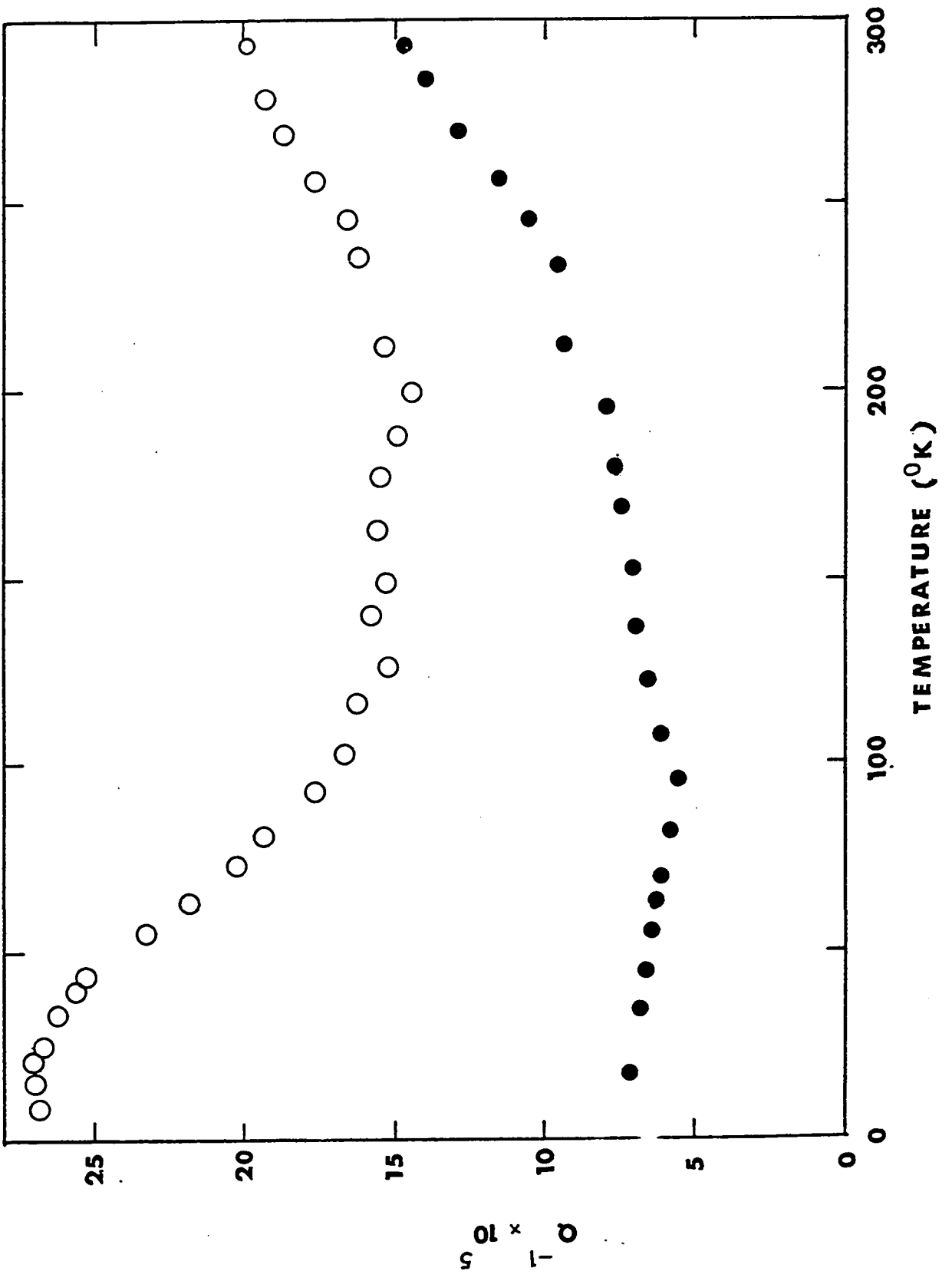
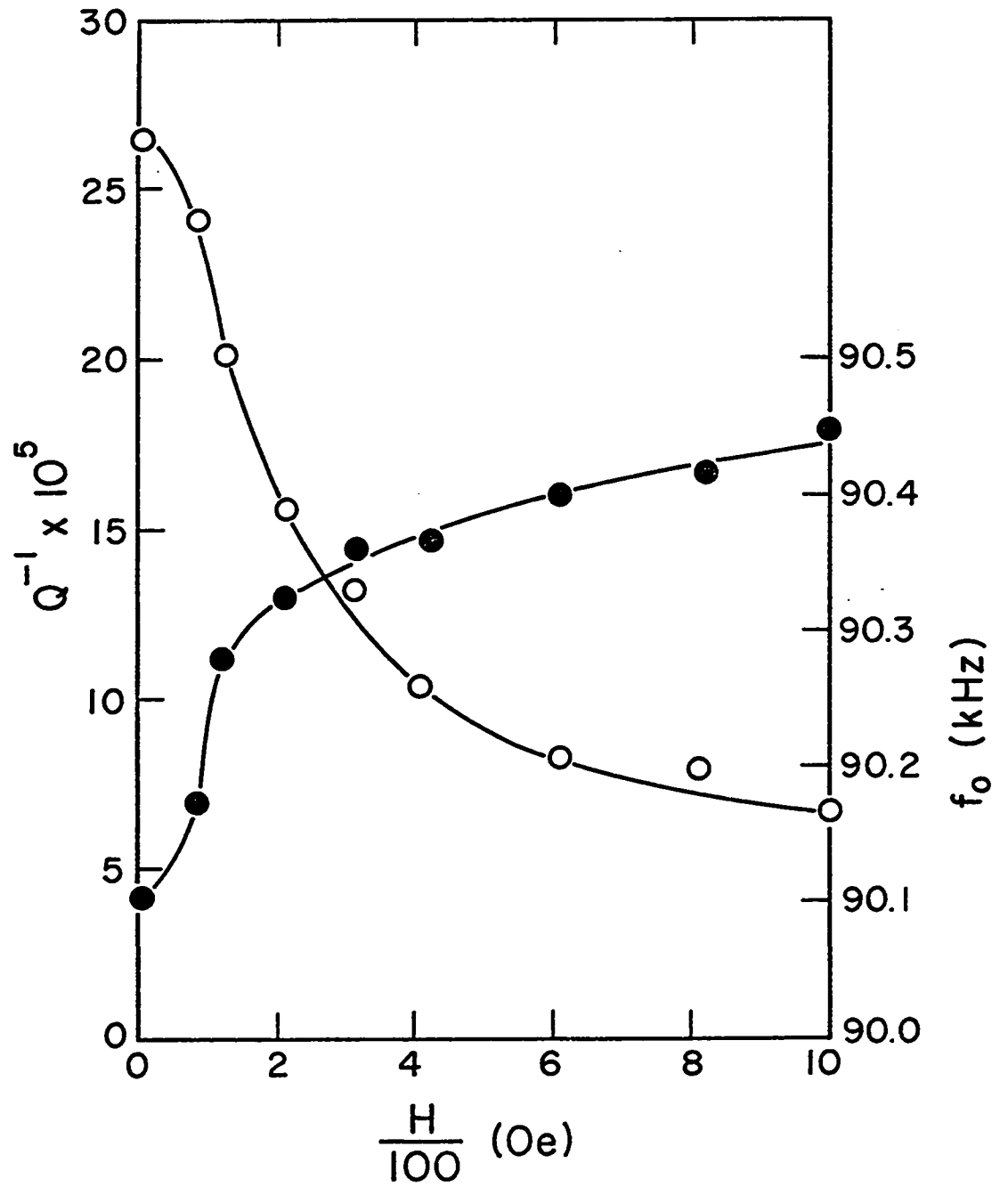


FIGURE 4.14

MAGNETIC FIELD DEPENDENCE OF Q^{-1} AND THE
RESONANT FREQUENCY f_0 OF THE SCHILLER SAMPLE
AT 4.2°K

○ — Q^{-1}

● — f_0



The low temperature magnetic damping observed here closely resembles the so called "plateau region" in the temperature dependence of Q^{-1} in iron, which was first observed by Bruner (1959) and Heller (1961). Investigations of this plateau have been reported by Vienneau (1968) and by Verdini and Vienneau (1968 a). (See Section D of this Chapter, dealing with magnetic damping in iron.)

B. Copper

The peak in the temperature dependence of Q^{-1} for cold worked copper was first observed by Bordoni (1949, 1954). Extensive studies of the Bordoni peak have since been carried out by numerous investigators and presently many reviews of these works are available; for example, Bordoni (1960), Niblett (1966), and Truell et al (1969).

The experimentally observed properties of the Bordoni peak, as listed by Truell et al are:

(1) The peak occurs in both single crystals and polycrystalline specimens, after slight plastic deformation.

(2) The height of the peak increases, and the peak maximum shifts slightly to higher temperatures with increasing amounts of plastic deformation; these effects tend to saturate at a few percent plastic strain.

(3) The peak disappears upon annealing at elevated temperature.

(4) The height and temperature of the peak are independent of wave amplitude.

(5) Impurities reduce the height of the peak and shift it to slightly lower temperatures.

(6) The main peak is accompanied by a subsidiary peak observed at lower temperatures (called Niblett-Wilks peak).

(7) The peak originates from a thermally activated relaxation process and exhibits, in a general way, an exponential temperature dependence of the relaxation time according to an Arrhenius-type equation. The activation energy is found to be 0.122 eV with $\ln \tau_0 = -28.5$ (Bordoni et al, 1959).

These characteristics are very similar to those observed for the P_1 peak in nickel. The only problem with the above comparison lies with the spectrum of relaxation times. It has been shown here that the shape of the P_1 peak is consistent with a spectrum of relaxation times the temperature dependence of which indicates that it is the result of a distribution of activation energies and a distribution of limiting relaxation times. It was also indicated that these two distributions are not independent of one another.

It has long been known that the Bordoni peak involves a spectrum of relaxation times (Bordoni et al, 1959), but the nature of this spectrum is still in dispute.

Bordoni et al have argued that their experimental results indicate the spectrum arises from a distribution of limiting relaxation times with a single activation energy. The argument used was based on the fact that the observed width of the peak did not vary significantly with T_m , the temperature of maximum damping. Niblett (1960) analysed the same set of data in essentially the same manner and arrived at the opposite result, a spectrum of activation energies with a single limiting relaxation time. The reason for the ambiguous result lies in the fact that the data used was taken from many different samples with various histories and the resulting scatter in the peak widths does not allow an unambiguous interpretation. At the same time, Thompson and Holmes (1959) observed several inflection points in the curve of resonant frequency versus temperature for lightly deformed copper samples. On this basis, they proposed a discrete spectrum with seven different activation energies for the Bordoni peak. Except for the Niblett-Wilks peak, there has been no evidence reported of this in the Q^{-1} versus temperature curve. Caswell (1958), Paré (1960) and more recently Hobart (1969) have shown that the Bordoni peak in copper can be fitted to a relaxation peak caused by a Gaussian distribution of activation energies and a single limiting relaxation time. These three studies however do not seem to take into account the subsidiary peak which would

significantly alter the peak shape on the low temperature side.

In order to resolve the problem, measurements were made of the Bordoni peak in copper and the analysis used in the study of the spectrum of the P_1 peak, was applied to them. The samples used in the measurements were polycrystalline OFHC copper disks which were machined from stock obtained from Anaconda American Brass Ltd. The samples were annealed at 700°C in vacuo for 5 hours before cold working. The cold working was produced by cross rolling in small stages.

The temperature dependence of Q^{-1} was measured for two modes of a copper sample rolled to 25% reduction in thickness. These data are presented in figure 4.15; the Bordoni peak appears at approximately 85°K while the subsidiary peak, called the Niblett-Wilks peak, is visible in the vicinity of 35°K .

i) The Bordoni peak

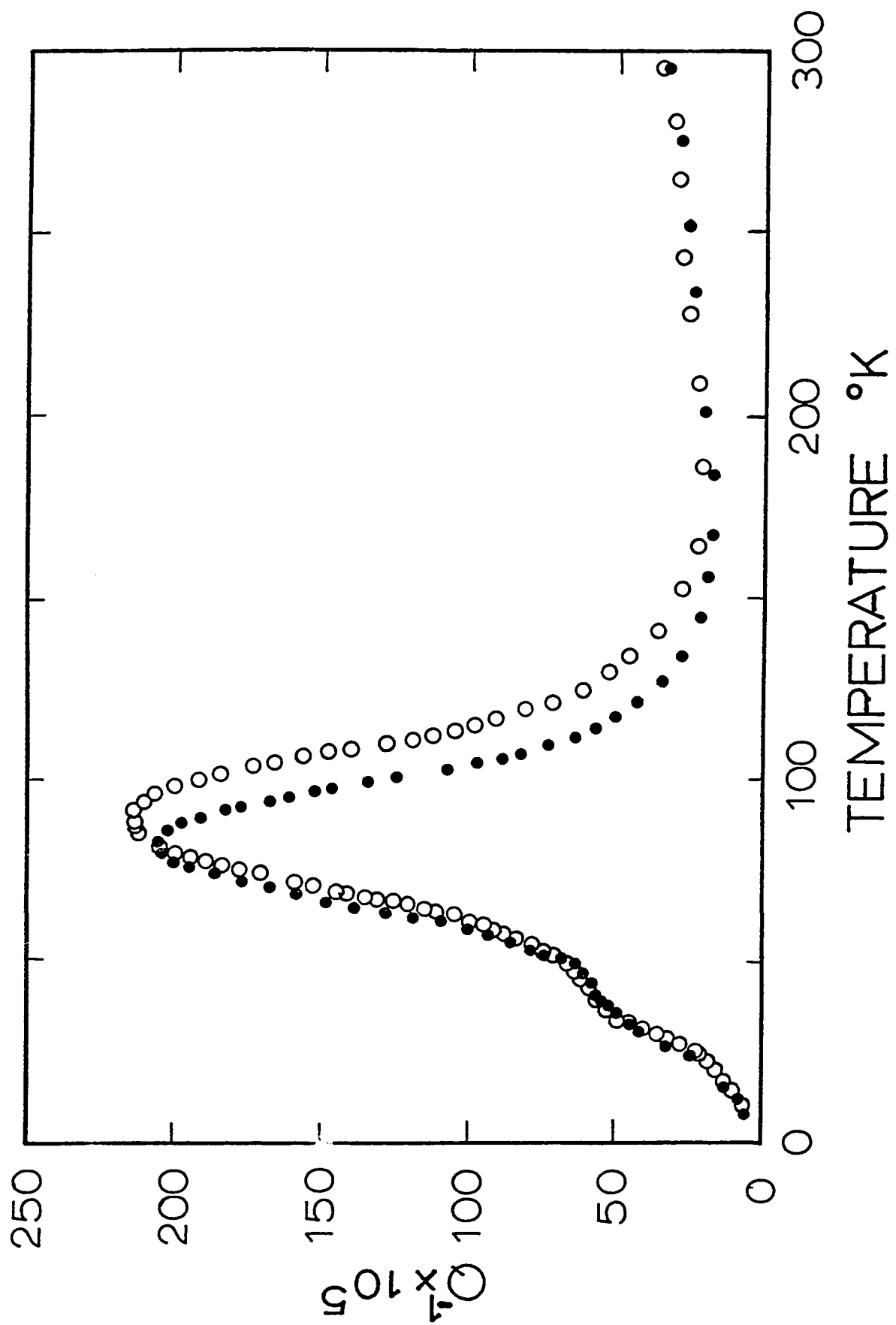
From these results, it is seen that the Bordoni peak is a thermally activated relaxation peak. The peak temperature T_m for each frequency has been compared with the measurements of Bordoni et al (1959). It is found that the activation energy of 0.122 eV deduced by those authors is applicable to the sample measured here. The temperature dependence of the spectrum parameter β was deduced just as

FIGURE 4.15

TEMPERATURE DEPENDENCE OF Q^{-1} FOR TWO MODES OF A
COPPER SAMPLE DEFORMED 25%

● - 19.1 kHz

○ - 71.5 kHz



it was for the P_1 peak in nickel (Section A). The result of this analysis is illustrated in figure 4.16. The behavior is seen to be of the form described by equation (2.38). The zero intercept of the line drawn through the data indicates that the Bordoni relaxation effect is characterized by a single limiting relaxation time. From the slope of the line, the activation energy spectrum parameter was found to be:

$$\beta_W = 0.035 \text{ eV} \quad . \quad (4.3)$$

It is noteworthy that the variation in the width of the peak with temperature, produced by an activation energy spectrum described by equation (4.9), falls within the scatter observed by Bordoni et al (1959). It can be concluded that the activation energy spectrum determined above is consistent with most of the available data on the Bordoni peak.

We see, from the inset in figure 4.16, that the relaxation spectrum is the same for a copper sample rolled to 10% deformation as for the sample with 25% deformation.

ii) The Niblett-Wilks peak

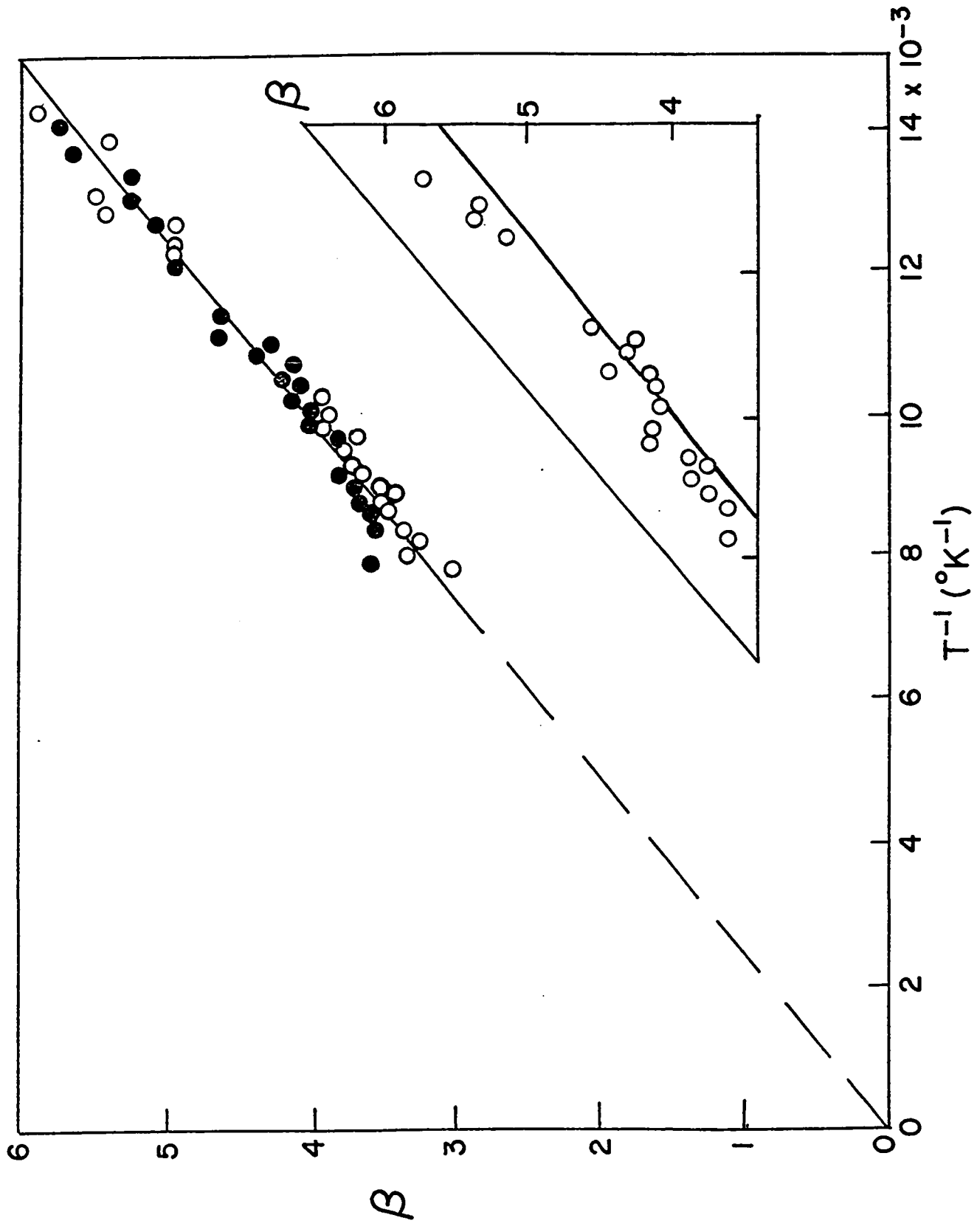
In order to study the Niblett-Wilks peak it is necessary to separate it from the Bordoni peak. This can be done in the same way that the P_2 peak was separated from the P_1 peak in nickel. The result of this procedure,

FIGURE 4.16

Temperature dependence of the spectrum width β deduces from the shape of the Bordoni peak in figure 4.15. The inset compares the result of a similar analysis (circles), for a sample rolled to 10% deformation, with the main curve (solid line).

0 - 19 kHz

0 - 71.5 kHz



carried out for the two curves in figure 4.15, is presented in figure 4.17. The most interesting feature of this curve is that the Niblett-Wilks peak is shown to consist of at least three distinct peaks (indicated by arrows), all of which appear to be thermally activated. This is the first concrete evidence observed in the Q^{-1} curve that coincides with the Thompson and Holmes (1959) observations of a discrete spectrum in the resonant frequency versus temperature curves.

In order to verify that this result was not linked in some way with the particular state of cold work in this sample, the Niblett-Wilks peak was separated from the total Q^{-1} in a second sample which was rolled to 10%. The separated peak is illustrated in figure 4.18 and it is clearly seen that the three peaks are present in this sample also. It was pointed out by Paré (1960) that the shape of the total Q^{-1} curve in the vicinity of the Niblett-Wilks peak strongly suggested the presence of two peaks. This author also suggested that the change in shape of the curve with different amounts of cold work indicated that each peak was affected differently by these treatments. This suggestion is confirmed here by the fact that the relative heights of the three individual peaks at 25% deformation (figure 4.17) are significantly different than for 10% deformation (figure 4.18).

FIGURE 4.17

The Niblett-Wilks peak separated from the total Q^{-1} in figure 4.15. The legend is the same as in the preceding figures. The arrows indicate the individual component peaks.

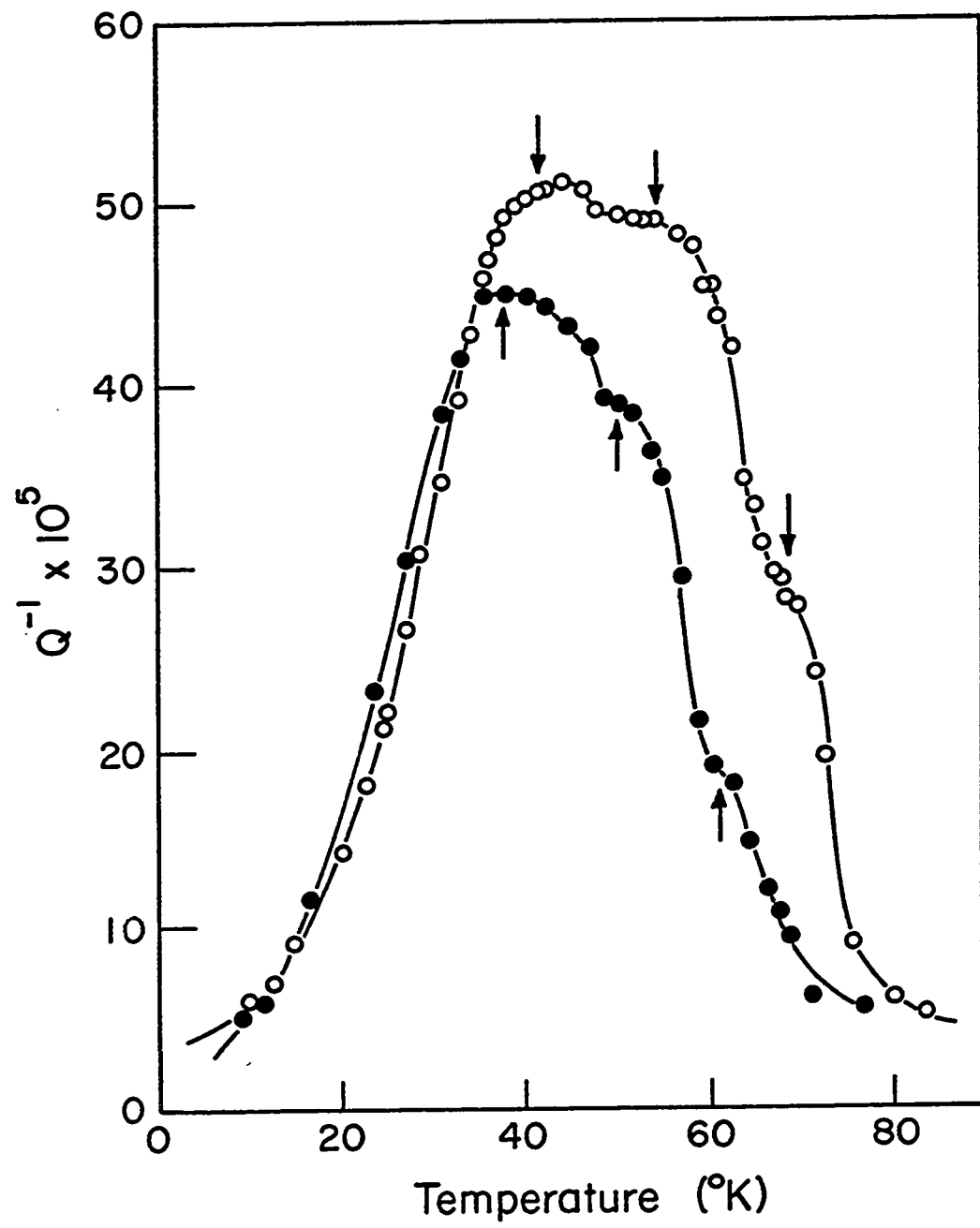
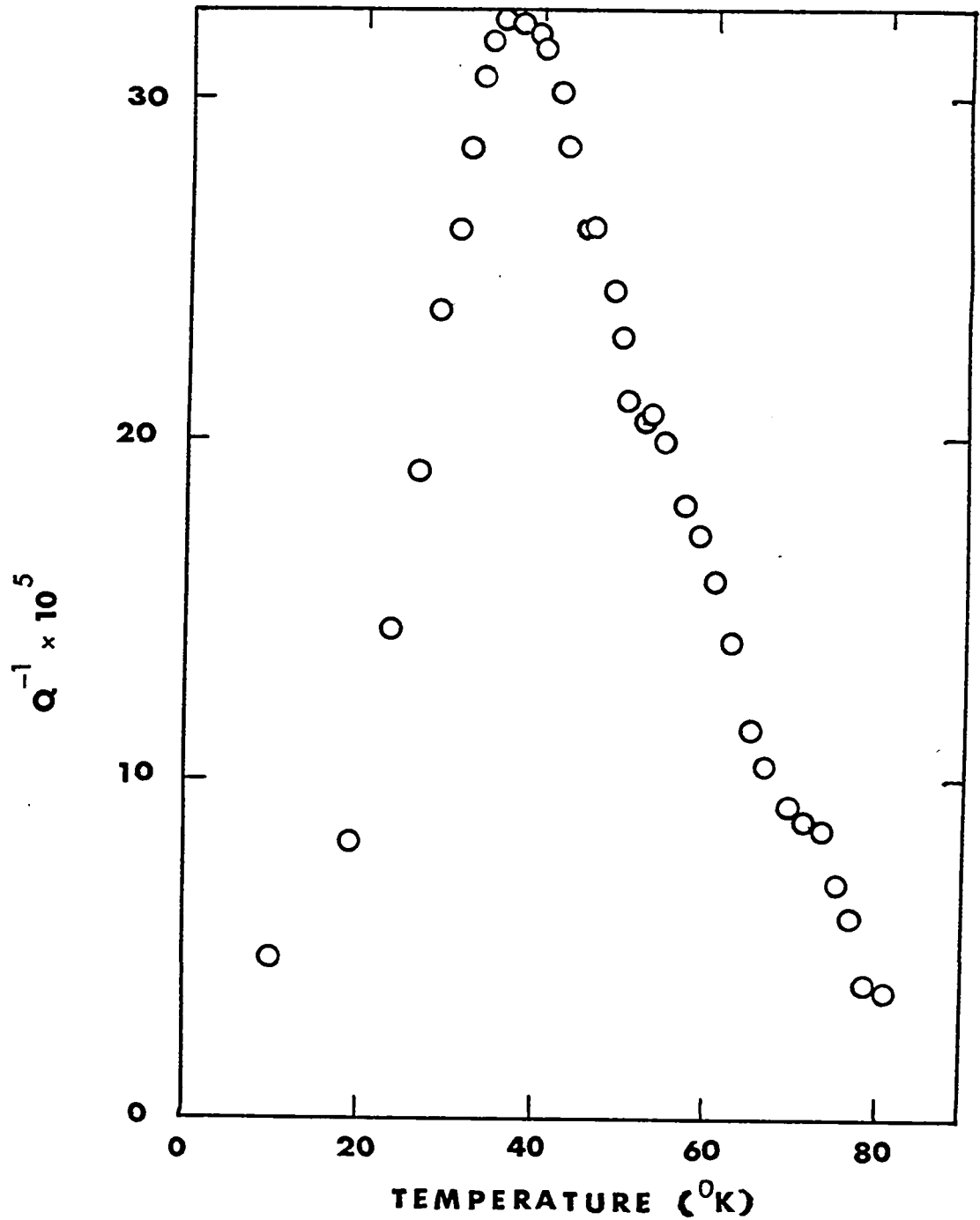


FIGURE 4.18

The Niblett-Wilks peak for a sample deformed 10%.
The frequency was approximately 17 kHz.



In view of the fact that at least part of the discrete spectrum proposed by Thompson and Holmes (1959) had been observed in the Niblett-Wilks peak, it was decided that a closer study of the Bordoni peak might further substantiate their proposal. This study was made in very slightly cold worked samples since this was the condition in which the Thompson and Holmes measurements were carried out. The graph of figure (4.19) shows the development of the Bordoni peak during early stages of cold working. The sample was aged for approximately twelve hours at room temperature before each measurement. There is good evidence in these measurements that the main Bordoni peak (83°K) is accompanied by a smaller peak (indicated by arrows) situated in the vicinity of 100°K . This peak appears to merge with the main peak for the larger amounts of cold working; however it is sufficiently removed from the main peak at $1\frac{1}{2}\%$ deformation to make the Bordoni peak appear 50% wider than it is at 10% deformation.

It may be said in summary that the Q^{-1} versus temperature curve of cold worked copper exhibits at least five distinct peaks in the vicinity of the Bordoni peak. At deformations somewhat greater than 3%, at least two of these peaks have merged to form the normally observed Bordoni peak. A detailed study of this Bordoni peak has revealed that its shape is consistent with that of a

FIGURE 4.19

THE EFFECT OF VARIOUS AMOUNT OF COLD WORKING ON THE
SHAPE OF THE BORDONI PEAK IN COPPER

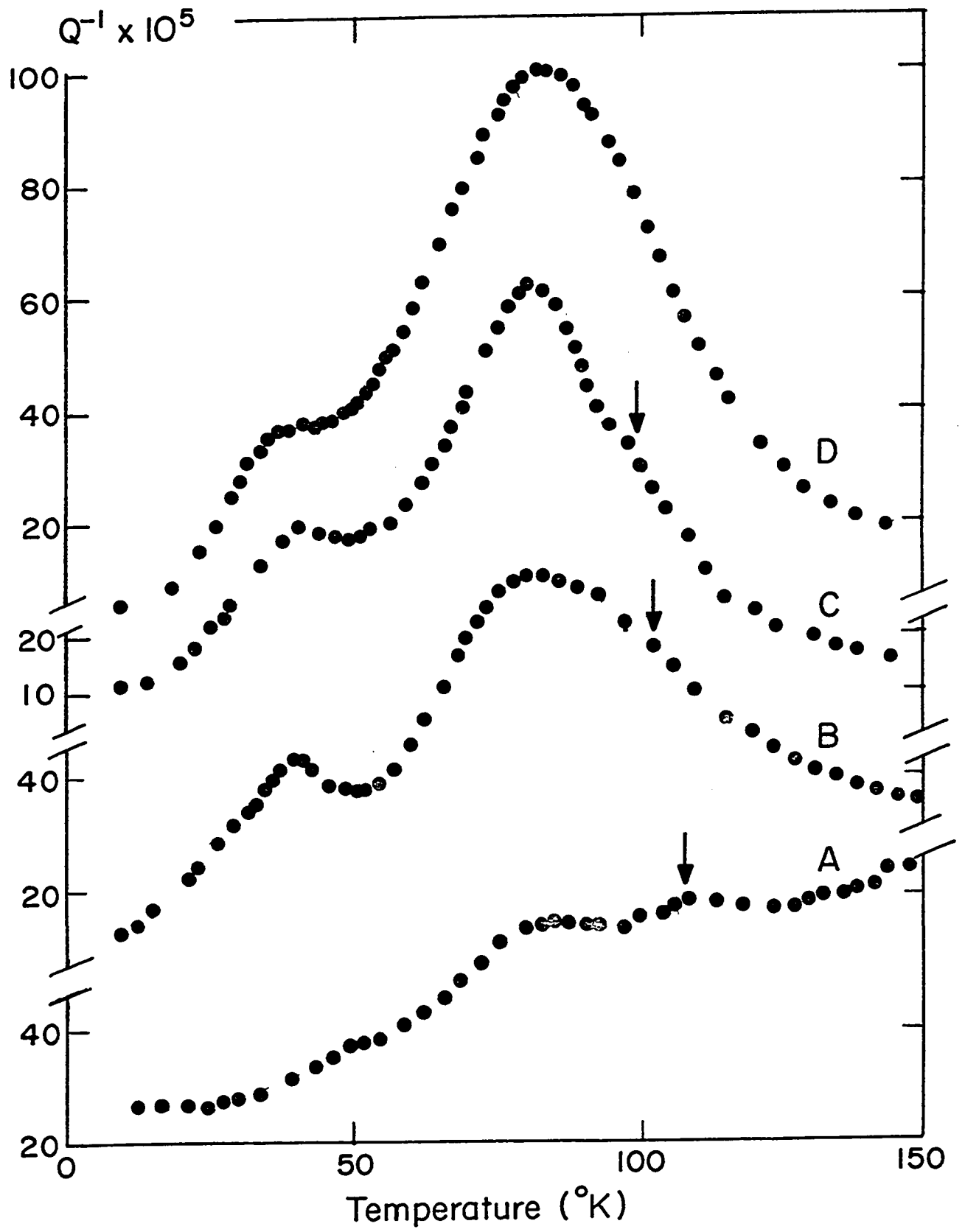
A - 1% cold rolled

B - 1.5%

C - 3%

D - 10%

Note: The scale of each curve is the same but they
are displaced for clarity.



relaxation peak characterized by a single limiting relaxation time and a spectrum of activation energies whose width is given by equation (4.3). It has also been observed that at least three peaks remain distinct from the main peak for deformations as large as 25%, and exhibit themselves as the so called Niblett-Wilks peak.

C. Tantalum

In the course of this study, it has been shown that the temperature dependence of nickel exhibits three prominent peaks which arise from thermally activated relaxation processes. One of these peaks was shown to require the presence of both cold working and dissolved hydrogen in order to be observed. The other two were found to be present with cold working only. The purpose of this section will be to present measurements on tantalum in order to show that this b.c.c. metal behaves in a strikingly similar manner.

Chambers (1966) has reviewed most of the internal friction measurements reported for cold worked tantalum. In the kilo Hertz frequency range, the internal friction below room temperature is dominated by the so called α - peak. It was reported by Chambers and Shultz (1962) that this peak is initiated by cold working. The height of the peak however is not a monotonically increasing function of cold work since the peak can be considerably reduced

by larger values of plastic deformation.

The temperature dependence of Q^{-1} in annealed tantalum is shown in figure 4.20. These measurements were made on polycrystalline high purity tantalum obtained from the Haynes Stellite Company (Kokomo, Indiana) and annealed for six hours in vacuo at 800°C. The peak which appears in the curve is the Snoeck peak (Cannelli and Verdini, 1966) which indicates the presence of dissolved hydrogen in the sample (Mazzolai and Nuovo, 1969). This is consistent with the wet analysis report of the supplier which indicated 0.0003% (wt.) H_2 in the sample. A similar sample in the "as received" condition (cold rolled) had a large α peak in the Q^{-1} versus T curve, as shown in figure 4.21. Further cold working of this sample reduced the height of the peak to less than 10% of its initial value (Verdini and Vienneau, 1968 b). Similar results have been reported for the α peak in niobium and molybdenum (Chambers, 1966). These characteristics are very similar to those of the P_3 peak in nickel and it is now known (Mazzolai and Nuovo, 1969) that the α peak in tantalum and niobium require both cold work and hydrogen to be visible. It would seem therefore reasonable to identify the α peak in these metals with the P_3 peak in nickel. Since extensive studies have been made of the α peak, reference is made to Chambers' (1966) review for its other properties.

FIGURE 4.20
THE TEMPERATURE DEPENDENCE OF Q^{-1} IN
ANNEALED TANTALUM

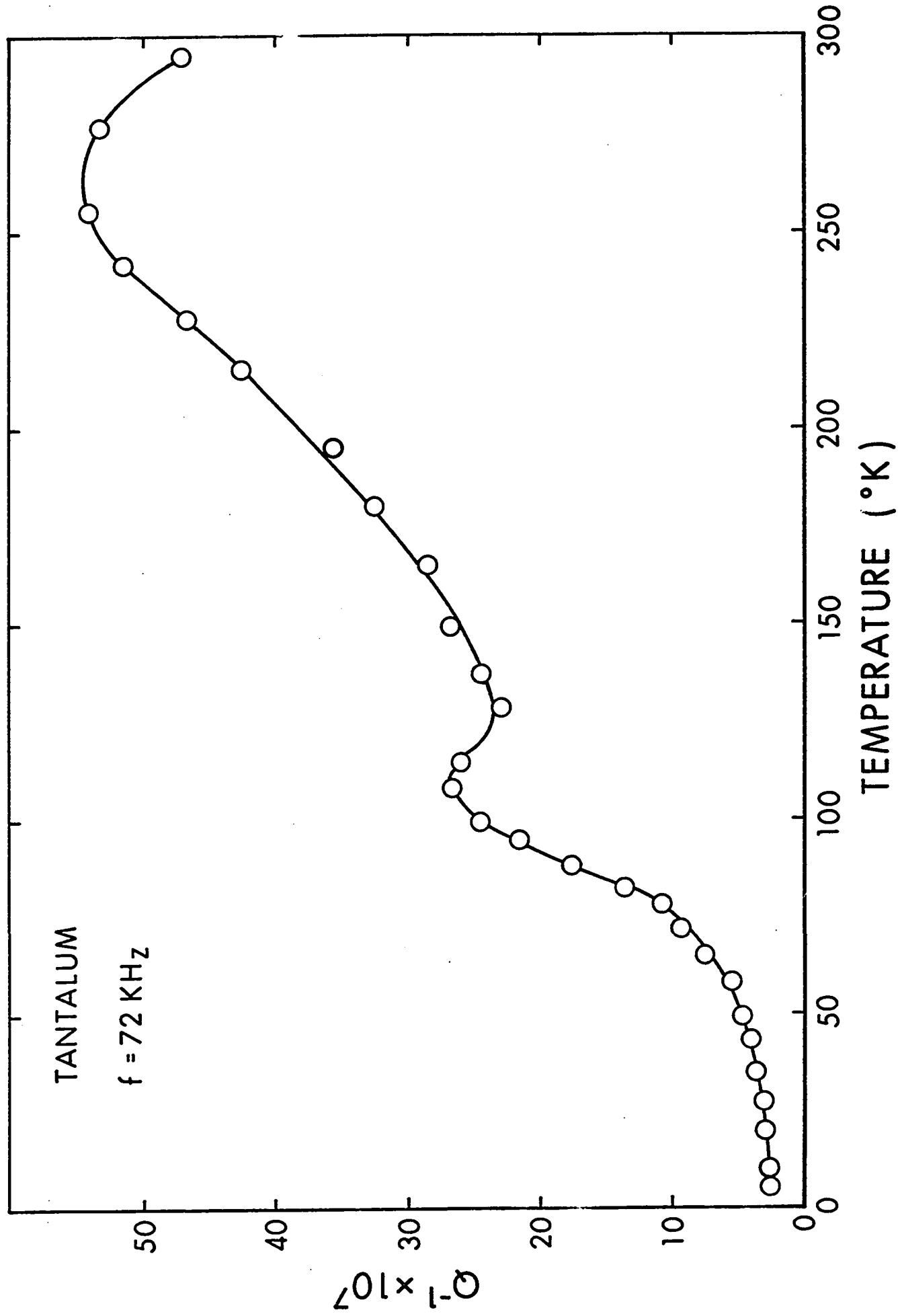
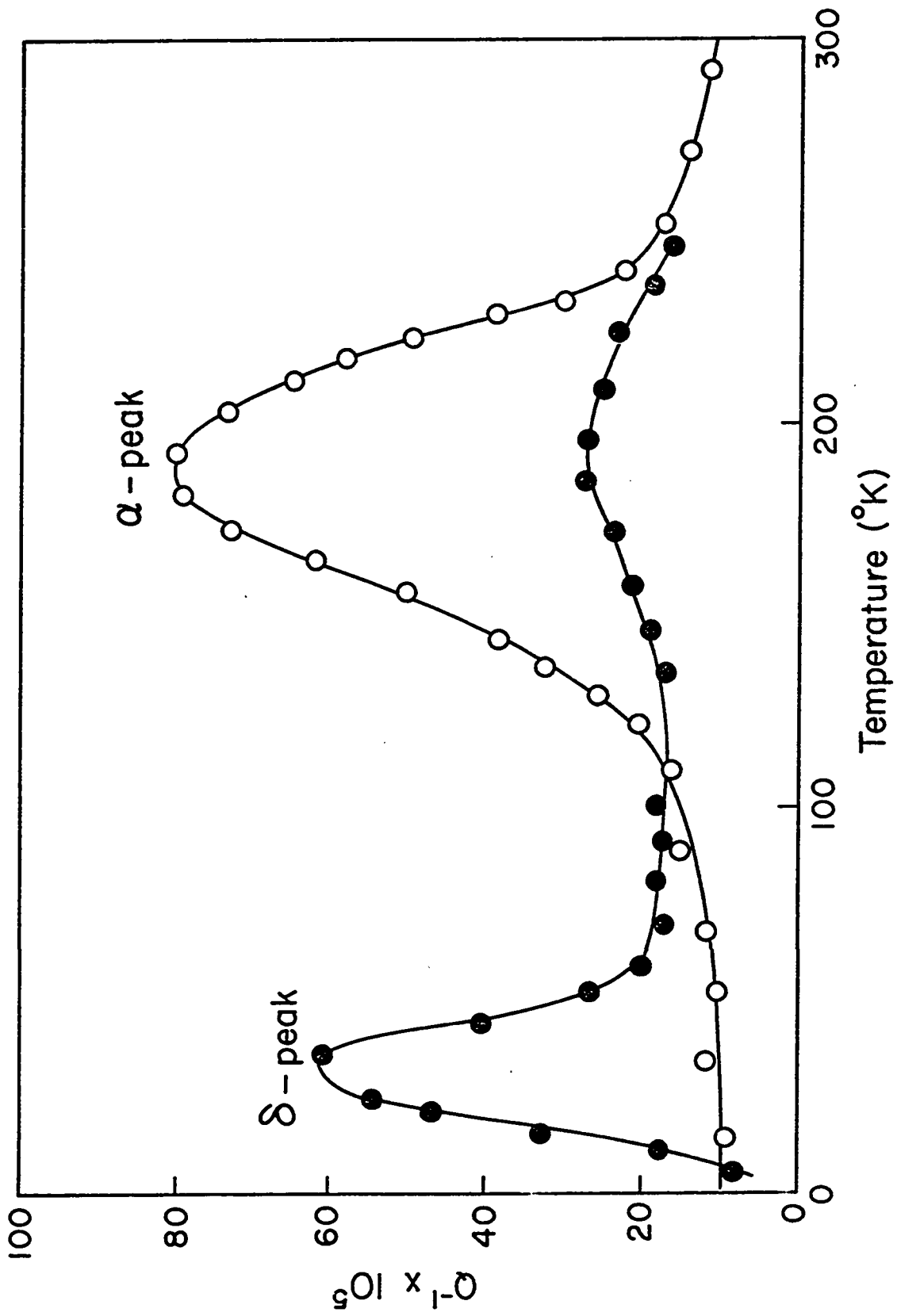


FIGURE 4.21

THE EFFECT OF COLD WORK ON Q^{-1} VERSUS
TEMPERATURE IN TANTALUM

- 0 - as received (cold worked unknown amount)
- - additional 7% deformation



Another interesting feature of the Q^{-1} versus temperature curve is a second peak which occurs at a lower temperature than the hydrogen cold work peak. This peak is clearly visible (figure 4.21) once the α peak has been reduced by "large" deformations. The presence of this peak was first reported by Verdini and Vienneau (1968 b) and has since been confirmed by Mazzolai and Nuovo (1969). This new peak will be referred to as the δ -peak in keeping with the Mazzolai-Nuovo notation.

The measurements of Q^{-1} were repeated for two frequencies after four months of aging at room temperature and the results for the lower range of temperatures are shown in figure 4.22. The δ -peak was slightly reduced in height by this aging treatment and the temperature of the maximum also appeared to be slightly lowered. The shift in the peak temperature with measuring frequency indicates that the δ -peak is a thermally activated relaxation process. This relaxation is also evident in the temperature dependence of the resonant frequency for each mode, as shown in figure 4.23.

The frequency dependence of the peak temperature is illustrated in figure 4.24. The results of Mazzolai and Nuovo are included for comparison. The two sets of results, at first glance, appear to be inconsistent. The sample for which the δ -peak was studied by Mazzolai

FIGURE 4.22

Q^{-1} VERSUS TEMPERATURE IN COLD WORKED TANTALUM
AT TWO FREQUENCIES

$$f_1 \approx 22.6 \text{ kHz}$$

$$f_2 \approx 81.0 \text{ kHz}$$

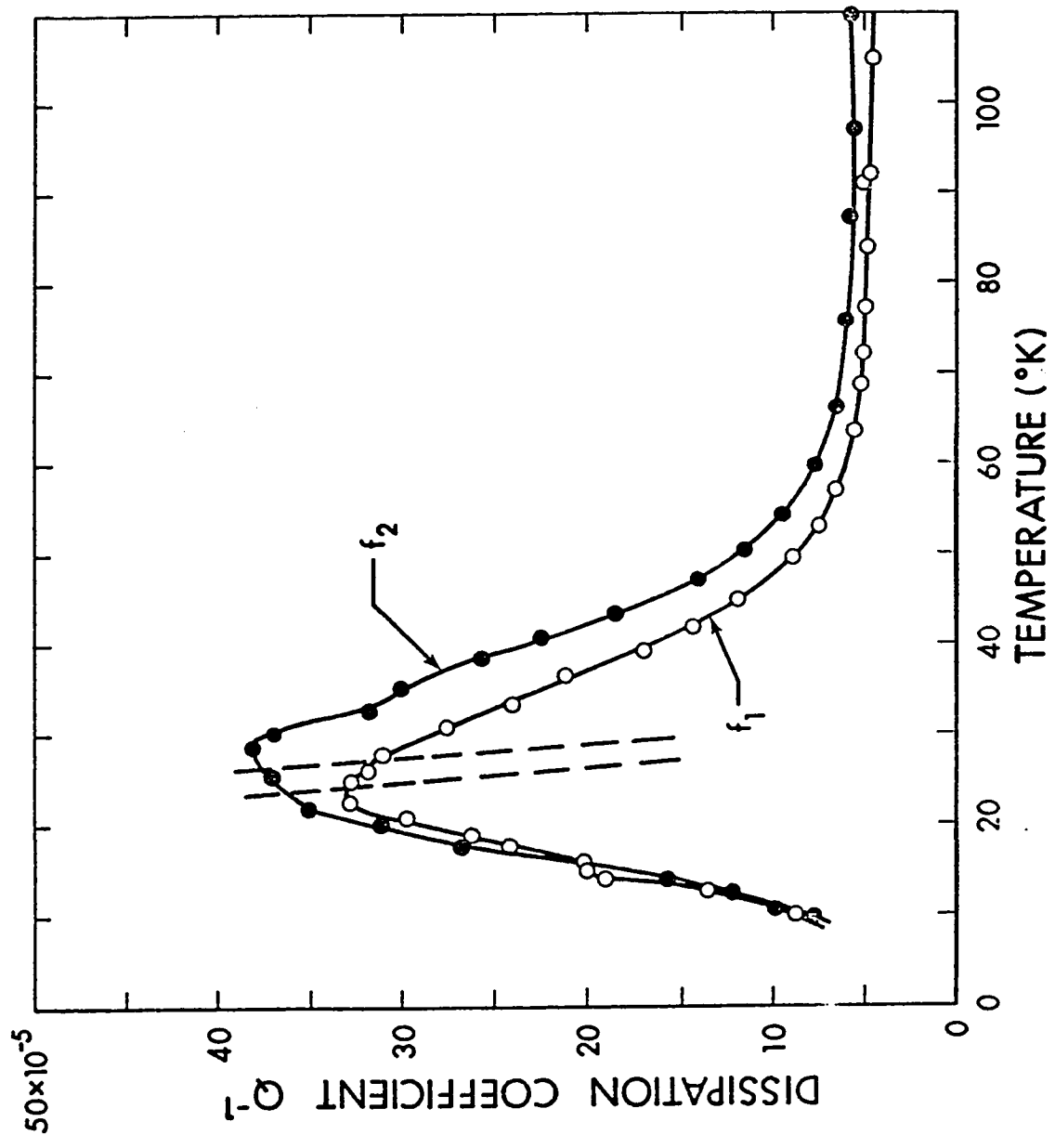


FIGURE 4.23

Resonant frequency as a function of temperature for the two modes f_1 and f_2 (figure 4.22). The dashed line represents temperature dependences for the resonant frequency of the sample in the annealed state. This frequency has been adjusted to fit the high temperature results in the cold worked samples. The change in shape of f versus T is obvious.

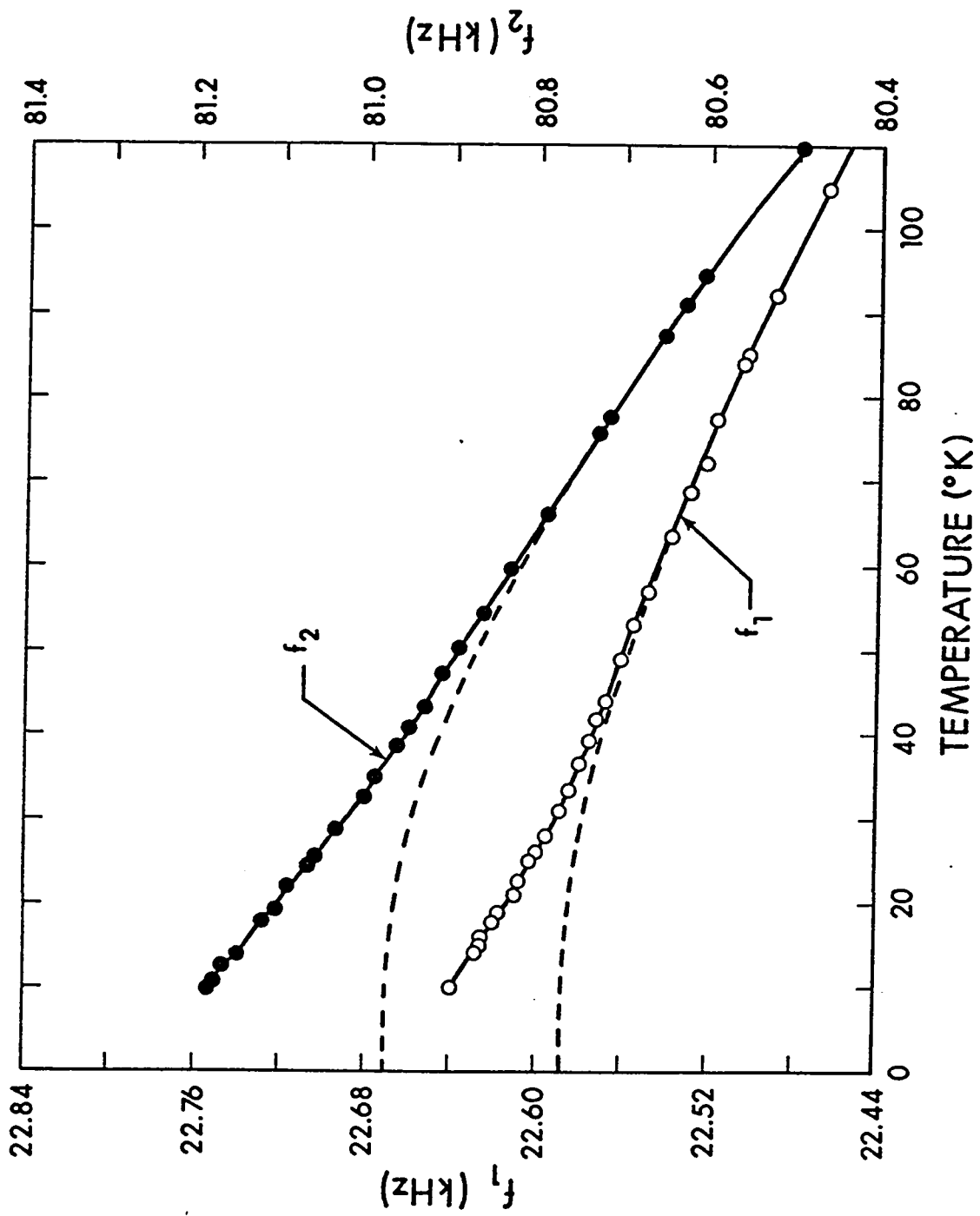
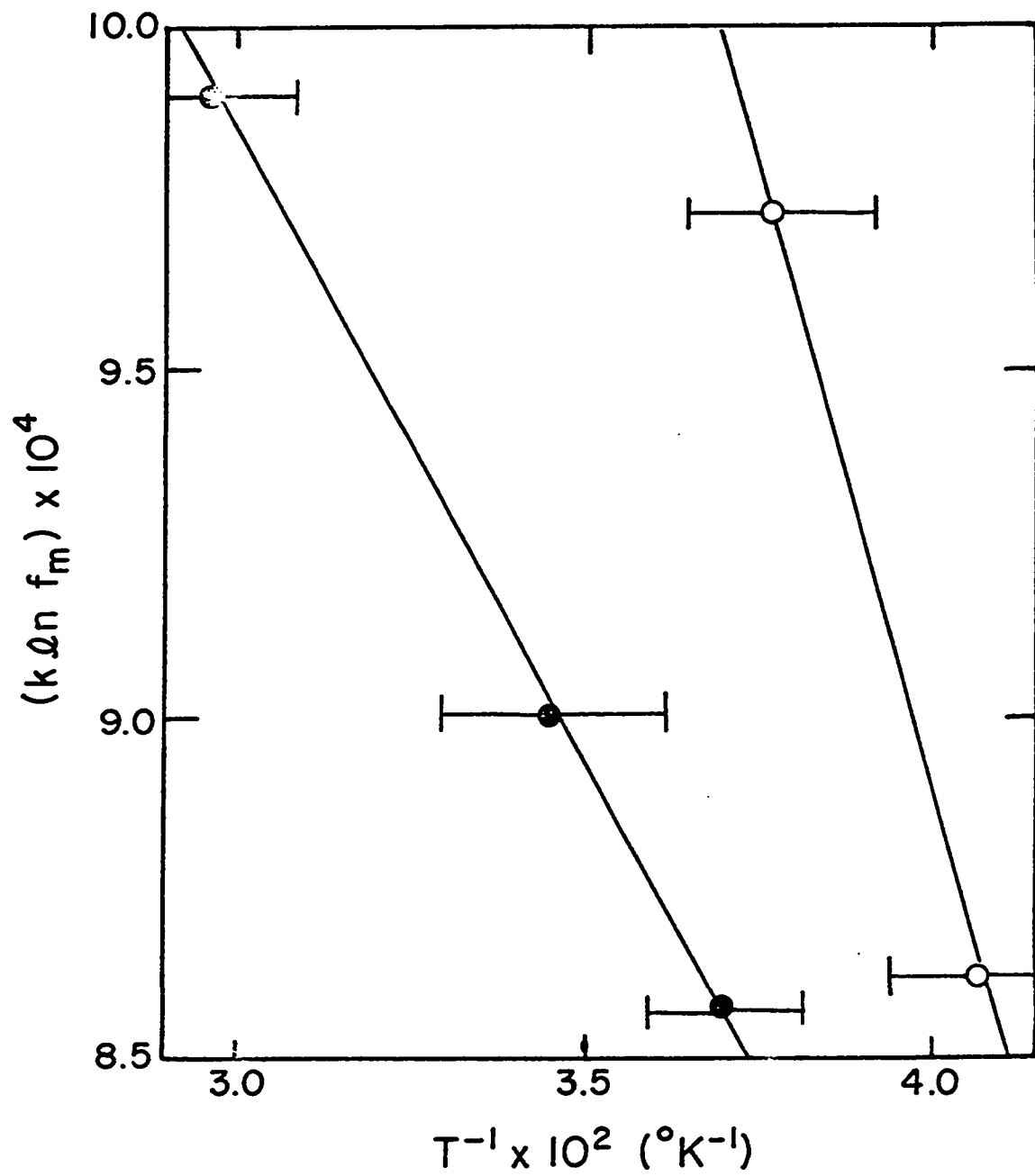


FIGURE 4.24

ACTIVATION ENERGY PLOT FOR THE δ -PEAK IN TANTALUM

O — this study

o — Mazzolai and Nuovo



and Nuovo contained too little hydrogen to produce the α -peak while the tantalum considered here showed a definite α -peak. M-N have shown that in the presence of hydrogen, the α -peak is visible and the δ -peak is shifted to lower temperatures, thus explaining the difference in the results. The slopes observed for the two sets of data in figure 4.24 are the same within the errors which reflect the difficulty of precisely determining the values of T_m^{-1} at these low temperatures. This is further complicated by the structure on both the high temperature and low temperature sides of the peak. This feature was confirmed by the M-N measurements. The average value of activation energy derived from the two lines in figure 4.24 is 0.027 ± 0.01 eV with $\ln \tau_0 \approx -26 \pm 2$.

It is easy to show (see figure 4.5 for the P_1 peak in nickel) that the δ -peak is wider than can be explained by a single relaxation time effect. At least part of this width can be explained by the presence of at least three overlapping peaks as mentioned earlier; the M-N results show this same structure. There is of course insufficient detail to determine whether the peaks have different activation energies, or different limiting relaxation times or both.

It has been shown here that the δ -peak is introduced by cold working and the M-N results indicate that

it is lowered by both annealing treatments and hydrogen charging. In these respects, the δ -peak system is very similar to the P_1 , P_2 peak system in nickel.

D. Iron

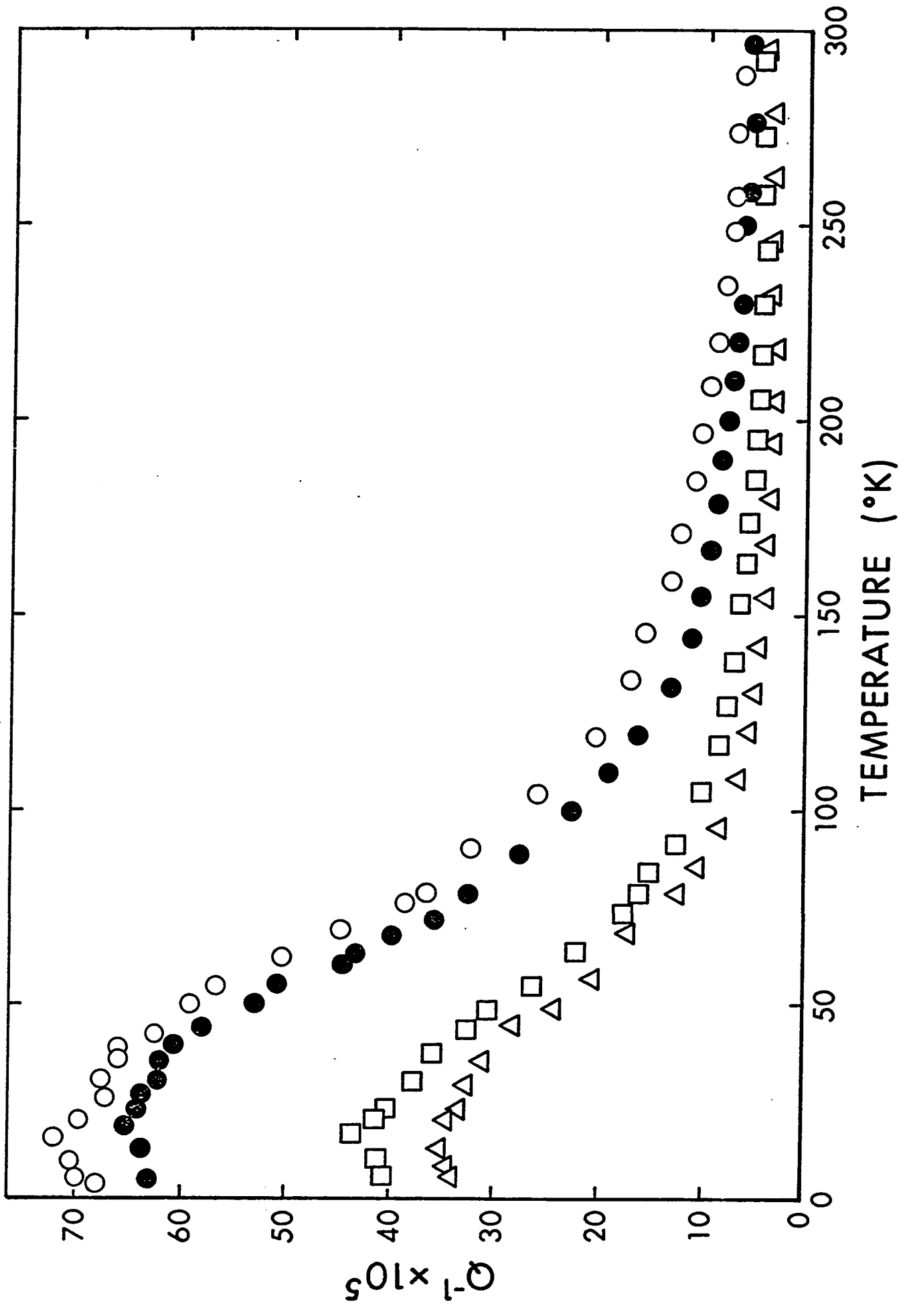
Measurements of internal friction in iron reported by Bruner (1960) and Heller (1961), have shown that this metal behaves anomalously at low temperatures. The internal friction was observed to increase as the temperature was lowered below 100°K and then level off and remain constant down to 4.2°K . Details of an investigation into this phenomenon were reported in the author's M.Sc. thesis (Vienneau, 1968) and by Verdini and Vienneau (1968 a). These results together with more recent measurements will be presented here in order to compare with the low temperature magnetic damping observed in nickel.

The samples used in this study were of polycrystalline spectrographically standardized material obtained from Johnson, Matthey Ltd. (London, England), the analysis of which showed an impurity content of less than 18 p.p.m. The temperature dependence typically observed for Q^{-1} in these samples is shown in figure 4.25. These data were taken for the first and second mode of two samples which were annealed together at 400°C for 6 hours, in vacuo. The internal friction is seen to increase as the temperature is lowered below 150°K and continues to do so until approximately 30°K where it tends to a near constant value. The effect is also shown to be an increasing function of frequency

FIGURE 4.25

DEPENDENCE OF Q^{-1} ON TEMPERATURE IN IRON
AT FOUR FREQUENCIES:

	Δ ———	26 kHz
Sample #1	\bullet ———	104 kHz
	\square ———	40 kHz
Sample #2	\circ ———	140 kHz



for the range of the measurements. It should also be pointed out that the damping at low temperatures was independent of stress amplitude for the range of stresses covered ($\sim 10^{-10}$ to 10^{-8}). The mounting technique did not permit measurements at larger stress amplitudes because of background vibrations set up in the pins.

The frequency dependence of the effect is illustrated in figure 4.26 for several temperatures. At high temperatures Q^{-1} increases with frequency while at low temperatures it appears to saturate at the highest frequencies.

The effect of annealing treatments on this internal friction phenomenon is shown in figure 4.27. In the highly cold worked sample it is seen that the internal friction at room temperature is comparable to that in ordinary metals. Its value increases, however, as the temperature is lowered. This low temperature increase becomes more prominent as the sample is annealed. A slight increase of the room temperature value is also noted. When the sample was annealed at 750°C (presumably sufficient for recrystallization, Gibala, 1967), the entire shape of the curve was changed. A large increase in Q^{-1} was observed at room temperature accompanied by the disappearance of the low temperature anomaly. When the recrystallized sample was slightly cold worked the

FIGURE 4.26

THE FREQUENCY DEPENDENCE OF THE ANOMALOUS
INTERNAL FRICTION IN IRON AT LOW TEMPERA-
TURES. A BACKGROUND EXTRAPOLATED FROM
ROOM TEMPERATURE HAS BEEN SUBTRACTED FROM
THE TOTAL Q^{-1} CURVE

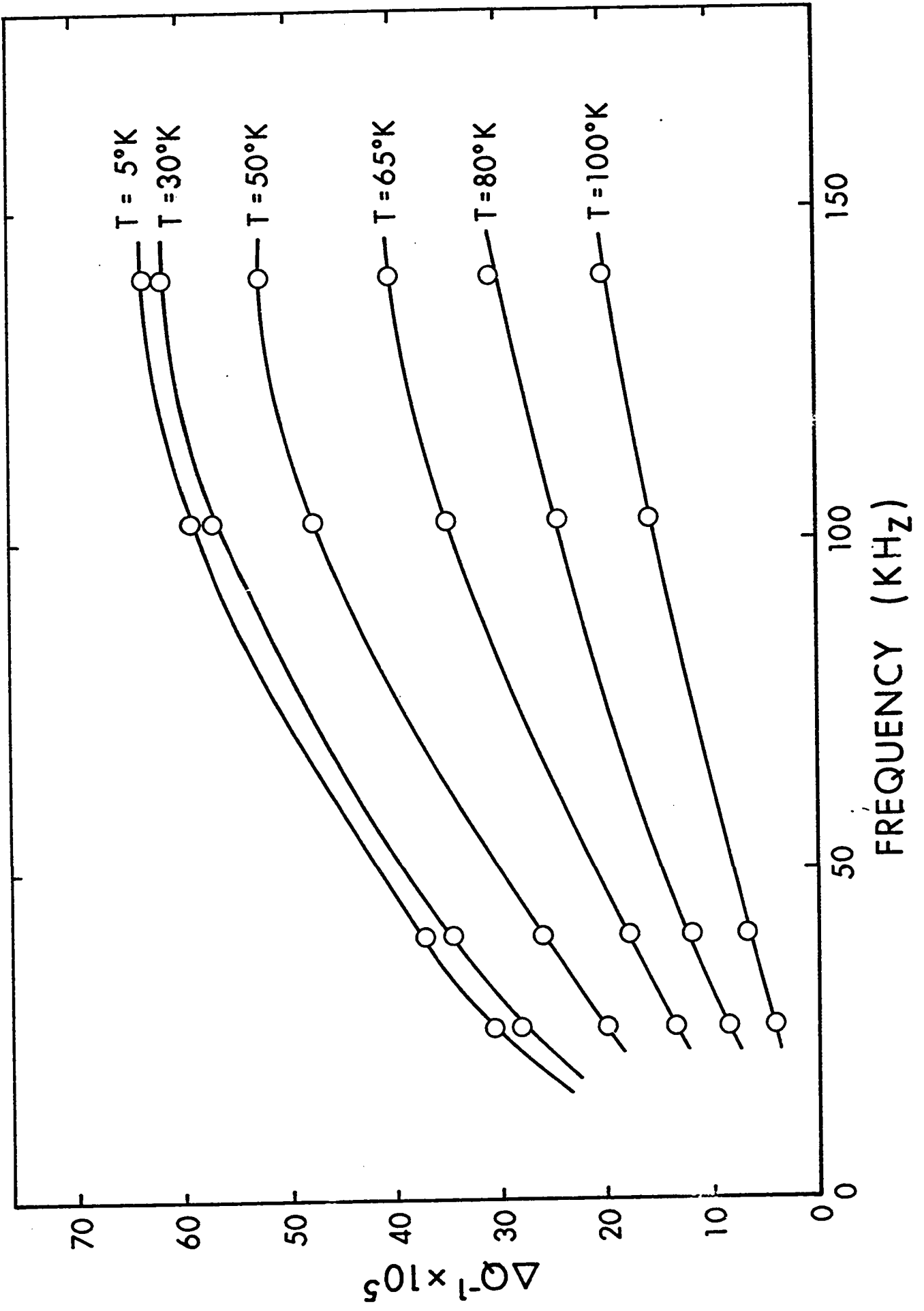
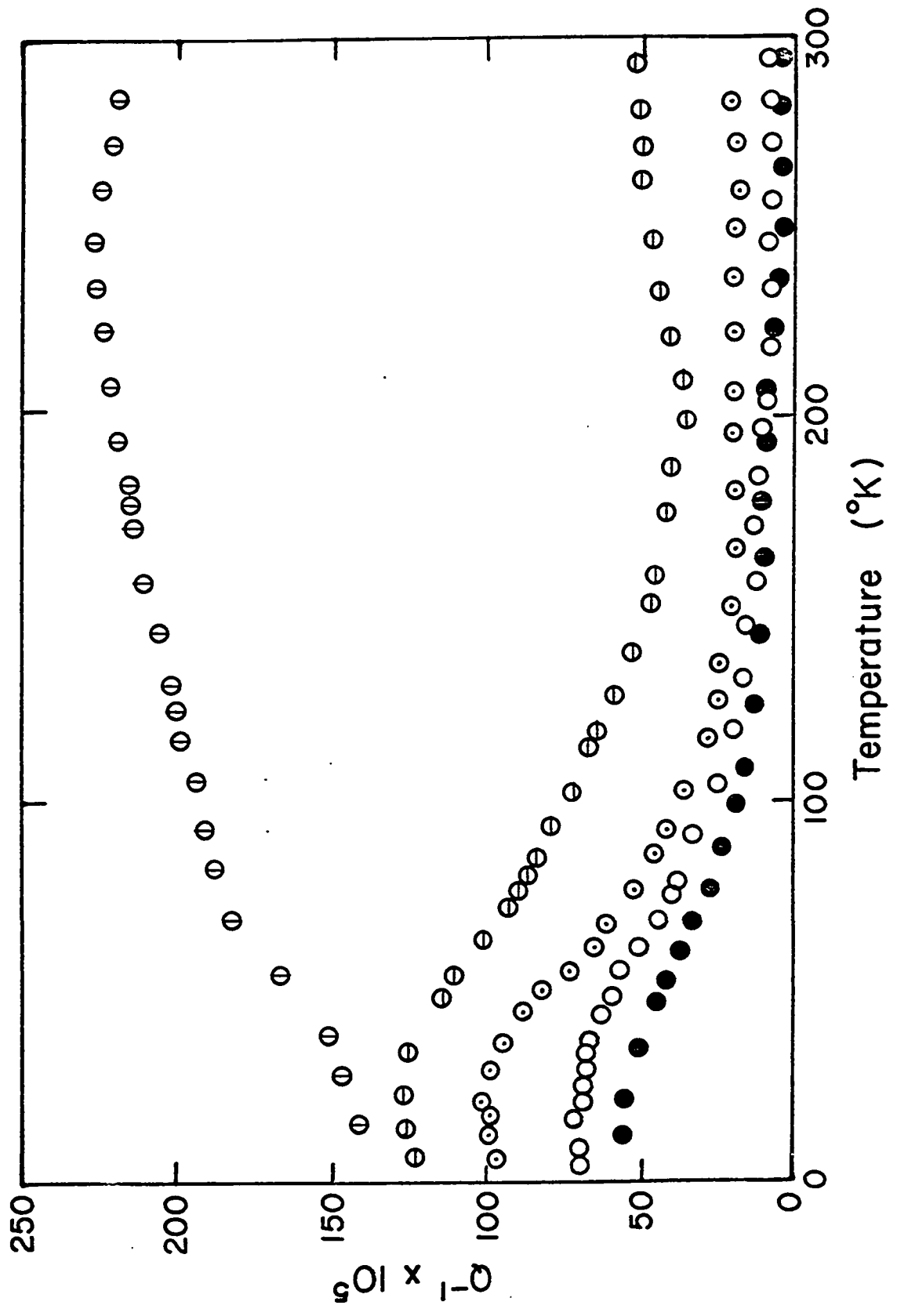


FIGURE 4.27

THE INTERNAL FRICTION IN IRON AT LOW
TEMPERATURES AFTER VARIOUS ANNEALING
TREATMENTS. (FREQUENCY $\approx 140 \text{ kHz}$)

- — As received (cold rolled unknown amount)
- — Annealed 6 hours at 300°C in vacuo
- ⊙ — Annealed 6 hours at 400°C in vacuo
- ⊖ — Annealed 6 hours at 550°C in vacuo
- ⊕ — Annealed 12 hours at 750°C in vacuo
(recrystallization)



anomalous behavior returned. This feature is substantiated by measurements reported by Gibala (1967) in his study of the hydrogen-Snoek peak in iron. There was however no discussion of the effect in Gibala's paper.

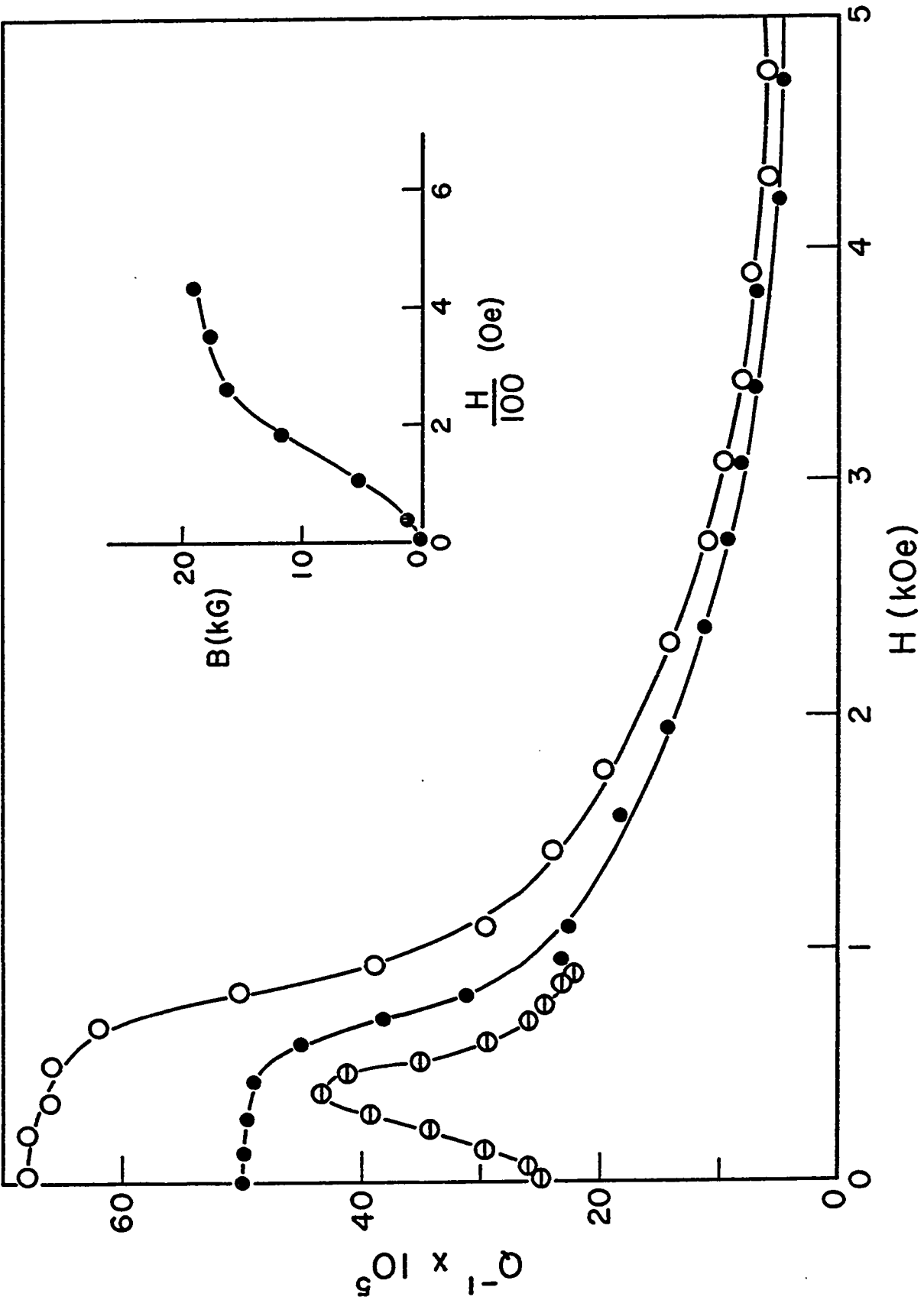
The effect of an applied magnetic field on a cold worked sample of iron was investigated. The sample was in the form of a bar (square cross section) and both extensional and torsional modes could be studied (see Chapter 3). The graph in figure 4.28 illustrates the magnetic field dependence of Q^{-1} at 4.2°K and 77°K . The sample was demagnetized prior to each run. The relatively large damping at 4.2°K is seen to be a monotonically decreasing function of applied field. At high fields it approaches the value of Q^{-1} at room temperature. The largest part of the reduction in damping coincides with magnetic saturation of the sample. Its occurrence at rather high fields is a reflection of the large demagnetization coefficient of the sample (see B-H curve in the inset). The Q^{-1} versus H curve at 77°K is significantly different from that at 4.2°K . It has a maximum that occurs near the onset of saturation. This is typical of the measurements made at room temperature in cold worked iron while the 4.2°K curve is similar to those measured in annealed iron at room temperature (Bratina, 1966).

FIGURE 4.28

MAGNETIC FIELD DEPENDENCE OF Q^{-1} FOR THE
EXTENSIONAL MODES OF A BAR-SHAPED IRON SAMPLE.

$T = 4.2^{\circ}\text{K}$	● — 52 kH_z
	○ — 105 kH_z
$T = 77^{\circ}\text{K}$	⊖ — 52 kH_z

The inset shows the B-H curve for this sample
at room temperature.



While the Q^{-1} versus temperature curve for torsional vibrations in this sample was similar to those for the extensional modes and for flexural modes of disks (figure 4.25), the effect of a magnetic field was somewhat different. The graph in figure 4.29 shows that in all cases Q^{-1} goes through a maximum as a function of magnetic field. What is most striking about this behavior is that the maximum value of Q^{-1} and the field at which it occurs is the same in all cases in spite of the large differences in the zero-field values of Q^{-1} .

The maximum in the curve of Q^{-1} versus magnetic field in cold worked samples is a complicating factor; however the general behavior is that the low temperature internal friction effect that has been observed in iron is absent at fields larger than the saturation field. This is an indication that the magnetic domain walls are involved in the effect. The fact that well annealed samples do not exhibit the anomalous effect is an indication that internal stresses (perhaps dislocations) also play a role in this internal friction. On the whole, the results are very similar to the effect observed in cold worked nickel (Section A of this Chapter).

It was shown in the author's M.Sc. thesis (Vienneau 1968) that the increase in the internal friction at low temperatures can be expressed in terms of electrical conductivity of the iron. This is illustrated in figure 4.30

FIGURE 4.29

THE MAGNETIC FIELD DEPENDENCE OF Q^{-1} FOR THE
TORSIONAL MODES OF A BAR-SHAPED IRON SAMPLE.

$T = 4.2^{\circ}\text{K}$	\odot — 60 kH_x
	\circ — 30 kH_z
$T = 77^{\circ}\text{K}$	\bullet — 60 kH_z
	\circ — 30 kH_z

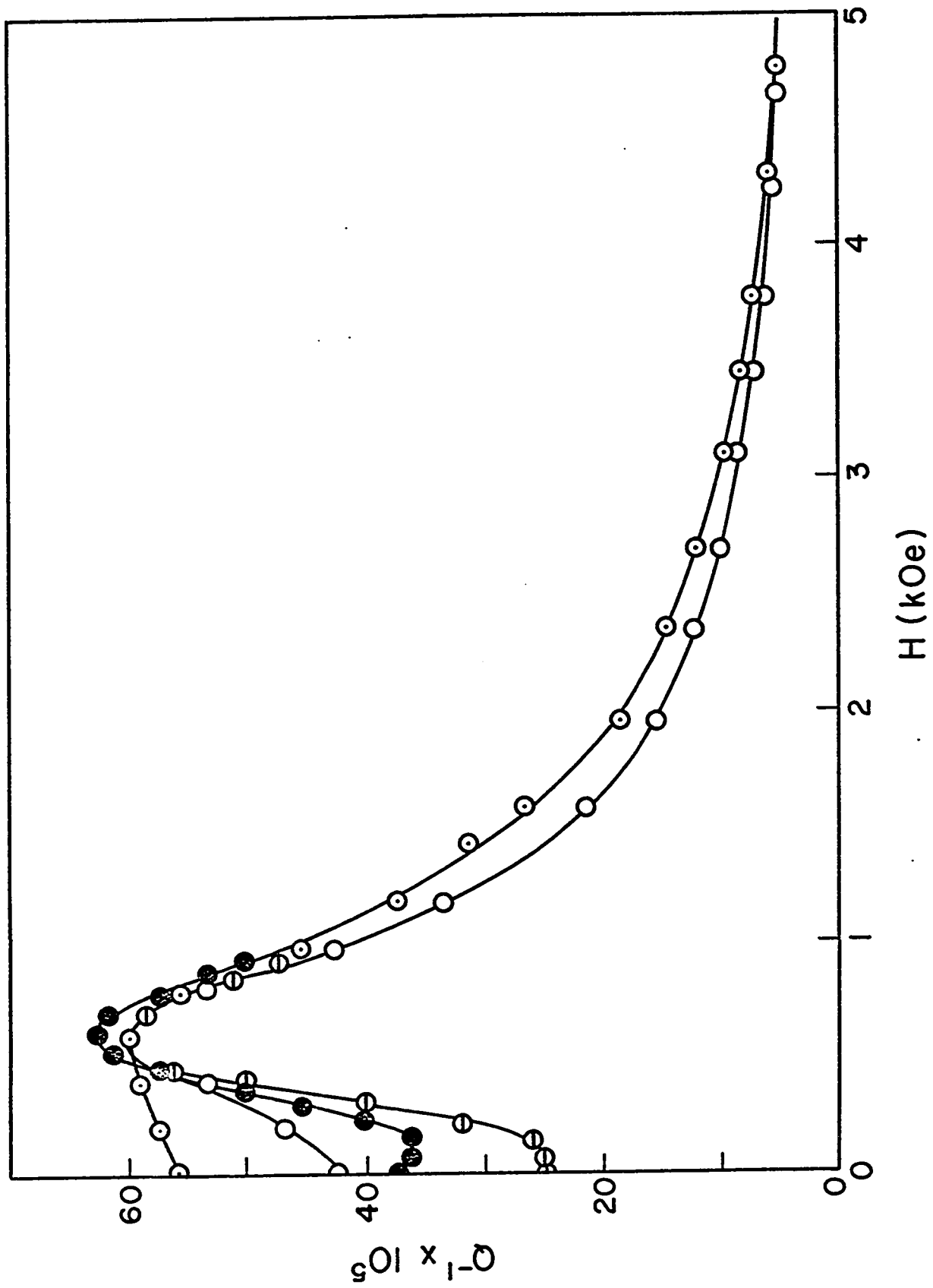
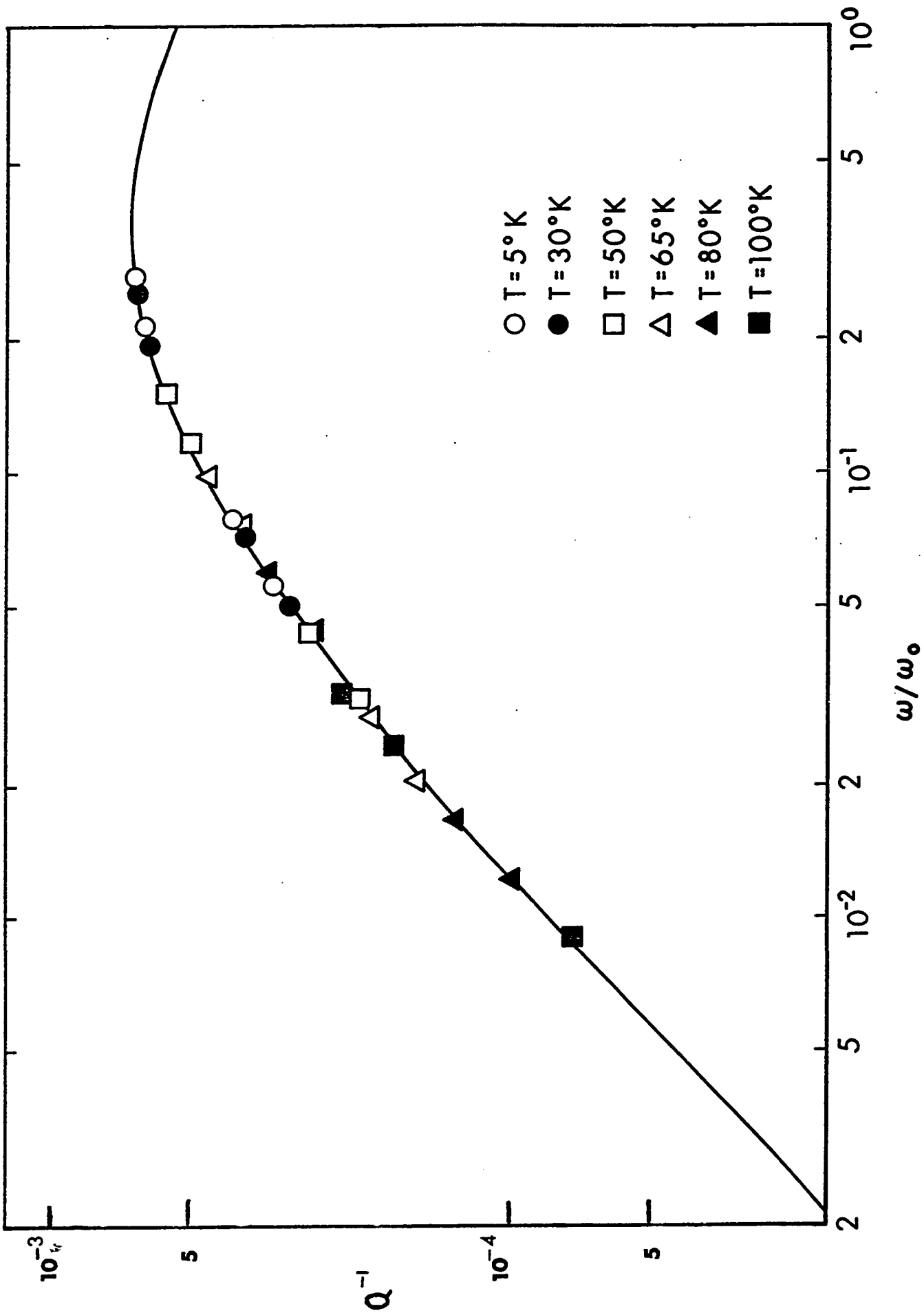


FIGURE 4.30

NORMALIZED FREQUENCY DEPENDENCE OF THE LOW
TEMPERATURE INTERNAL FRICTION IN IRON. THE
SOLID LINE REPRESENTS THE DISLOCATION INTERNAL
FRICTION THEORY OF OEN ET AL (1960).

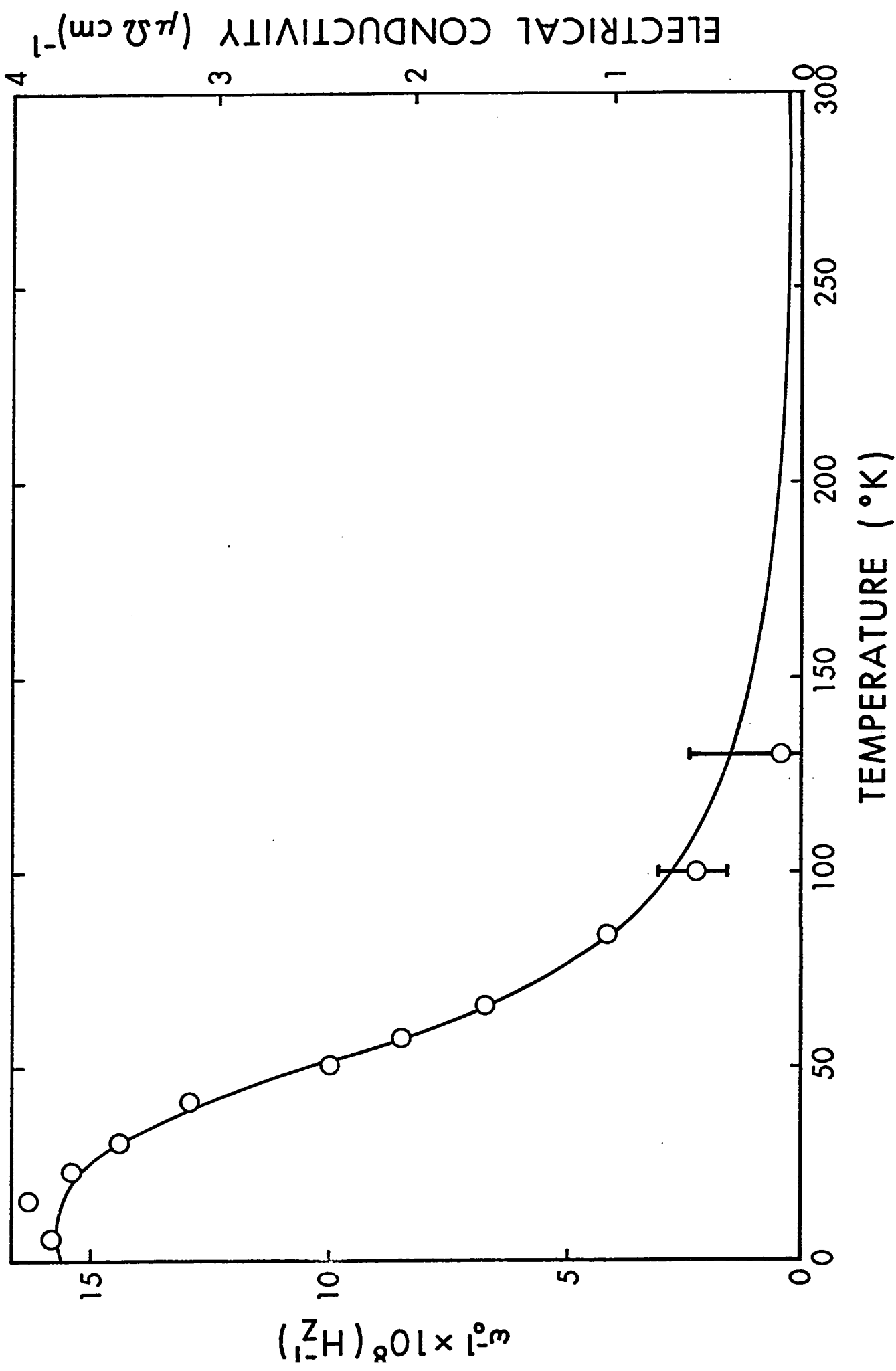


where Q^{-1} is plotted against the vibration frequency normalized by ω_0 a temperature dependent parameter. The solid line in the diagram represents the theoretical prediction for internal friction arising from overdamped dislocation motion as treated by Oen et al (1960). This theory can be looked at as a relaxation process with a most probable relaxation time $\tau_m \approx \omega_0^{-1}$. The associated spectrum of relaxation times was accounted for numerically by Oen et al. The parameter ω_0 is related to the frictional forces which cause the damping of the dislocation. The temperature dependence of ω_0 resulting from the fit in figure 4.30 is illustrated in figure 4.31. The solid line represents the electrical conductivity of the sample derived from the results of White and Woods (1959) using a residual resistivity of $0.265 \mu\Omega \text{ cm}$.

It was concluded from these results that the anomalous internal friction in iron was caused by the motion of dislocations that were damped by the conduction electrons in the iron. Mason (1966) has proposed that the motion of dislocations in metals is damped by the conduction electrons through their interaction with the strain field surrounding the dislocations. Mason's theory combined with the Oen et al model was able to account qualitatively for the results; however there was gross disagreement between theory and experiment on the magnitude

FIGURE 4.31

TEMPERATURE DEPENDENCE OF THE NORMALIZING
FREQUENCY ω_0 . THE SOLID LINE IS THE
ELECTRICAL CONDUCTIVITY OF THE SAMPLE AFTER
WHITE AND WOODS (1959) USING $\rho_0 = 0.265 \mu\Omega \text{ cm.}$



of ω_0 . The failure of the dislocation model to explain ω_0 does not however invalidate the experimental results in figures 4.30 and 4.31. Since it has been postulated here that the internal friction arises from domain wall motion, it should be possible to associate ω_0 with this type of internal friction.

The effect of annealing treatments on the curve in figure 4.30 was investigated. The graph of figure 4.32 shows the internal friction in iron plotted against ω/ρ where ρ is the electrical resistivity. The increase in Q^{-1} with annealing that was noted in figure 4.27 is reflected in this curve. The value of ω/ρ at which Q^{-1} begins to level off seems however to be relatively insensitive to annealing. In the context of the preceding discussion, the value of ω_0 does not seem to be sensitive to annealing treatments. It has also been found that γ irradiation does not alter the internal friction effect. In figure 4.33, the temperature dependence of Q^{-1} is plotted against temperature for measurements made before and after the sample received 40 Mr of 1.3 MeV γ -radiation. Both of these results favor the magnetic damping interpretation over the dislocation model since the Oen et al calculation indicates that ω_0 should be altered by annealing and that the damping should be reduced by γ irradiation.

FIGURE 4.32

Q^{-1} VERSUS ω/ρ FOR VARIOUS ANNEALING TREATMENTS.

A - 300°C

B - 400°C ; for 6 hours

C - 550°C

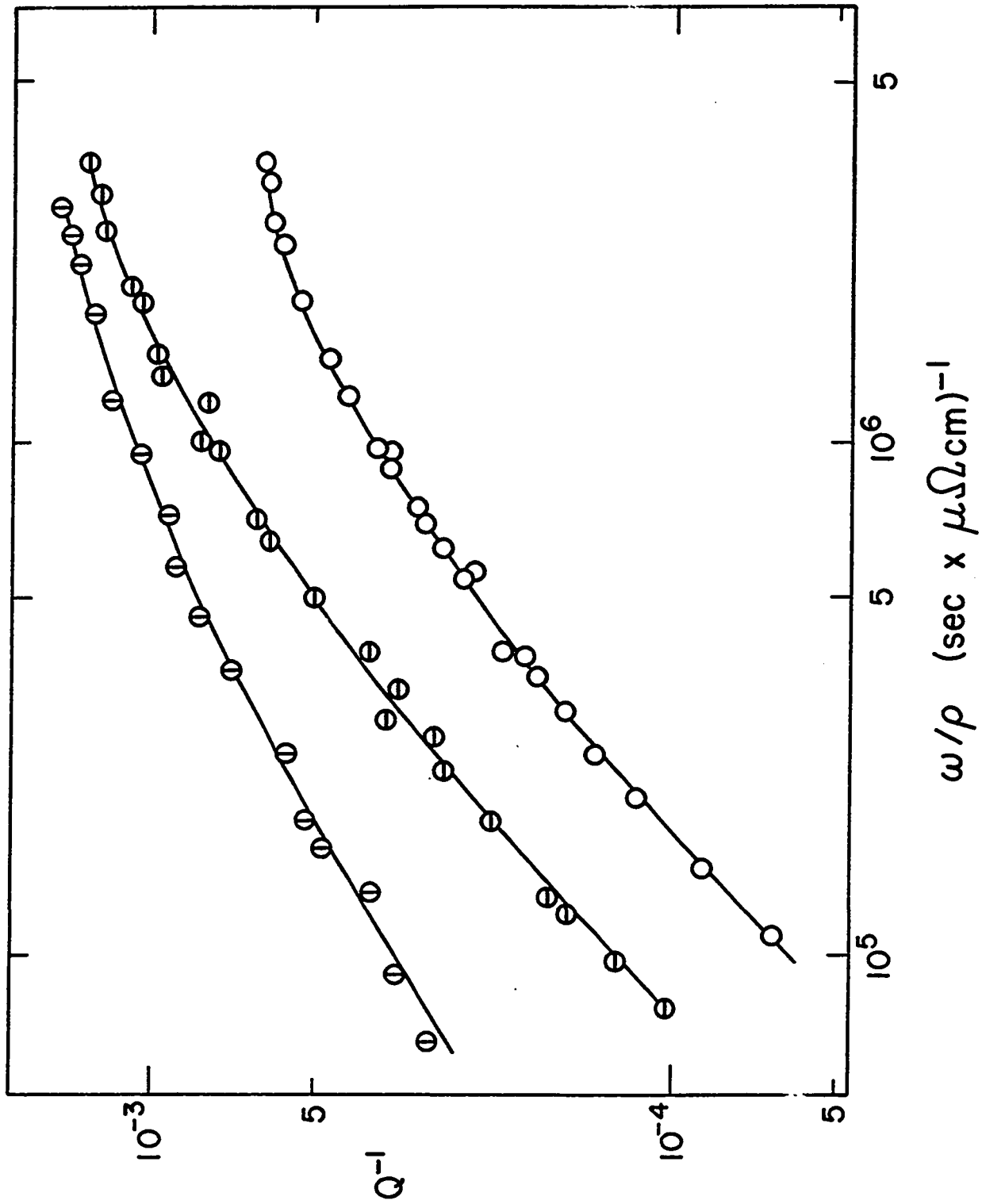
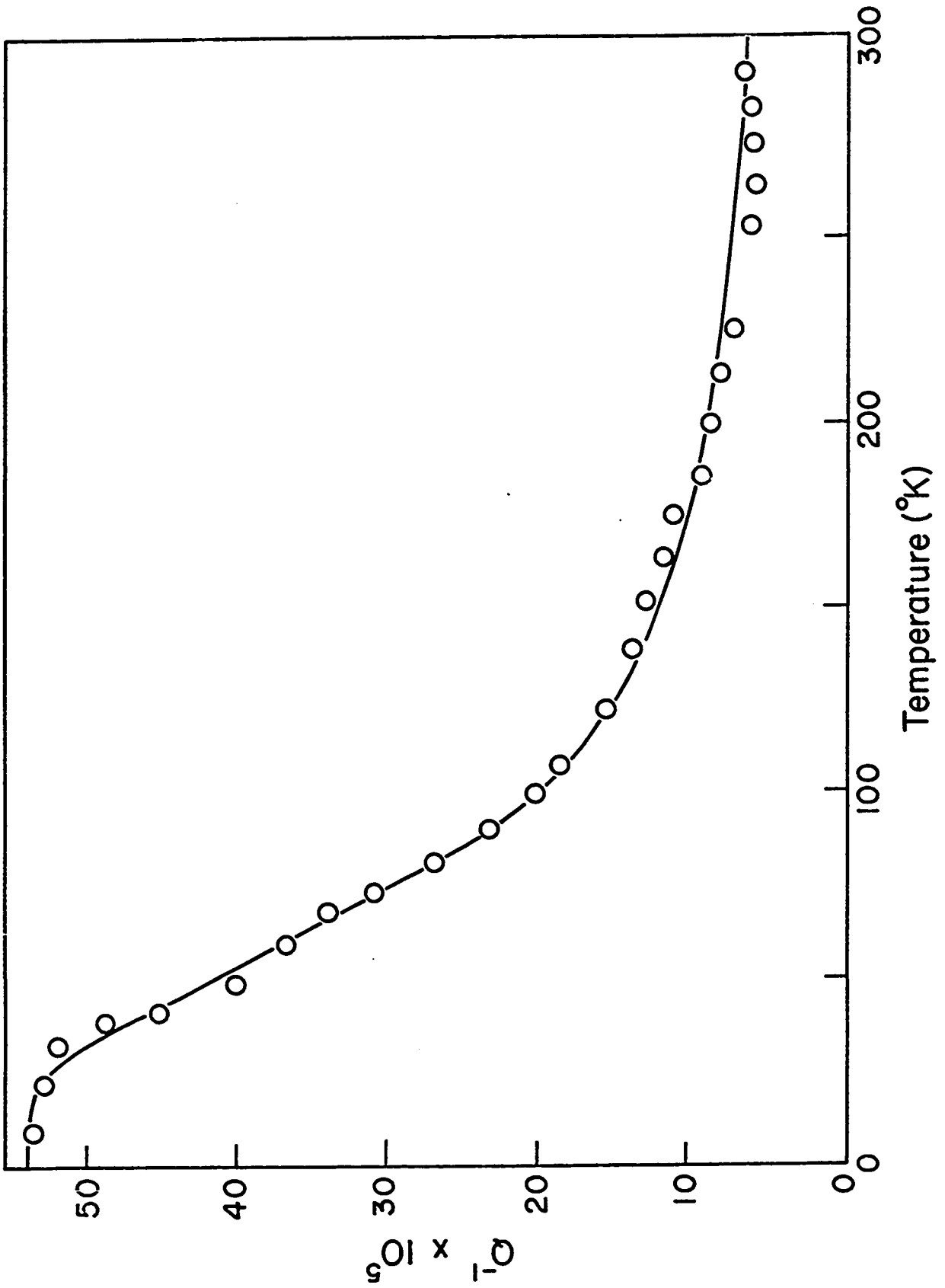


FIGURE 4.33

THE TEMPERATURE DEPENDENCE OF Q^{-1} AFTER
 γ IRRADIATION. DOSAGE: 40 Mr AT 1.5 MeV.

———— - "as received"

o - after irradiation



CHAPER 5

DISCUSSION

A. The relaxation peaks

It has been shown in the experiments done here (Chapter 4, A) that cold worked nickel exhibits three relaxation peaks which have been called P_1 , P_2 and P_3 . The P_1 and P_2 peaks were shown to be present in relatively pure material while the P_3 peak required the presence of hydrogen to be observed. Measurements of similar peaks in copper and tantalum have also been presented for comparison purposes. We will first examine the P_1 and P_2 peaks and their relation to relaxations in other metals.

i) The Bordoni peaks

The experimental results for the P_1 and P_2 peaks have shown that they are caused by cold work. We have also seen that they are hindered by the presence of an impurity such as hydrogen. These basic properties are very similar to those of the Bordoni relaxation peak in copper (Chapter 4, B). We will now make a detailed comparison between the P_1 , P_2 system in nickel and the Bordoni peak with its subsidiary (Niblett-Wilks peak) to show that these two systems can be identified with one another. The comparison will be made on the basis of experimental results.

1) We have previously pointed out that the P_1 peak in nickel is produced by cold working in a manner similar to that of the Bordoni peak. The heights of both the P_1 peak and the Bordoni peak increase monotonically with cold work.

This effect has been shown to saturate for the Bordoni peak in copper (Caswell, 1958). The results for the P_1 peak in nickel (figure 4.1) are in agreement with this in that the increase in Q_m^{-1} in going from 5% to 10% deformation is much less marked than in going from 1% to 5%. A second effect observed by Caswell, is that the maximum of the Bordoni peak shifts to slightly higher temperatures with increasing cold work. This is also the case for the P_1 peak as shown in figure 4.1.

2) It is known that the Bordoni peak disappears upon annealing at elevated temperatures. The same effect has been found for the P_1 peak in nickel by Sommer and Beshers (1966) and the present study. The annealing temperature (600°C) for the disappearance of the Bordoni peak has been identified with the onset of recrystallization (Niblett, 1966). Niblett also discusses complicated annealing behaviors which have occasionally been observed in copper. The annealing behavior of the P_1 peak is difficult to study because of the very large background (magnetic) damping which is initiated by nickel annealing and interferes with the observation of the peak. The P_1 peak maximum has, however, been observed to shift to lower temperatures upon annealing (figure 4.7) which is in agreement with the observations made on the Bordoni peak.

3) Caswell has observed that the height of the Bordoni peak and the temperature of maximum damping are also reduced

by the addition of impurities to the sample. The effect of dissolved hydrogen on the P_1 peak in nickel (figure 4.10) is very similar to this behavior.

4) The Bordoni peak in copper is known to be accompanied by a smaller subsidiary peak on its low temperature side (Niblett and Wilks, 1956). We have shown that the P_1 peak in nickel is also accompanied by a subsidiary peak (P_2) in a similar manner.

5) The Bordoni peak and the Niblett-Wilks peak originate from a thermally activated process and exhibit, in a general way, an exponential temperature dependence of the relaxation time according to an Arrhenius equation (Bordoni et al, 1959). However, they cannot be described by a single relaxation process; a range of relaxation times is involved in each case. The P_1 and P_2 peaks in nickel have been shown here to exhibit the same properties.

In view of the large number of properties which the P_1 and P_2 peaks in nickel have in common with the Bordoni peak and its subsidiary in copper, it is probable that both systems arise from the same relaxation effects. We would therefore expect the relaxation time spectra for the Bordoni peaks in copper and nickel to be similar in nature. We have shown in Chapter 4.A that the shape of the P_1 peak is consistent with a spectrum of relaxation times which arises from a distribution of limiting relaxation times and activation energies. We have also inferred that these

two distributions are not independent of one another. In Section B of Chapter 4 it was shown that the shape of the Bordoni peak is consistent with a spectrum of activation energies with a single limiting relaxation time. It would appear that the spectra for nickel and copper are not compatible since the inferred linear dependence would not allow a single limiting time in the presence of an activation energy spectrum.

The answer to this contradiction may lie with the errors in the analysis, for example, the width of the limiting relaxation time spectrum for the Bordoni peak in copper may in fact be small but non-zero (see figure 4.16). Another possibility is that the width of the relaxation time spectrum in nickel (figures 4.6 and 4.7) may not vary linearly with the inverse temperature. The conclusion that the time and energy spectra are linearly dependent on one another, in this case, would be erroneous.

The most likely answer to the problem lies in the basic assumptions made in the analysis. We assumed that the spectrum of $\ln \tau$ could be described by a log normal distribution function which is both continuous and symmetric about the most probable value $\ln \tau_m$. The assumption of continuity may however be questioned. We have seen that the Bordoni peak in copper and nickel is not well formed at small deformations. The high temperature side of the peak displayed structure (figures 4.1 and 4.19) indicating

the possible existence of a separate peak which contributes to the relaxation. This same type of structure has been observed by Bordoni et al (1962) and by König et al (1964) on the Bordoni peak in copper. If we assume that the Niblett-Wilks peak (and P_2 peak in nickel) arises from the same type of relaxation process (Seeger and Schiller, 1966), then the conclusion that the Bordoni peak consists of at least 2 overlapping peaks is made more plausible. We have shown that the Niblett-Wilks peak consists of at least three overlapping peaks (figures 4.17 and 4.18). Similar structure could not be resolved on the P_2 peak in nickel because of the greater uncertainty in the data which was mainly due to the much larger background damping present in this metal.

We can now understand the inconsistencies in the shape of the Bordoni peaks in nickel and copper. Under the simplest assumption the Bordoni peak consists of a large peak which is slightly disturbed by the presence of a lesser peak on its high temperature side. In copper we have seen that the effect of this additional relaxation is more marked for small amounts of cold work (figure 4.19) while the shape of the peak becomes more stable for larger deformations (figure 4.16). The results were similar for the measurements in nickel. Although the high temperature peak cannot be uniquely separated from the total curves (see the discussion of discrete spectra by Bordoni, 1959),

the consistency in the deduced spectra indicates that the disturbance in the shape is more marked for nickel than copper. Further comment on the spectrum of the Bordoni peak will be reserved until the specific nature of relaxation process has been examined.

As mentioned in Chapter 1, the most commonly accepted explanation of the Bordoni peak is based on stress relaxation through the generation of double kinks along dislocation lines. This proposal was first put forward by Mason (1955) and was subsequently modified by Seeger et al (1957). Since that time, a great many studies have been published concerning the stress induced generation and motion of double kinks and their relation to internal friction (see, for example: Niblett, 1966 and Seeger and Schiller, 1966). Only the most important development can be presented here for comparison with the experimental results.

For the basic concepts of dislocations, reference is made to Hirth and Lothe(1968). For our purposes a dislocation is a linear defect in a crystal lattice that is surrounded by a strain field. The strength of the dislocation (and its associated strain field) is given by the Burgers vector \vec{b} . In the presence of an applied stress σ , a dislocation experiences an effective force F per unit length given by:

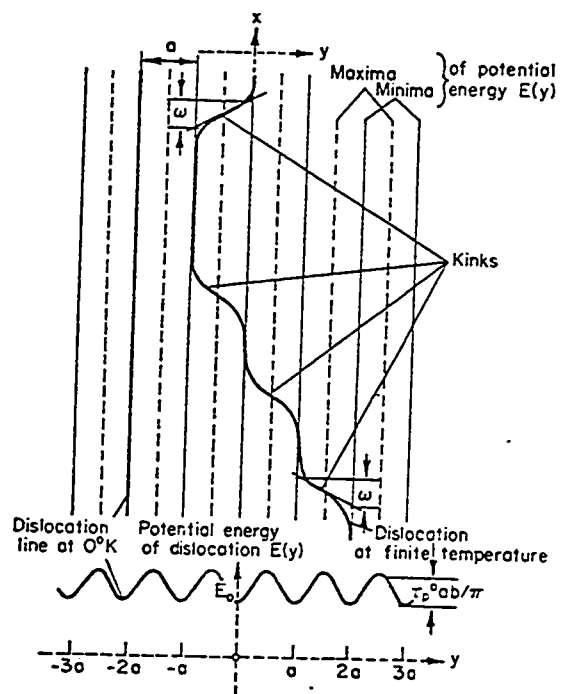
$$F = \sigma_s b \quad , \quad (5.1)$$

where σ_s is the projection of the shear component of σ onto a line perpendicular to the dislocation line. As a result of this effective force, the dislocation will tend to move in the direction of σ_s . This motion will result in a strain ϵ_d associated with the dislocation. The strain ϵ_d , however, is not produced instantaneously since the velocity of the dislocation will be limited by the frictional forces arising from the interaction of the dislocation with its surroundings. If the applied stress is in the form of an acoustic wave, the result of this delayed strain will be an internal friction effect (see Chapter 2, Section A) with a specific relaxation time τ .

A very important form of frictional force encountered by a moving dislocation is that associated with the periodicity of the lattice (Peierls stress). If we examine a dislocation lying parallel to a close packed direction in an f.c.c. crystal, each unit length of the strain field has associated with it an elastic energy. When the dislocation is displaced perpendicular to its direction, the energy per unit length is a periodic function of the displacement (Peierls, 1940). The period a of this energy function is in general simply related to the dislocation strength b . The situation is illustrated in figure 5.1. At zero temperature the dislocation will lie along a position of minimum energy and will require a shear stress (Peierls stress) to be displaced into the adjacent minimum

FIGURE 5.1

THE ELASTIC ENERGY OF A DISLOCATION SHOWING THE
EFFECT OF THE LATTICE PERIODICITY. (AFTER SEEGER
ET AL, 1957).



energy position. At finite temperatures (Seeger et al, 1957), the dislocation will not lie along a single potential energy minimum. Thermal agitation will cause it to jump the barrier and the dislocation will contain kinks (figure 5.1) and bulges consisting of kinks of opposite sense. The probability of forming kinks on either side of the zero temperature line should be equal and thus the dislocation will suffer no net displacement due to thermal fluctuation. The effect of applying a stress in one direction will be to offset this balance so that the dislocation undergoes a net displacement in the direction of the stress. Seeger and Schiller (1966) have shown that the internal friction due to this type of redistribution can be calculated by a rate theory similar to that used by Mason (1955).

Let us assume that the rate of formation of kink pairs (two kinks of opposite sense) in the presence of an applied stress is given by Γ for a dislocation of length L . Let us number the Peierls valleys (solid lines in figure 5.1) which a dislocation line of total length L may reach by forming thermal kinks by $i=0, \pm 1, \pm 2$ etc. The total length over which the dislocation lies in the i th valley is denoted by L_i and the number of kinks lying between the i th and the $(i+1)$ st valley is N_i . We define the probability

$$g_{i, i+1} = \frac{\Gamma}{L_i} \quad (5.2)$$

for the formation of a kink pair (between valleys i and $i+1$) per unit time per unit length of the dislocation line. The rate of change of N_i is given by

$$\frac{dN_i}{dt} = G_i - R_i \quad , \quad (5.3)$$

where G_i is the rate of generation of kinks between the valleys i and $i+1$ and R_i is the corresponding recombination rate (annihilation of two kinks of opposite sign by recombination). The rate of formation is given by:

$$G_i = 2g_{i,i+1} L_i + 2g_{i+1,i} L_{i+1} \quad , \quad (5.4)$$

and because of the preferential direction due to the applied stress, we note $g_{i,i+1} \neq g_{i+1,i}$. The recombination rate is not as straightforward as the generation since a detailed knowledge of the motion of kinks is required for its determination. Let us assume that the dislocation terminates at strong pinning points which are situated in the zeroth valley. In this situation, neighboring kinks are always of opposite sign. They may thus move together, along the line of the dislocation to annihilate one another. The motion of the kinks along the dislocation consists of random thermal motions at high velocity superimposed on a small drift velocity due to the applied stress. Stenzel (1965) has shown that the recombination rate under these assumptions is given by:

$$R_i = 2|v_d| \frac{N_i^2}{L} + DN_i^3 \left(\frac{1}{L_i^2} + \frac{1}{L_{i+1}^2} \right) , \quad (5.5)$$

where v_d is the drift velocity and D is the diffusion coefficient of the kinks. Thus the complete expression for the rate of change of N_i is:

$$\begin{aligned} \frac{dN_i}{dt} = & 2g_{i,i+1} L_i + 2g_{i+1,i} L_{i+1} \\ & - 2|v_d| \frac{N_i^2}{L} - DN_i^3 \left(\frac{1}{L_i^2} + \frac{1}{L_{i+1}^2} \right) . \end{aligned} \quad (5.6)$$

We now write the equation governing the change in lengths L_i due to kink formation. To do this, we introduce the minimum separation d which the two kinks of a newly formed pair must have in order that their motion be independent. The resulting equation is:

$$\begin{aligned} \frac{dL_i}{dt} = & -(g_{i,i+1} + g_{i,i-1})L_i d + g_{i+1,i} L_{i+1} d \\ & + g_{i-1,i} L_{i-1} d + (N_{i-1} - N_i)|v_d| , \end{aligned} \quad (5.7)$$

with the condition

$$\sum_i L_i = L . . \quad (5.8)$$

The motion of the dislocation is thus defined by a system of n nonlinear differential equations (5.6 and 5.7). On solving these equations, we would find that under the influence of an oscillating stress the area swept out by

the dislocation is given by:

$$A(t) = a \sum_{i=-i_{\max}}^{+i_{\max}} i L_i . \quad (5.9)$$

The resulting strain ϵ due to the dislocation is then given by (see, for example, Mason, 1955):

$$\epsilon(\sigma, t) = b A(t)/L , \quad (5.10)$$

and the internal friction is found from equation (2.8) to be:

$$Q^{-1} = \frac{\text{Im } \epsilon(\sigma, t)}{\text{Re } \epsilon(\sigma, t) + \mu\sigma} , \quad (5.11)$$

where μ is the shear modulus of the material. Summation over all the dislocation in a unit volume would then give the total internal friction.

There have been a great many problems in applying this general theory. The generation rate Γ has been calculated using different approaches (see, for example, Alefeld et al, 1965 and Seeger and Schiller, 1966). This calculation is rendered difficult because of a lack of knowledge concerning the form of the periodic Peierls potential (Seeger and Schiller, 1966, Lothe and Hirth, 1968). The evaluation of the draft velocity v_d in equations (5.6) and (5.7) is also a problem. This velocity is assumed to be the result of an equilibrium between the force on the kinks due to the applied stress

and the frictional forces due to the interaction of the kinks with their surroundings. Brailsford (1961) has suggested that the rate controlling mechanism for kink drift along the dislocation line is the period potential of the lattice. Seeger and Schiller (1962, 1966) have argued that the activation energy for this motion is small compared to kT except at very low temperatures (typically, $T < 0.5^{\circ}\text{K}$), and therefore should be negligible. They therefore suggested that the dominating friction force would be due to the interaction of the kinks with the phonons and other kinks.

The major problem with this treatment is the highly nonlinear character of equations (5.6) and (5.7). They cannot be solved in closed form and would require extensive numerical calculations. Such calculations have not been reported, largely because of the uncertainty in the values for the various terms in the equation. Seeger and Schiller (1966) have reported that an attempt at linearizing the equations by considering small deviations from equilibrium values of N_i and L_i have yielded physically meaningless results. The reason is that the linearized equations do not limit L_i to positive values presumably because the recombination term is not properly taken into account by the procedure.

Let us examine a simplified version of this theory which is typical of those reported in the literature. The

discussion will be based on the model of Seeger et al (1957). If we treat the dislocation line (lying nearly parallel to the x direction in figure 5.1) as a string of mass m per unit length, we obtain the following partial differential equation for the shape $y(x,t)$ of the dislocation line (t =time):

$$E(y) \frac{d^2 y}{dx^2} = \frac{dE(y)}{dy} + m \frac{\partial^2 y}{\partial t^2} - b\sigma \quad (5.12)$$

This is the normal equation of motion for a forced vibrating string with the force per unit length (last term on right hand side) given by equation (5.1). The energy per unit length $E(y)$, as mentioned earlier, is a periodic function of y , and will be represented by a second order Fourier expansion:

$$E(y) = E_0 - \alpha_1 \cos \frac{2\pi y}{a} - \alpha_2 \cos \frac{4\pi y}{a} \quad (5.13)$$

where σ_0 P(Peierls stress) is the stress required to move a dislocation over the maximum in $E(y)$ without the assistance of thermal or quantum activation. The constant E_0 is always much larger than α_1 or α_2 (Seeger, 1956); therefore we replace $E(y)$ by E_0 over the left hand side of equation (5.12) and the equation is rewritten as:

$$E_0 \frac{d^2 y(x)}{dx^2} = \frac{2\pi\alpha_1}{a} \left(\sin \frac{2\pi y(x)}{a} + 2\gamma \sin \frac{4\pi y(x)}{a} \right) + m \frac{\partial^2 y}{\partial t^2} - b\sigma \quad (5.14)$$

where $\gamma = \alpha_2/\alpha_1$. The time independent solution to this equation corresponding to a single kink in the dislocation line is given by (Seeger 1956)

$$y = \frac{a}{\pi} \tan^{-1} \left[\frac{(1 + 48)^{1/2}}{\sinh[2\pi\alpha_1(1+48)/E_0]^{1/2}/a} \right] \quad (5.15)$$

for the case of $\tau = 0$. By inserting this expression into the potential energy equation for a stretched string we find that the energy of a kink is given by:

$$W_k = \frac{2a}{\pi} \left(\frac{2E_0 ab \sigma_P^0}{\pi} \right)^{1/2}, \quad (5.16)$$

where σ_P^0 , called the Peierls stress, is given by:

$$\sigma_P^0 = 2\pi\alpha_1/ab \quad (5.17)$$

This solution corresponds to the approximation $\gamma = 0$ and σ_P^0 is the minimum stress required to overcome the Peierls potential (at $\gamma = 0$).

Seeger et al (1957) have studied the solutions to equation (5.12) for $\gamma = 0$ and find that the dislocation undergoes normal modes of vibration with energy W per wavelength. They are ordinary harmonic waves (as for stretched string) when $W \ll 2W_k$ but are related to bulges over the maximum in $E(y)$ when $W \approx 2W_k$. These modes were assumed to represent double-kink generation when the separation between the two kinks was greater than a distance d allowing the kinks to move along the dislocation independently

of one another under the influence of the applied stress. This distance was assumed to be the separation at which the work done by the applied stress plus the potential energy of the double kink were at a maximum. The situation is an unstable equilibrium and the applied stress causes the kink pair to separate further.

The solution to equation (5.12) was carried out numerically by Seeger et al (1957) and Wonth (1957) to show that the frequency ν with which double kinks (separation $> d$) are formed is given by the equations

$$\ln(\nu/B) = F_1(\gamma, \alpha) \quad , \quad (5.19)$$

$$B = \frac{\pi^2 \mu b^2 kT}{32a^2 v_m^2 E_0^{3/2}} \quad , \quad (5.20)$$

where k is the Boltzmann constant, T is the absolute temperature and v is the velocity of sound. The numerical results for $F_1(\gamma, \alpha)$ were given by Seeger et al. The parameters γ and α are given by:

$$\gamma = 2W_k/kT \quad (5.21)$$

and

$$\alpha = 1 - \frac{\pi\sigma}{8\sigma_P^0} \quad . \quad (5.22)$$

Paré (1961) has approximated the function $F_1(\gamma, \alpha)$ by:

$$F_1(\gamma, \alpha) = \frac{-4.56W_k}{kT} \left[1 - 0.785 \left(\frac{\sigma}{\sigma_P^0} \right)^{0.592} \right] \quad . \quad (5.23)$$

The frequency ν may be interpreted in the following way. A number of dislocations in the crystal are assumed to lie initially in valleys of the Peierls potential. A constant stress σ is applied to the crystal at $t = 0$. The dislocation, which is vibrating in its normal modes due to thermal agitation, will form a double kink by bulging into the next valley. At a frequency ν , these double kinks will be separated by the critical distance d and will be torn apart by the applied stress, thus the dislocation will be pushed into the next valley. The length of dislocation which is pushed over the barrier is equal to the maximum distance which the kinks can be separated, that is the distance between pinning points (an intersecting dislocation or immobile point defect). Thus under a constant stress the dislocation will produce a strain due to its motion which relaxes at a rate $1/2\pi\nu$. This is the relaxation time τ_σ in equation (2.1) which also applied for the case of sinusoidal stress with the usual approximations (equation 2.9). The internal friction will therefore be given by:

$$Q^{-1} = \frac{\Delta}{(1+\Delta)^{1/2}} \frac{\omega\tau}{1+(\omega\tau)^2}; \quad \tau = (2\pi\nu)^{-1} \quad (5.24)$$

The relaxation time is therefore given by:

$$\ln \tau = \ln(2\pi B)^{-1} - \frac{4.56W_k}{kT} \left[1 - 0.785 \left(\frac{\sigma}{\sigma_P} \right)^{0.592} \right] \quad (5.25)$$

Equation (5.25) indicates that the process of double kink generation is a thermally activated process with the limiting relaxation time $\tau_o = B^{-1}$ and an activation energy W given by:

$$W = 4.56 W_k \left[1 - 0.785 \left(\frac{\sigma}{\sigma_p^o} \right)^{0.592} \right] . \quad (5.26)$$

It is easy to show that in internal friction experiments the applied stress σ is much smaller than σ_p^o (Paré, 1961) and therefore the activation energy is expected to be

$$W_o = 4.56 W_k . \quad (5.27)$$

Bordoni et al (1959) have shown that the activation energy and the limiting relaxation time (average values) for the Bordoni peak in copper are in reasonable agreement with equations (5.27) and (5.20) respectively. These equations however predict a single activation energy and limiting relaxation time and thus cannot account for the width of the Bordoni peak (Seeger et al, 1957).

Paré (1961) has proposed a very simple modification to the Seeger et al theory to explain the width of the peak. He suggested that the internal stresses σ_i present in a cold worked metal be included in the σ dependence of W (equation 5.26). If we assume that $\sigma_i \gg \sigma$, the applied stress, then:

$$W = 4.56 W_k \left[1 - 0.785 \left(\frac{|\sigma_i|}{\sigma_p^o} \right)^{0.592} \right] . \quad (5.28)$$

Paré assumed the internal stress to have a normal distribution with mean value zero and standard deviation $\Delta\sigma_i$. It is then a simple matter to arrive at the expectation value and width of the resulting activation energy spectrum. The most probable value W_m of the activation energy is given by:

$$W_m = \int_{-\infty}^{+\infty} W(|\sigma_i|) \psi(\sigma_i) d\sigma_i \approx W_o \left[1 - 0.6 \left(\frac{|\Delta\sigma_i|}{\sigma_p^o} \right)^{0.592} \right] , \quad (5.29)$$

where $\psi(\sigma_i)$ is the normal distribution function for σ_i .

The standard deviation ΔW is given by:

$$\Delta W = \left[\int_{-\infty}^{+\infty} (W - W_m)^2 \psi(\sigma_i) d\sigma_i \right]^{1/2} \quad (5.30)$$

and was estimated by Paré to be:

$$\Delta W = 0.3 \left(\frac{|\Delta\sigma_i|}{\sigma_p^o} \right)^{0.592} . \quad (5.31)$$

The quantity ΔW is related to β_W used in Chapter 2 (equation 2.28) by

$$\beta_W = \sqrt{2} \Delta W . \quad (5.32)$$

The measured values of W_m and β_W for copper are 0.122 eV and 0.035 eV (Chapter 4, Section B) and by inserting into equations (5.29) and (5.31) we find:

$$W_0 \approx 0.15 \text{ eV}, \quad (5.33)$$

$$\Delta\sigma_i \approx 0.45 \sigma_p^0 .$$

Paré pointed out that the width of the stress distribution indicated by these results would require internal stresses of the order of the flow stress ($\sim \sigma_p^0$). It is not expected that a crystal could maintain these large stresses without relaxation. He therefore concluded that the internal stress distribution could not completely account for the width of the Bordoni peak.

More recently, Hobart (1969) has suggested that in addition to the σ_i distribution one might expect a distribution in the value of W_0 . It is known that under suitable energy conditions a dislocation line may break up into partial dislocations which are separated by a stacking fault (see, for example, Lothe and Hirth, 1968). Hobart (1968) has suggested that the oscillating part of the dislocation energy $E(y)$ [equation (5.13)] for the split dislocation can be represented by the sum of the contributions from each partial. Thus he arrives at

$$E(y) = E_0 - \alpha_1 \left[\cos\left(\frac{2\pi y}{a} - \frac{\pi s}{a}\right) + \cos\left(\frac{2\pi y}{a} + \frac{\pi s}{a}\right) \right], \quad (5.34)$$

where s is the separation between the partials. By taking this into account in equations (5.16) and (5.27), Hobart (1969) has suggested that:

$$W = W_0 \left[1 - 0.785 \left(\frac{|\sigma_i|}{\sigma_P^0} \right)^{0.592} \right] \left(\left| \cos \frac{\pi s}{a} \right| \right)^{\frac{1}{2}}. \quad (5.35)$$

It was assumed that the partial separation s is distributed normally about a mean value \bar{s} with a standard deviation Δs . Using the following values:

$$\Delta \sigma_i = 0.13 \sigma_P^0, \quad ,$$

$$\Delta s = a, \quad ,$$

$$\bar{s} = 10a, \quad ,$$

Hobart was able to account for the width of the Bordoni peak in copper. It is easy to show that approximately the same values of the above quantities would also account for the width of the Bordoni peak in nickel.

The above argument, that the simplified theory of double kink generation can be modified in this way to account for the width of the Bordoni peak, is moot. Let us examine the first contribution to the activation energy spectrum, namely the internal stresses. As shown by equation (5.29), W_m is a decreasing function of $\Delta \sigma_i$. As a consequence T_m , the peak temperature, is also a decreasing function of $\Delta \sigma_i$ (equation 2.14). It should be expected that $\Delta \sigma_i$ would increase with the amount of cold working and we would therefore expect the peak maximum to shift to lower temperatures with increases in cold work. Experimentally the opposite behavior is observed

(Chapter 4). Alefeld et al (1965) have argued that the Pare proposal is substantiated by the fact that T_m of the α -peak in niobium behaves in the predicted manner. The same argument has been put forth by Sommer and Beshers (1966) based on their observation of the P_3 peak in nickel. We have shown in Chapter 4 that neither of these peaks can be classified as Bordoni peaks because of their enhancement in the presence of hydrogen.

We would also expect mild annealing to reduce the internal stresses thus reducing $\Delta\sigma_i$ with an accompanying increase in T_m . Again, the Bordoni peak has been observed to behave in the opposite manner. It is doubtful whether other, unaccounted for, effects would mask the predicted changes in T_m since both Hobart (1969) and Paré (1961) have shown that T_m is reduced by approximately 20°K upon increasing $\Delta\sigma_i/\sigma_p^0$ from 0 to 0.2.

We would expect, from Paré's model (and from Hobart's modification of it), that the width of the activation energy spectrum would be dependent on $\Delta\sigma_i$ and therefore on cold work and annealing treatments. We have shown in figures 4.7 and 4.16 that this is, in fact, not the case in nickel and copper where the spectrum width is left essentially unaltered by cold working and annealing treatments. The changes in shape of the peak in the early stages of deformation (figures

4.1 and 4.19) cannot be accounted for by this model since they are not consistent with an activation energy spectrum as predicted.

The contribution due to splitting of dislocation is also in doubt. The average separation between partials \bar{s} is determined by a balance between the reduction in dislocation energy caused by the splitting and the increase in the crystal energy due to the presence of the stacking fault plane (Loth and Hirth, 1968). As a consequence, in metals with high stacking fault energies the average separation between partials is expected to be smaller than in low stacking fault energy metals. The stacking fault energy of copper is (Hirth and Loth, 1968) approximately 100 ergs/cm^2 while in nickel it is $\sim 400 \text{ ergs/cm}^2$. The partial separation is then expected to be $\sim 3a$ in copper and $\sim 1.5a$ in nickel (Van Buren, 1960). We therefore do not see the justification in assuming $\bar{s} = 10a$ as done by Hobart. Furthermore we would expect that, since the separation of partials is less marked in nickel than in copper, it should have less effect on the width of the Bordoni peak. The experimental results however indicate that the Bordoni peak in nickel is significantly wider than in copper (figures 4.6 and 4.16).

It is apparent from the above discussion that the Seeger-Hobart proposal cannot account for the relaxation spectrum of the Bordoni peak. This conclusion would tend

to substantiate Seeger and Schiller's (1966) contention that the σ dependence of W (equation 5.26) should not include internal stresses. A reasonable discussion of the dislocation splitting effect is not possible in view of the large uncertainties in the concept of kink generation in split dislocations (Lothe and Hirth, 1968 and Friedel, 1968). The discrepancies between the Paré-Hobart model and the experimental results are not linked with the use of the Seeger et al kink generation model since all the other kink models presented in the literature have qualitatively the same dependence on kink energy and applied stress for the activation energy (see, for example, Seeger and Schiller, 1966; Alefeld et al, 1965 and Asenault, 1967).

Seeger and Schiller (1962 and 1966) have suggested that the width of the Bordoni peak might be explained by taking into account the time required for the kinks in a pair that has been thermally activated to separate under the influence to an applied stress. They proposed that the relaxation time τ for the Bordoni peak could be represented by:

$$\tau = \tau_k + \tau_s \quad , \quad (5.36)$$

where τ_k is the relaxation time for double kink generation (to critical separation d) and τ_s is the relaxation time for the further separation of the kinks under the applied

stress. The value of τ_s could be made appreciable compared to τ_k by viscous drag forces on the kinks due to kink-kink interactions and phonon viscosity. The time τ_k decreases exponentially with temperature while τ_s due to phonon drag might be expected to increase (much more slowly) with temperature. As pointed out by Seeger and Schiller (1966), this would broaden the Bordoni peak particularly at high temperatures where τ_s becomes comparable with τ_k . This qualitative argument was used by these authors to explain the structure on the high temperature side of the Bordoni peak. We have discussed this structure at the beginning of this Chapter and compared its effect on the shape of the peaks in copper and nickel. Until further development of this theory is made, we cannot comment on the validity of the Seeger-Schiller proposal; however their suggestion that the total width of the peak might be explained in this way does not seem to be correct. The analysis on the shape of the Bordoni peak, given in Sections A and B of Chapter 4, has shown that the most significant broadening of the peak occurs on the low temperature side of T_m and produces the characteristic asymmetry. The contribution to τ_s arising from kink-kink interactions cannot account for this effect either. Kink-kink interactions should be increased by increasing the number of dislocations and thus the number of kinks. However, except for

the very early stages of deformation, it has been shown that the shape of the peak is independent of the amount of cold work (figures 4.7 and 4.16).

The preceding discussion has indicated that the simple theories of double kink generation and the proposed modifications to these theories by Paré (1961), Seeger and Schiller (1962), and Hobart (1969) cannot account for the spectrum of the Bordoni peak. It would appear at this time that an explanation of the spectrum must await further development of the rate theory given by Seeger and Schiller (1966) and outlined at the outset of this discussion. This would require a much more detailed calculation of the rate of generation of double kinks which has not been reported as yet. The effects of dragging forces on kinks due to various defects such as other kinks, phonons and point defects would also have to be taken into account. The fact that many dislocations will be pinned at points which do not all lie in the same Peierls valley must also be considered since these dislocations would cross the Peierls potential at all temperatures. They would therefore contain kinks (called geometric kinks) which are not thermally activated. These kinks would be expected to drift under an applied stress and interact with thermally activated kink pairs (Alefeld, 1967). Until the uncertainties, in the above listed interactions, are resolved a numerical solution of the

non linear rate theory is not warranted. The successful theory will be required to explain the changes in peak temperature that are produced by cold work, annealing and impurities. It should also yield a spectrum which is relatively insensitive to these treatments. The spectrum must produce a broadening of the peak which is more marked at low temperatures as might be expected from an activation energy spectrum. Finally this theory should determine the relationship of the structure on the high temperature side of the peak and the three peaks composing the Niblett-Wilks peak (P_2) to the main Bordoni peak.

ii) The δ peaks in tantalum and niobium

We have shown (Section C, Chapter 4) that the internal friction versus temperature curve for cold worked tantalum exhibits a relaxation peak at approximately 25°K (22 kHz). A peak, similar to this δ -peak, has also been observed in niobium by Mazzolai and Nuovo (1969) and by Chambers (1966). It was suggested by the authors (Verdini and Vienneau 1968 b) and subsequently Mazzolai and Nuovo (1969) that this peak arises from the same relaxation mechanism as the Bordoni peak. The latter authors, however, used the Brailsford (1961) abrupt kink model in their analysis of the peak. Before commenting on the different

models used, let us examine the basis and consequence of identifying the δ -peak with the Bordoni peak.

In reviewing the properties used to define the Bordoni peak in nickel and copper (Chapter 5, A i) we find that the δ -peak does in fact fit the definition reasonably well. The effects of cold work, annealing and hydrogen impurity on the peak height and temperature, as outlined in Chapter 4, C, agree well with observations made on the Bordoni peak. The width of the peaks indicates the presence of a relaxation time spectrum which is also the case for the Bordoni peak. We were not able to make a quantitative comparison between the spectra of the δ -peak and that of the Bordoni peak because of the structure on the high and low temperature sides of the former. If, however, we identify this structure with the Niblett-Wilks peak and the structure on the high temperature side of the Bordoni peak, the δ -peak fits the definition of the Bordoni peak quite well.

The assumption that the δ -peak is a Bordoni peak has very important consequences. The activation energy for the Bordoni peak according to the Seeger et al (1957) model is given by equation (5.27) for very small applied stress. The proportionality of W to W_k is a common feature of all double kink generation models presented in the literature (see, for example, Niblett, 1966).

The proportionality constant (4.56 in the Seeger et al model) however varies by a factor of two from model to model. In spite of this, we can make a comparison of the values of σ_p^0/μ derived from equations (5.16) and (5.27) using the measured value of the activation energy W . In table III we find the measured value of the activation energy W for the Bordoni peak in copper and nickel and the δ -peak in tantalum and niobium accompanied by the corresponding values of σ_p^0/μ .

The results in table III indicate that the Peierls stress is much smaller for the b.c.c. metals, niobium and tantalum, than the f.c.c. metals, nickel and copper: although the theoretical estimates of σ_p^0/μ are very uncertain and cover the range given in table III, it is generally expected that the values for tantalum and niobium should be somewhat higher than in copper and nickel (Loth and Hirth, 1968; Seeger and Schiller, 1966). The qualitative argument for this rests on the fact that the interatomic forces in b.c.c. metals tend to be more directional than in f.c.c. crystals. This results in greater resistance to shearing and therefore a larger Peierls stress.

In the Mazzolai-Nuovo interpretation of the δ -peak, use is made of the abrupt kink model for the Bordoni peak (Brailsford, 1961). In this description the Bordoni peak

TABLE III

COMPARISON OF σ_P^0/μ FOR VARIOUS METALS

	W (eV)	$\sigma_P^0/\mu \times 10^4$ *
Copper	0.122 (1)	1.3
Nickel	0.195 (2)	1.7
Tantalum	0.027 (2)	0.012
Niobium	0.1 (3)	0.52

* Derived from equations (5.16) and (5.27) using;
 $a=b$, $E_0 = \mu b^2/2$ (Seeger et al, 1957).

(1) Bordoni et al (1959)

(2) This study

(3) Chambers (1966)

is assumed to arise from motion of kinks along the dislocation line rather than through the nucleation of kink pairs. This motion is assumed to be thermally activated because of the presence of a periodic energy barrier analogous to the Peierls barrier. If we assume that this model contains the explanation of the Bordoni peak, then it is easily seen that the discrepancy in table III is not removed. Since the activation energy for kink motion along the dislocation line is expected to be much less than that of double kink nucleation, we might assume that the Bordoni peak in copper and nickel arises from the Seeger et al mechanism while the δ -peak is due to the Brailsford mechanism. Further discussion on this point would require more justification for Brailsford's assumption of an energy barrier. The effective Peierls barrier for kink motion along the dislocation line is estimated to be much less than kT down to $0.5^\circ K$ or lower (Loth and Hirth, 1968; Seeger and Schiller, 1966).

We will close this discussion by pointing out that reconsideration of the basic concepts of the Peierls barrier might be avoided by identifying the δ -peaks with a similar peak observed in polycrystalline magnesium by Tsui and Sack (1967) in the same temperature range. They report that the peak, which is very similar to the

δ -peaks, is only visible in the polycrystalline material and not in single crystals. They therefore interpret the peak as a grain boundary effect. Measurements of the internal friction in high purity single crystal of tantalum and niobium would therefore be the deciding factor here. A Bordoni peak should be present in both polycrystal and single crystal specimens (as in Copper, Mongy et al, 1964) while grain boundary effects should only occur in the former. The mechanism for the magnesium peak is not known at this time; however further experimental study may yield the information required for an interpretation.

The striking similarity of the δ -peak and the magnesium peak to the Bordoni peak in copper points out the discretion required in identifying relaxation peaks in cold worked metals with the Bordoni peak in copper. A very good example of this is the long standing identification of the α -peaks in b.c.c. metals with the Bordoni peak. As we have shown in Chapter 4, C, this requires reccnsideration because of the role hydrogen apparently plays in this relaxation.

iii) The hydrogen cold-work peaks

We now turn our attention to the P_3 peak in nickel and its counterpart, the α -peak in tantalum. These peaks are basically different from the Bordoni peaks with regard

to their behavior in the presence of dissolved hydrogen. The α -peak in niobium is similar to that in tantalum (Mazzolai and Nuovo, 1969). We have shown the following properties to be common to the P_1 peak in nickel and the α -peak in tantalum and niobium:

(1) For a fixed amount of cold work, the height of the peak, and its temperature T_m increases with hydrogen concentration.

(2) For a fixed hydrogen concentration, the height of the peak increases with the amount of cold work up to a critical value after which it decreases to very small values.

(3) The temperature of the peak maximum tends to decrease slightly with increasing amounts of cold work.

(4) The peak is relatively insensitive to the stress amplitude of the sound wave.

(5) The peak temperature T_m varies with frequency according to an Arrhenius equation, indicating that it arises from a thermally activated relaxation process. The width of the peak cannot be explained by a single relaxation process and a range of relaxation times is involved in each case. Because of their similarities, we will assume that the P_3 peak in nickel and the α -peaks in niobium and tantalum arise from the same relaxation process.

From the properties (1) and (2), it would appear that the hydrogen cold work peaks are due to dislocation motion in the presence of dissolved hydrogen or visa versa. Since the peak arises irrespective of the order in which the dislocations and the hydrogen are introduced into the crystal we can assume that the relaxation does not require the peculiar dislocation structures which could be produced by deformation in the presence of hydrogen (a difference in structure has been observed by Wilcox and Smith, 1964).

The hydrogen cold work peak in tantalum has been interpreted by Mazzolai and Nuovo (1969) using the Schoeck (1963) atmosphere dragging model. This model assumes that the internal friction arises from the stress induced motion of dislocations experiencing a frictional force caused by the impurity (hydrogen) atmosphere around them. The Schoeck model has recently been modified by Ino and Sugeno (1967) to take into account the effects of internal stresses. The treatment due to the latter authors will be presented here.

The equation of motion for a dislocation is written in a similar fashion to equation (5.12); however the energy per unit length of the dislocation is presumed to have a constant value E_0 (no lattice interaction). The result is:

$$B \frac{\partial y}{\partial t} - E_0 \frac{\partial^2 y}{\partial x^2} - f_i(y, x) = \sigma b \quad , \quad (5.36)$$

where the first term on the left hand side is the frictional force due to the solute atmosphere (proportional to dislocation velocity) and $f_i(x, y)$ is the force caused by the internal stresses. The inertia term in the equation of motion is assumed to be very small compared to the friction term and is therefore neglected. The y coordinate is the direction of displacement while the x coordinate is parallel to the dislocation line. With no external stresses σ present the equilibrium position of the dislocation is given by:

$$- E_0 \frac{\partial^2 y_0}{\partial x^2} - f_1(y_0, x) = 0 \quad . \quad (5.37)$$

By expanding $f_1(y, x)$ about the point y_0 and retaining only first order terms, we can write equation (5.36) as

$$B \frac{\partial \xi(x)}{\partial t} - E_0 \frac{\partial^2 \xi(x)}{\partial x^2} - a_1(x) \xi(x) = \sigma b \quad , \quad (5.38)$$

where $a_1(x) = \partial f_i / \partial y |_{y_0}$ and $\xi(y) = y - y_0$. For simplicity we assume that we are able to replace $\xi(x)$ by an average value $\bar{\xi}$ and replace $a_1(x)$ by its average value \bar{a}_1 . With these substitutions, it is shown that the solution of equation (5.38) is given by:

$$\bar{\xi} = \frac{\sigma b \left(\frac{\alpha E_0}{l^2} - \bar{a}_1 - i\omega B \right) e^{i\omega t}}{\left(\frac{\alpha E_0}{l^2} - \bar{a}_1 \right)^2 + \omega^2 B^2} \quad , \quad (5.39)$$

for the conditions:

$$\sigma = \sigma_0 e^{i\omega t}$$

$$y = \xi = 0 \quad \text{at} \quad x = 0, \ell .$$

The constant α (≈ 10) is related to the average displacement approximation and is the length of the dislocation segment. Equation (5.39) reduces to the results of Schoeck (1963) for $\bar{a}_1 = 0$ (zero or uniform internal stresses). The strain resulting from this displacement for all the dislocation segments (see equation 5.10) is then given by:

$$\epsilon_d = b \int_0^{\infty} \rho(\ell) \bar{\xi}(\ell) \ell d\ell ,$$

where $\rho(\ell)$ is the density of dislocation segments of length ℓ . The internal friction is derived from the imaginary part of the dislocation strain, according to equation (5.11), to be:

$$Q^{-1} = \int_0^{\infty} \frac{\mu b^2 \ell}{\alpha E_0 \frac{\ell^2}{2} - \bar{a}_1} \rho(\ell) \frac{\omega \tau}{1 + \omega^2 \tau^2} d\ell . \quad (5.40)$$

The relaxation time τ is given by:

$$\tau = \frac{B}{\alpha E_0 \frac{\ell^2}{2} - \bar{a}_1} , \quad (5.41)$$

and L , the total length of dislocations per unit volume, is given by:

$$L = \int_0^{\infty} \rho(\ell) \ell d(\ell) \quad . \quad (5.42)$$

If the average value of ℓ is given by ℓ_0 we can rewrite equation (5.40) as:

$$Q^{-1} = \frac{\mu b^2 L}{\alpha E_0 \ell_0^2 - \bar{a}_1} \int_0^{\infty} \rho(\ell) \frac{\omega \tau}{1 + \omega^2 \tau^2} d\ell \quad . \quad (5.43)$$

By comparison with equation (2.19) we see that the dislocation drag model yields a relaxation process with a spectrum of relaxation times governed by $\rho(\ell)$. The relaxation time is evaluated using the Einstein mobility relation for diffusing particles.

In equation (5.41) we see that the relaxation time is controlled by B the frictional drag coefficient in equation (5.36) which is given by:

$$B = \frac{F}{\ell v} \quad , \quad (5.44)$$

where F is the total friction force on the dislocation moving with velocity v . The Schoeck model is based on the Cottrell drag model (Cottrell and Jaswon, 1949). The dislocation motion is assumed to be retarded by the necessity to move the surrounding impurity atmosphere. The force exerted on the dislocation by its atmosphere

is equal to the force required to move the atmosphere at the velocity v of the dislocation. This force F is given by the Einstein mobility relation:

$$F = \frac{\ell v N k T}{D} \quad , \quad (5.45)$$

where N is the excess number of impurity atoms per unit length of dislocation and D is the diffusion coefficient of the impurity atom. By assuming that the impurity atoms which contribute to the dragging force are all within a radius R of the dislocation axis Schoeck (1963) demonstrated that:

$$N = \frac{9\pi R^2 C_d}{4\sqrt{3} b^3} \quad , \quad (5.46)$$

where C_d is the excess concentration of impurities bound to the dislocation (atomic fraction). The relaxation time is then derived from equation (5.41) to be:

$$\tau = \left(\frac{9\pi R^2 C_d k T}{4\sqrt{3} b^3 D} \right) / \left(\frac{\alpha E_0}{\ell^2} - \bar{a}_1 \right) \quad . \quad (5.47)$$

The diffusion coefficient D is assumed to have its usual temperature dependence

$$D = D_0 \exp(-Q/kT) \quad (5.48)$$

where Q is the activation energy for bulk diffusion of the impurity. The concentration C_d is assumed to be

proportional to $C \exp [E_B/kT]$ where E_B is the binding energy of the impurity atom to the dislocation and C is the hydrogen concentration in the bulk. The relaxation time can then be written as:

$$\tau = \frac{KCT}{\left[\frac{\alpha \mu b^2}{2\ell^2} - \bar{a}_1 \right]} \exp [(Q + E_B)/kT] \quad (5.49)$$

where K is a constant and E_0 has been replaced by $\mu b^2/2$ (Seeger et al, 1957). We see that the atmosphere dragging model results in a thermally activated relaxation process with an activation energy W given by the sum of Q and E_B . The limiting relaxation time has a spectrum of values caused by the spectrum in both ℓ and \bar{a}_1 , the internal strain gradient.

The measured values of the activation energy W are compared in table IV with the values of Q and E_B determined by other techniques. We have included the results for tantalum, niobium, iron, and palladium for comparison purposes. Some identifications of the activation energy of diffusion that occurs in the Schoeck atmosphere dragging model with that derived from the Snoek relaxation peak have been made in the literature (Mazzolai and Nuovo, 1969 and Gibala, 1967). It is known that the measured activation energy for diffusion depends on the method used (see, for example, Barrer, 1961; Smithells, 1967), and therefore the choice of the

TABLE IV
SUMMARY OF ENERGIES RELATED TO HYDROGEN COLD
WORK PEAK (eV)

	W	* Q	† E _B
Nickel	~0.5 ⁽¹⁾	A.— B.0.4 (4) C.0.4 (5)	A. 0.1 (1) B. 0.08 (4)
Tantalum	0.25 ⁽²⁾	A. 0.12±0.01 (6) B. — C. —	A. 0.13 (2)
Niobium	0.25 ⁽²⁾	A. 0.18±0.01 (6) B. 0.38 (7) C. 0.04 (5)	A. 0.07 (2)
Iron	0.36 ⁽³⁾	A. 0.09 (3) B. — C. 0.13 (5)	A. 0.27 (3)
Palladium	0.35± 0.05 ⁽⁸⁾	A. 0.13 (9) B. — C. 0.23 (5)	A. 0.22

* The letters refer to the method used in measuring Q
 A - internal friction experiments (Snoek effect).
 B - serrated yielding or strain aging techniques.
 C - various bulk diffusion methods at high temperatures (>100°C).

† A - Derived from W-Q (Q_A for all except N_i where Q_B is used)
 B - Derived from serrated yielding experiments.

(1) This study

(2) Chambers, 1966

(3) Gibala, 1967

(4) Boniszewski and Smith, 1963

(5) Smithells, 1967

(6) Mazzolai and Nuovo, 1969

(7) Wilcox and Huggins, 1961

(8) Fanti, 1965

(9) Arons et al, 1967

Snoek activation energy seems somewhat arbitrary. The better choice is perhaps that derived from serrated yielding measurements. The activation energy enters the theory of serrated yielding (due to dissolved hydrogen) in exactly the same way that it does the Schoeck model. In examining the case of nickel in table IV we see that the binding energy of hydrogen to dislocations is known from two sources. The first was obtained by subtracting the value of Q derived from serrated yielding experiments from the activation energy W (of the cold work peak). The resulting value is in excellent agreement with the value of E_B derived independently from the same experiment in which Q was determined.

In niobium, the only other metal in the table for which Q has been obtained from serrated yielding effects, the situation is quite different. The measured value of Q is larger than the value of W . This leads to a negative value of E_B . The value of E_B could in fact be negative and would indicate a repulsive force between the dislocation and the hydrogen impurity. It has however been tacitly assumed in the Schoeck model that the excess concentration of impurities around the dislocation is a positive quantity. A slightly more refined treatment (Loth and Hirth, 1968) of the frictional force due to an impurity atmosphere shows that

the absolute value of the binding energy E_B enters the theory. Thus, the activation energy of the hydrogen cold work peak should be given by:

$$W = Q + |E_B| \quad . \quad (5.50)$$

We see from equation (5.50) that $(W-Q)$ should be a positive number, that is $|E_B|$.

The use of Q as deduced from measurements of the hydrogen Snoek peak would resolve the problem but this procedure is uncertain. This approach was used by Mazzolai and Nuovo (1969) and, as shown in the table, the resulting value of E_B is comparable with that for nickel. This result cannot be considered as conclusive, since the relationship between Q_A (Snoek peak at low temperature) and Q (at the temperature of the hydrogen cold work peak) is as yet not understood. The classical theory of diffusion is not expected to apply to hydrogen at low temperatures because of its small mass (see, for example, Mueller, 1965). In view of the lack of knowledge concerning the diffusion activation energy, we must conclude that agreement between the measured values of W and that predicted in equation (5.50) is at best speculative.

The value of the relaxation strength as given in equation (5.43) is independent of the hydrogen concentration. This is not in agreement with the experimental

results for the hydrogen cold work peak in nickel (figure 4.10). Mazzolai and Nuovo have noted this discrepancy in their measurements of the peak in tantalum and niobium. It is to be expected from the Schoeck model that the peak would not exist in the absence of hydrogen. The Schoeck model assumes that the frictional force caused by the interstitial hydrogen can be described by a uniform force per unit length resulting in a peak which is independent of hydrogen concentration. This description can only be considered valid when the distance between hydrogen atoms near the dislocations is very small compared to the distance between pinning points (typically 10^{-5} cm). It is easy to show that the distance between hydrogen atoms at a concentration as small as 1 p.p.m. is approximately 2×10^{-6} cm, so according to our argument the peak should increase with hydrogen concentration up to a value on the order of 1 p.p.m. where the Schoeck description becomes valid. The concentration of hydrogen at the dislocations is very difficult to estimate even if the total amount of hydrogen dissolved in the sample is accurately known. Various attempts have been made to estimate the hydrogen concentration at the dislocations (Gibala, 1967; Sturges and Miodownik, 1969) in connection with measurements of the hydrogen cold work peak

in iron. The results are somewhat uncertain; however they generally indicate that, in the range for which the height of the peak increases with hydrogen charging, the excess concentration is of the order 0.3 to 1 p.p.m. For further hydrogen charging, the peak height saturates, which is consistent with the view that the Schoeck model is only valid when the hydrogen concentration is high enough that the friction force can be considered uniform along the length of the dislocation.

The procedure used by Gibala (1967) to estimate the excess hydrogen concentration near the dislocations cannot be used in the case of nickel. The procedure makes use of the relaxation strength of the Snoek peak which is not present in nickel since it is an f.c.c. metal (see, for example, Berry and Nowick, 1966). It does not seem unreasonable however to expect similar values to apply and the explanation of the concentration dependence of the peak height would proceed in the same way as for iron.

Let us next examine the relaxation strength Δ of the peak as influenced by cold work. From equations (5.43) and (2.9) we can write:

$$\Delta = \frac{\mu b^2 L}{\frac{\alpha E_0}{\rho_0^2} - \bar{a}_1} \quad (5.51)$$

If we assume that the dislocations are randomly oriented it is easy to show that the average distance ℓ_i between points of intersection for two dislocations can be approximated by:

$$\ell_i^2 = 3/L \quad . \quad (5.52)$$

These intersections form pinning points for the dislocations (Loth and Hirth, 1968). The large immobile impurities in the sample will generally form pinning points which are closer together than the network length ℓ_i in an annealed crystal, that is

$$\ell_i > \ell_0 \quad . \quad (5.53)$$

Thus, assuming $\bar{a}_1 = 0$ in equation (5.51) and replacing E_0 by $\mu b^2/2$ (Seeger et al, 1957) we find that:

$$\Delta = \frac{2L\ell_0^2}{\alpha} \quad . \quad (5.54)$$

We find that when equation (5.53) applies (annealed and lightly cold worked samples), the relaxation strength increases with L which increases with cold working. For larger amounts of cold work ℓ_i becomes less than ℓ_0 and must replace it in equations (5.51) and (5.54) since the product $L\ell_i^2$ is a constant, the relaxation strength (of equation 5.54) must become constant for large amounts of cold work. As the dislocation density increases they interact more strongly with one another, that is, the

value of \bar{a}_1 becomes larger. Let us consider the case where \bar{a}_1 is a negative number. This would occur, for example, in a group of interacting edge dislocations arranged in the form of a Taylor net (Weertmann and Koehler, 1953). The value of Δ as derived from equation (5.51) should then decrease as \bar{a}_1 becomes more negative. This could qualitatively explain the experimental observations as outlined by property (2) at the beginning of this section.

The qualitative arguments presented above show that the atmosphere dragging model can account for the hydrogen cold work peak. The theoretical development of this model as given by Schoeck (1963) and Ino and Sugeno (1967) however requires further development in order to get a realistic quantitative comparison. The interpretation of the results would also be aided by reliable measurements of the activation energy for the diffusion of hydrogen. This would be best achieved by serrated yielding experiments near the temperature of the peak.

B. Magnetic damping effects

In both cold worked iron and nickel it has been shown that the internal friction exhibits a plateau region in its temperature dependence. We have also shown that this internal friction effect depends on the magnetic state of the sample as well as the state of cold work. It was pointed out in Chapter 4,D that the plateau region in iron

and nickel are very similar. In view of the fact that this damping in nickel is observed only for a limited range of cold work (~3-12%) and is heavily masked by other damping effects, we will restrict our discussion to the results in iron and assume that the conclusions apply equally well in both cases.

It was originally thought (Vienneau, 1968; Verdini and Vienneau, 1968a) that the plateau arose from dislocation damping. Recalling the results in figure 4.30 we see that the frequency dependence of the low temperature internal friction can be fit to the Oen et al (1960) theory. The Oen et al theory is simply a general solution of equation (5.36) used in the Schoeck model. The internal stresses are assumed to be zero ($f_i=0$) and no assumptions are made concerning the frictional force coefficient B. The quantity ω_0 in the calculation roughly corresponds to:

$$\omega_0 = \tau^{-1} \quad (5.55)$$

where τ is the relaxation time as given by equation (5.41) with $\bar{a}_1 = 0$. The experimentally determined temperature dependence for ω_0 given in figure 4.31 indicates that the relaxation time is proportional to the electrical conductivity. Mason (1966 b) has suggested that in pure metals, the strain field around a dislocation would interact with the free electrons in the metal and therefore produce a

relaxation time which is proportional to the electrical conductivity. This conductivity dependence is in agreement with the results in figure 4.31; however the author has shown (Vienneau, 1968) that the relaxation time predicted by Mason's theory is much too small to account for the experimental results.

Recently Hasiguti et al (1968) have reported measurements of ultrasonic attenuation at room temperature in iron which they attributed to dislocation damping with long relaxation times, comparable to those in figure 4.31. With this in mind, we sought an alternative model for dislocation damping in ferromagnetic metals. It is known that the strain field around a dislocation interacts, via magnetostriction, with the magnetization in a ferromagnetic metal (Brown, 1941; Kronmüller and Seeger, 1961). Kosevich and Fel'dman (1968) have shown that this effect can be treated as a small perturbation on the normal magnetization vector. By minimizing the elastic and magnetic energy around a dislocation they have shown that the internal fields in a metal can be expressed as:

$$H = H_0 + h \quad , \quad (5.56)$$

$$M = M_0 + m \quad ,$$

where h is a small deviation from a uniform internal magnetic field strength H_0 and depends on the position relative

to the dislocation line. The quantity m is the corresponding deviation in magnetization M_0 . It is easy to see that a moving dislocation would produce a time dependent magnetic induction given by the time dependence of $(h + 4\pi m)$. The resulting induced e.m.f. would generate eddy currents and consequently power dissipation and a frictional force on the dislocation. The author has derived the frictional force coefficient B and the dislocation relaxation time τ starting from the values of h and m given by Kosevich and Fel'dman (1968). It is sufficient to say that the resulting relaxation time is of the same order as that of Mason's theory and therefore cannot account for the results in figure 4.31.

From equation (5.54) we expect the magnitude of the internal friction due to dislocation relaxation to increase as the $N\ell_0^2$. The best check on this behavior comes from the effect of radiation in the internal friction (Thompson and Paré, 1966). The effect of high energy irradiation is to displace some of the atoms from their lattice sites into interstitial sites, that is, interstitial and vacancy defects are produced. These defects are able to migrate to the dislocations and produce pinning points. We thus have a situation where L the total length of dislocations is unchanged but ℓ_0 is effectively shortened. Equation (5.54) would then predict a reduction in the internal friction due to dislocation

relaxation. The internal friction in the plateau region clearly does not follow this behavior (figure 4.33).

The above discussion indicates that dislocations do not play a direct role in the plateau internal friction. As pointed out in the last chapter, the fact that the internal friction is greatly reduced by the application of a magnetic field and that the largest part of the reduction approximately coincides with magnetic saturation (figure 4.28) favors the interpretation that domain wall motion is responsible for the relaxation. The motion of domain walls in the presence of internal stresses is as yet an unresolved problem (Truell et al, 1969), so it is possible to make only qualitative remarks at this time. The irreversible motion of domain walls (in the presence of internal stresses) known as the Barkhausen effect has been applied in the study of magnetic damping. The resulting hysteresis type of damping has been observed in both iron and nickel (Roberts and Barrand, 1969a) and accounts for a large portion of the damping in these metals when they are well annealed (figure 4.27, upper curve). This hysteresis damping is however independent of frequency (see, for example, Bozorth, 1951). Cold working is expected to reduce this damping to negligible amounts (Bozorth, 1951 and Roberts and Barrand, 1969b). The results in figure 4.27 are in agreement with

this picture. The frequency independent hysteresis damping is however replaced by a frequency dependent relaxation damping (the plateau region).

The motion of domain walls in connection with acoustic relaxation has been considered by several authors (Mason, 1951; Simon, 1961; and Dietz, 1969). As pointed out by Dietz, these models have not been particularly successful in explaining the relaxation part of magnetic damping in annealed metals. In the case of the plateau, they are even less appropriate since none of them take into account the effect of internal stresses which seem to play a significant role here.

In the simplest model, the domain wall is considered as a membrane of finite thickness. The application of an internal stress (sound waves) causes the wall to vibrate and change thickness. As it does so, eddy currents are generated which could produce the desired relaxation. The treatment depends on the type of domain wall (Mason, 1951); therefore one would expect a different behavior in nickel, which has predominantly 180° walls, than in iron which has predominantly 90° walls. This might account for the fact that the plateau in iron is larger and more easily seen than in nickel. It might also account for the limited range of cold working for which the plateau is appreciable in nickel as compared to iron.

One might consider the motion of domains as analogous to that of dislocations. The internal stresses were taken into account in the dislocation model by introducing a static position dependent force f_i into the equation (5.36) of motion. It should be expected that this would be reflected in the relaxation time as was the case for dislocations (equation 5.41). The results of figure 4.32 show that the relaxation curve is not significantly shifted in frequency by annealing contrary to the qualitative argument given above. Although the experimental results favor an explanation involving the motion of magnetic domain walls in the presence of internal stresses, a quantitative comparison must await further theoretical development. It would be hoped that the successful theory would explain the maximum in the internal friction versus magnetic field which was observed here (figure 4.29) and by others (Bratina, 1966). This effect is known to be associated with the cold worked state of the metal (Bratina, 1966) and probably involves internal stresses. No explanation however is available as yet.

CHAPTER 6

CONCLUSIONS

The internal friction of cold worked nickel has been measured as a function of several parameters (including temperature, frequency and degree of cold work). The temperature dependence exhibits a large peak accompanied by a subsidiary peak on its low temperature side. These are identified with the Bordoni peak and Niblett-Wilks peak in copper. Another relaxation peak occurring at a higher temperature than the Bordoni peak is identified with the hydrogen cold work peak. A magnetic relaxation effect was also observed below the temperature of the Bordoni peak.

The Bordoni peak in nickel was found to have an activation energy of 0.195 ± 0.02 eV with a limiting relaxation time given by $\ln \tau_0 \approx -28$. The peak width indicates a relaxation time spectrum similar to that in copper. The results are discussed in terms of the double kink generation theory. We find that the spectrum of the Bordoni peak cannot be explained by the proposals of Paré (1961), Seeger and Schiller (1962) and Hobart (1969). The more detailed theory of double kink generation outlined by Seeger and Schiller (1966) is discussed, but a quantitative comparison with this theory would require more information about the dislocation parameters than are presently available for real metals.

The Niblett-Wilks peak in nickel was found to have an activation energy of 0.140 ± 0.035 eV with a limiting relaxation time given by $\ln \tau_0 = -25 \pm 2$. There is a spectrum of relaxation times associated with this peak similar to that of the Bordoni peak. Measurements made of the Niblett-Wilks peak in copper for comparison purposes show that this peak is made up of three overlapping peaks. Poorly defined structure observed on the Niblett-Wilks peak in nickel is thought to correspond to the clearer results in copper. Our measurements of the Bordoni peak in lightly cold worked copper show the same structure on the high temperature side as was discussed by Seeger and Schiller (1962). The Bordoni peak in nickel is observed here to exhibit this same structure. Together with the results for the Niblett-Wilks peak, this lends strong support for the Thompson and Holmes (1959) proposal that several relaxation peaks are present in the vicinity of the Bordoni peak.

The addition of hydrogen to cold worked nickel is shown to produce a large relaxation peak above the temperature of the Bordoni peak. A comparison shows that this peak is the same as that observed by Sommer and Beshers (1966) and identified by them to be the Bordoni peak. The activation energy for the peak was found to be approximately 0.5 eV. We interpret this peak to be the hydrogen cold work peak in terms of the Schoeck (1963)

atmosphere dragging model. The activation energy of 0.5 eV is in agreement with Schoeck theory. The effects of cold work and hydrogen charging on the relaxation strength are discussed in terms of the Ino and Sugeno (1967) modification of the Schoeck theory. It is argued on qualitative grounds that the Schoeck model is not applicable for very small hydrogen concentrations. The experimental results are shown to be comparable with the hydrogen cold work peak in other metals, particularly tantalum.

Our measurements on tantalum have revealed a previously unreported relaxation peak which occurs at a lower temperature than the hydrogen cold work peak and is introduced by cold working. It is suggested that the peak is similar to that reported in magnesium by Tsui and Sacks (1967) and interpreted as a grain boundary effect. More work, including measurements on single crystals, would be very useful in interpreting these results further.

Nickel samples cold worked by amounts between approximately 3% and 12% strain show an internal friction effect similar to the plateau region reported in iron by Bruner (1960) and Vienneau (1968). We find that our original suggestion (Vienneau, 1968) of a dislocation damping effect involving the conduction electrons and

a recent modification of it which takes into account magnetostrictive effects, when subjected to quantitative comparison, cannot explain the results. Measurements presented for both iron and nickel favor a magnetic relaxation effect involving the motion of domains in the presence of internal stresses. A complete description of this effect is not yet available.

BIBLIOGRAPHY

- Alefeld, G., Chambers, R.H., and Firle, T.E. (1965)
Phys. Rev. 140, A1771.
- Alefeld, G. (1967) in "Lattice defects and their interactions", p. 407, Ed. R. Hasiguti, Gordon and Breach publ., New York.
- Arons, R.R., Bouman, J., Wijzenbeek, M., Klaase, P., Tuyn, C., Leferink, G., De Vries, G. (1967)
Acta Met. 15, 144.
- Arsenault, R.J. (1967) Acta Met. 15, 501.
- Barrer, R.M. (1951) "Diffusion in and through Solids"
Cambridge Univ. Press.
- Berry, B.S. (1962) I.B.M. Annual Res. Rep. to U.S.A.E.C.
Cont. No. AT (30-11-2811).
- Berry, B.S. and Nowick, A.S. (1961) I.B.M. J. Res. Develop.
5, 297, 312.
- Berry, B.S. and Nowick, A.S. (1966) in "Physical Acoustic"
Vol. IIIA, p. 1, Mason (1966) Loc. cit.
- Boniszewski, T. and Smith, G.C. (1963) Acta Met. 11, 165.
- Bordoni, P.G. (1949) Ricerca Sci. 19, 851.
- Bordoni, P.G. (1954) J. Acoust. Soc. Am. 26, 495.
- Bordoni, P.G. (1959) "Proceedings 3rd International Congress on Acoustics" Stuttgart, p. 146.
- Bordoni, P.G. (1960) Nuovo Cimento, Suppl. no.1, 17, 1518.
- Bordoni, P.G. (1961) Meteaux Corrosion Industries n. 427.
- Bordoni, P.G., Nuovo, M. and Verdini, L. (1959) Nuovo Cimento 14, 273.
- Bordoni, P.G., Gina, P.E. and Verdini, L. (1962) "Proceedings of the 4th International Congress on Acoustics", Copenhagen.
- Bozorth, R.M. (1951) "Ferromagnetism" Van Nostrand.

- Brailsford, A.D. (1961) Phys. Rev. 122, 778.
- Bratina, W.J. (1966) in "Physical Acoustics", Vol. IIIA
p. 223, Mason (1966) loc. cit.
- Brown, W.F. (1941) Phys. Rev. 60, 139.
- Bruner, L.S. (1959) Phys. Rev. 118, 399.
- Caswell, H.L. (1958) J. Appl. Phys. 29, 1210.
- Chambers, R.H. (1966) in "Physical Acoustics" Vol. IIIA,
p. 123, Mason (1966) loc. cit.
- Chambers, R.H. and Schultz, J. (1962) Acta Met. 10, 466.
- Cottrell, A.H. (1953) "Dislocations and Plastic Flow in
Crystals", Oxford Univ. Press.
- Cottrell, A.H. and Jaswon, M.A. (1949) 199A, 104.
- Dietz, G. (1969) Z. Angew. Phys. 27, 82.
- Donth, H. (1957) Quoted by Seeger et al (1957) loc. cit.
- Echigoya, J. and Hoyashi, S. (1969) Japan J. Appl. Phys.
8, 964.
- Fanti, F. (1965) Nuovo Cimento 38, 728.
- Friedel, J. (1968) Comments on Solid State Physics 1, 24.
- Gibala, R. (1967) Trans. Mat. Soc. AIME 239, 1574.
- Gnanato, A. and Lücke, K. (1956) J. Appl. Phys. 27, 583.
- Guberman, H. (1963) Quoted by Sommer and Beshers (1966)
loc. cit.
- Haywood, C.T. (1969) Ph.D. thesis "Electrical Resistivity
of Palladium/Hydrogen" Univ. of Alberta, Edmonton.
- Heller, W.R. (1961) Acta Met. 9, 600.
- Hirth, J.P. and Loth, J. (1968) "Theory of Dislocations"
McGraw-Hill, New York.
- Hobart, R. (1968) J. Appl. Phys. 39, 1907

- Hobart, R. (1969) J. Appl. Phys. 40, 3065.
- Ino, H. and Sugeno, T. (1967) Acta Met. 15, 1197.
- Jenkins, G. and Watts, D. (1968) "Spectral Analysis", Holden-Day.
- Konig, D., Völkl, J. and Schilling, W. (1964) Phys. Stat. Sol. 7, 577.
- Kosevich, A.M. and Fel'dman, E.P. (1968) Sov. Phys. - Sol. State 9, 2696.
- Kronmüller, H. and Seeger, A. (1961) J. Phys. Chem. Solids 18, 93.
- Mason, W.P. (1951) Phys. Rev. 83, 683.
- Mason, W.P. (1955) J. Acoust. Soc. Am. 27, 643.
- Mason, W.P. (1966 a) "Physical Acoustics", Vol. IIIA, Academic Press, New York.
- Mason, W.P. (1966 b) Phys. Rev. 143, 229.
- Mazzolai, F.M. and Nuovo, M. (1969) Sol. Stat. Com. 1, 103.
- Mongy, M., Saloma, K. and Beckman, O. (1964). Nuovo Cimento 34, 869.
- Mueller, W.M. (1965) "Energetics in Metallurgical Phenomena" Vol. I, Gordon and Breach, New York.
- Niblett, D.H. (1961) J. Appl. Phys. 32, 895.
- Niblett, D.H. (1966) in "Physical Acoustics" Vol. IIIA p. 77, W.P. Mason (1966) loc. cit.
- Niblett, D.H. and Wilks, J. (1956) Phil. Mag. 1, 415.
- Nuovo, M. (1961) Ricerca Sci. 31(II-A), 212.
- Oens, O.S., Holmes, D.K. and Robinson, M.T. (1960) U.S.A.E.C. Report ORNL-3017, p.3.
- Paré, V.K. (1961) J. Appl. Phys. 32, 332.
- Peierls, R. (1940) Proc. Phys. Soc. 52, 34.
- Powell, R.L., Bunch, M.D., Corruchini, R.J. (1961) Cryogenics 1, 139.

- Read, T.A. (1941) Trans. AIME 143, 30.
- Roberts, J.T.A. and Barrand, P. (1969a) Acta Met. 17, 757.
- Roberts, J.T.A. and Barrand, P. (1969b).
- Schiller, P. (1955) Nuovo Cimento 2, 1328.
- Schoeck, G. (1963) Acta Met. 11, 617.
- Seeger, A. (1956) Phil. Mag. 1, 651.
- Seeger, A., Donth, H. and Pfaff, P. (1957) Disc. For. Soc. 23, 19.
- Seeger, A. and Schiller, P. (1962) Acta Met. 10, 348.
- Seeger, A. and Schiller, P. (1966) in "Physical Acoustic"
Vol. IIIA, p. 361, Ed. W.P. Mason, Academic Press,
New York.
- Simon, V. (1961) Aran. der Phys. 7, 140.
- Smithells, C.J. (1967) "Metals Preference Book", Vol. II,
Butterworths, London.
- Sommer, A.W. and Beshers, D.N. (1966) J. Appl. Phys. 37,
4603.
- Staverman, A.J. and Schwarzl, F. (1956) in "Die Physik Der
Hochpolymeren", Vol. 4, p. 1, Ed. by H.A. Stuart,
Springer-Verlag, Berlin.
- Stenzel, G. (1965) Quoted by Seeger and Schiller (1966)
loc. cit.
- Sturges, C.M. and Miodownik, A.P. (1969) Acta Met. 17,
1197.
- Thompson, D.O. and Paré, V.K. (1966) in "Physical Acoustic"
Vol. IIIA; p.293, loc. cit.
- Thompson, D.O. and Holmes, D.K. (1959) J. Appl. Phys. 10,
525.
- Truell, R., Elbaum, C. and Chick, B.B. (1969) "Ultrasonic
Methods in Solid State Physics", Academic Press,
New York.

- Tsui, R.T.C. and Sack, H.S. (1967) Acta Met. 15, 1715.
- Van Bueren, H.G. (1960) "Imperfections in Crystals"
North-Holland, Amsterdam.
- Verdini, L. and Vienneau, L.A. (1968a) C.A.P. Congress,
Calgary, Abstract in Phys. in Can. 24, 29.
- Verdini, L. and Vienneau, L.A. (1968b) Can. J. Phys. 46,
2715.
- Vienneau, L.A. (1968) M.Sc. thesis "Anelasticity in Iron
at Low Temperatures", Univ. of Alberta, Edmonton.
- Weertman, J. and Koehler, J.S. (1953) J. Appl. Phys. 24,
624.
- White, G.K. and Woods, S.B. (1959) Phil. Trans. A, 251,
274.
- Wilcox, B.A. and Huggins, R.A. (1961) in "Niobium, Tantalum,
Molybdenum and Tungsten", p. 289, Ed. by A.G.
Quarrel, Elsevier, New York.
- Wilcox, B.A. and Smith, G.C. (1964) Acta Met. 12, 371.
- Yager, W.A. (1936) J. Appl. Phys. 1, 434.
- Zener, C. (1948) "Elasticity and Anelasticity of Metals"
Univ. of Chicago Press, Chicago, U.S.A.